Midwest States' Regional Pooled Fund Research Program
Fiscal Year 1998-1999 (Year 9)
Research Project Number SPR-3(017)
NDOR Sponsoring Agency Code RPFP-99-01(a)

DEVELOPMENT OF STANDARDS FOR PLACEMENT OF STEEL GUARDRAIL POSTS IN ROCK

Submitted by

Jason E. Herr, B.S.C.E., E.I.T.
Graduate Research Assistant

John R. Rohde, Ph.D., P.E.
Associate Professor

Dean L. Sicking, Ph.D., P.E.
Professor and MwRSF Director

John D. Reid, Ph.D.
Associate Professor

Ronald K. Faller, Ph.D., P.E.
Research Assistant Professor

James C. Holloway, M.S.C.E., E.I.T.
Research Associate Engineer

Brian A. Coon, M.S.C.E., P.E.
Graduate Research Assistant

Karla A. Polivka, M.S.M.E., E.I.T.
Research Associate Engineer

MIDWEST ROADSIDE SAFETY FACILITY
University of Nebraska-Lincoln
527 Nebraska Hall
Lincoln, Nebraska 68588-0529
(402) 472-6864

Submitted to

MIDWEST STATES' REGIONAL POOLED FUND PROGRAM
Nebraska Department of Roads
1500 Nebraska Highway 2
Lincoln, Nebraska 68502

MwRSF Research Report No. TRP-03-119-03

May 30, 2003

Technical Report Documentation Page

1. Report No.	2.	3. Recipient's Accession No.
SPR-3(017)		

4. Title and Subtitle	5. Report Date
Development of Standards for Placement of Steel Guardrail Posts in Rock	May 30, 2003
	6.

7. Author(s)	8. Performing Organization Report No.
Herr, J.E., Rohde, J.R., Sicking, D.L., Reid, J.D., Faller, R.K., Holloway, J.C., Coon, B.A., and Polivka, K.A.	TRP-03-119-03

9. Performing Organization Name and Address	10. Project/Task/Work Unit No.
Midwest Roadside Safety Facility (MwRSF) University of Nebraska-Lincoln 527 Nebraska Hall Lincoln, NE 68588-0529	11. Contract © or Grant (G) No. SPR-3(017)

12. Sponsoring Organization Name and Address	13. Type of Report and Period Covered
Midwest States' Regional Pooled Fund Program Nebraska Department of Roads 1500 Nebraska Highway 2 Lincoln, Nebraska 68502	Final Report 1998-2003
	14. Sponsoring Agency Code RPFP-99-01(a)

15. Supplementary Notes

Prepared in cooperation with U.S. Department of Transportation, Federal Highway Administration

16. Abstract (Limit: 200 words)

A steel post W-beam guardrail system was developed for installation in rock-soil foundations. The guardrail system was constructed with a 2.66-mm (12-gauge) thick W-beam rail, 53.34 m in length. The W-beam guardrail was supported by twenty-seven W152x13.4 by 1,346-mm long steel posts, spaced at 1,905 mm on center. The posts were installed in drilled holes in concrete, constructed by drilling three 203-mm diameter holes on 165-mm centers to a depth of 610 mm. The drilled holes were backfilled with compacted ASTM C33 coarse aggregate, size no. 57.

One full-scale vehicle crash test, using a ¾-ton pickup truck, was performed on the W-beam guardrail system. The test was conducted and reported in accordance with the requirements specified in the National Cooperative Highway Research Program (NCHRP) Report No. 350, *Recommended Procedures for the Safety Performance Evaluation of Highway Features*. The safety performance of the W-beam guardrail system with post placed in rock was determined to be acceptable according to the Test Level 3 (TL-3) evaluation criteria specified in NCHRP Report No. 350.

Further, guardrail post placement recommendations were also developed for situations where rock is located below the surface. These recommendations were developed through an analysis of bogie testing of posts.

17. Document Analysis/Descriptors	18. Availability Statement
Highway Safety, Guardrail, Longitudinal Barrier, Post Testing, Posts in Rock, Roadside Appurtenances, Crash Test, Compliance Test	No restrictions. Document available from: National Technical Information Services, Springfield, Virginia 22161

19. Security Class (this report)	20. Security Class (this page)	21. No. of Pages	22. Price
Unclassified	Unclassified	174	

DISCLAIMER STATEMENT

The contents of this report reflect the views of the authors who are responsible for the facts and accuracy of the data presented herein. The contents do not necessarily reflect the official views or policies of the University of Nebraska-Lincoln, the State Highway Departments participating in the Midwest States' Regional Pooled Fund Research Program, nor the Federal Highway Administration. This report does not constitute a standard, specification, or regulation.

ACKNOWLEDGEMENTS

The authors wish to acknowledge several sources that made a contribution to this project: the Midwest States' Regional Pooled Fund Program funded by the Connecticut Department of Transportation, Iowa Department of Transportation, Kansas Department of Transportation, Minnesota Department of Transportation, Missouri Department of Transportation, Montana Department of Transportation, Nebraska Department of Roads, Ohio Department of Transportation, South Dakota Department of Transportation, Texas Department of Transportation, and Wisconsin Department of Transportation for sponsoring this project and the MwRSF personnel for constructing the barrier and conducting the crash tests.

A special thanks is also given to the following individuals who made a contribution to the completion of this research project.

Midwest Roadside Safety Facility

R.W. Bielenberg, M.S.M.E., Research Associate Engineer
B.A. Coon, M.S.C.E., P.E., Graduate Research Assistant
K.L. Krenk, B.S.M.A., Shop Manager
A.T. Russell, Laboratory Mechanic II
M.L. Hanau, Laboratory Mechanic I
G.L. Schmutte, Laboratory Mechanic I
Undergraduate and Graduate Assistants

Connecticut Department of Transportation

Dionysia Oliveira, Transportation Engineer 3

Iowa Department of Transportation

David Little, P.E., Assistant District Engineer
Will Stein, P.E., Design Methods Engineer

Kansas Department of Transportation

Rod Lacy, P.E., Road Design Leader
Ron Seitz, P.E., Assistant Bureau Chief

Minnesota Department of Transportation

Ron Cassellius, former Research Program Coordinator
Andrew Halverson, P.E., former Assistant Design Standards Engineer
Jim Klessig, Implementation Liaison
Mohammad Dehdashti, P.E., Design Standards Engineer

Missouri Department of Transportation

Dan Smith, P.E., Research and Development Engineer

Montana Department of Transportation

Susan Sillick, Research Bureau Chief

Nebraska Department of Roads

Leona Kolbert, former Research Coordinator
Amy Starr, Research Engineer
Phil Tenhulzen, P.E., Design Standards Engineer

Ohio Department of Transportation

Monique Evans, P.E., Administrator
Dean Focke, Roadway Safety Engineer

South Dakota Department of Transportation

David Huft, Research Engineer
Bernie Clocksin, Lead Project Engineer

Texas Department of Transportation

Mark Bloschock, P.E., Supervising Design Engineer
Mark Marek, P.E., Design Engineer

Wisconsin Department of Transportation

Peter Amakobe, Standards Development Engineer
Beth Cannestra, P.E., Chief in Roadway Development

Federal Highway Administration

John Perry, P.E., Nebraska Division Office
Danny Briggs, Nebraska Division Office

Dunlap Photography

James Dunlap, President and Owner

TABLE OF CONTENTS

Page

List of Figures

Page

List of Tables

Page

1 INTRODUCTION

1.1 Problem Statement

In many states, the underlying bedrock can be quite close to the surface if not at the surface. This leads to problems in the installation of guardrail systems alongside roadways. Normally, guardrail posts are embedded 1,090 mm (43 in.) into *insitu* soil. However, if the bedrock is close to the surface, this standard practice for installing guardrail posts is not feasible. Currently, if bedrock is found within 1,090-mm (43-in.) of the ground surface, the Missouri Department of Transportation (MoDOT) specifies that the posts be placed in 915 mm (3 ft) diameter holes and backfilled with concrete. Not only does this placement procedure make guardrail installation more difficult and expensive, but it may also adversely affect the guardrail's ability to redirect vehicles during impact events. For the vehicle to be properly redirected without undue risk to the occupant, the guardrail must properly dissipate some of the kinetic energy. One mechanism that aids in the dissipation of this kinetic energy is by the rotation of posts in soil. Posts installed in rigid foundations are hampered in this respect, and as a result, leads to premature post failure without significant energy dissipation, thus resulting in increased strain in the guardrail and subsequently unacceptable performance.

1.2 Objective

The objective of this research was to develop guidelines for the placement of guardrail posts in rock and to evaluate the safety performance of a guardrail system using this post placement procedure through full-scale vehicle crash testing. The guardrail system was to be evaluated according to the Test Level 3 (TL-3) safety performance criteria found in the National Cooperative Highway Research Program (NCHRP) Report No. 350, *Recommended Procedures for the Safety Performance Evaluation of Highway Features* (1).

1.3 Scope

The research objective was achieved through both computer simulation and physical testing. First, a literature review was conducted on previous post testing as well as crash testing of guardrail systems installed in rigid foundations. Next, parameters for the placement of posts in rock were determined. This included the selection of critical conditions for post installation, post type, hole size and geometry, and soil backfill material. Initial computer simulation modeling was then used to determine optimum post/soil properties. Bogie testing of posts, placed in drilled holes using different backfill materials, was then conducted in an effort to determine which backfill material would best fulfill the requirements identified by computer simulation. Once the critical post placement design was finalized, additional computer simulation runs were conducted in order to determine the critical impact point for this new guardrail system. A full-scale vehicle crash test was then performed using a ¾-ton pickup truck, weighing approximately 2,000 kg (4,409 lbs), at a target impact speed of 100.0 km/hr (62.1 mph) and at a target impact angle 25 degrees. The results from testing were then analyzed and evaluated. Further analysis of the post placement methods was conducted for cases where the rock was at varying depths below the surface. Finally, conclusions and recommendations were made as to the safety performance of the post-in-rock guardrail system.

2 LITERATURE REVIEW

W-beam guardrail, and in particular guardrail posts and the material they are embedded in, has been the subject of a significant amount of study over the past 40 years. In 1961, researchers at General Motors studied guardrail systems to determine their safety performance (2). The existing guardrail on their test track was found to perform poorly, providing virtually no protection to vehicles impacting it, even at speeds as low as 56 km/hr (35 mph). Through full-scale vehicle crash testing of barriers and static testing of posts of different types, new improved barrier designs were developed. During the post testing phase, 254-mm x 254-mm (10-in. x 10-in.) square and 152-mm (6-in.) diameter circular reinforced concrete, 152-mm x 203-mm (6-in. x 8-in.) timber, and W152x12.7 (W6x8.5) steel posts were statically tested in soil using the following guidelines:

1. Posts should yield under impact to reduce lateral accelerations on the vehicle.
2. Posts should not bend nor yield above the ground surface since this would tend to pull the guardrail down.
3. Posts should provide longitudinal strength to prevent pocketing.

It was found that the reinforced concrete posts did not perform satisfactorily due to being more rigid and failing sooner than steel and timber posts.

In 1967, the New York State Department of Public Works (3) completed six years of research on standard barrier designs for roadsides, medians, and bridges to check that their performance was satisfactory. This research led to the development of new guardrail designs, many of which are considered standard guardrail designs today. For W-beam guardrail, it was determined that:

1. The minimum post spacing should be 1,905 mm (75 in.).

2. Addition of blockouts between the posts and rail would decrease wheel snag.

3. Anchoring of end posts would prevent rail tension from pulling posts over in the longitudinal direction.

The researchers also found post strength to be a very important factor for the proper functioning of a barrier. They also determined that for a barrier impacted by a vehicle with an initial velocity of 96.6 km/hr (60 mph) and an impact angle of 25 degrees, the posts would be subjected to a maximum lateral velocity of 32.2 km/hr (20 mph).

In 1970, the Southwest Research Institute (4) tested posts in soil to study the post-soil interaction under both static and dynamic conditions. Seventy-two tests were conducted in two types of soils, with posts embedded at four different embedment depths and with three different post widths. The dynamic peak and average resistive loads as well as the absorbed energy were found to be directly related to embedment depth and post width, as well as to the shear strength of non-cohesive soils. Dynamic loads and absorbed energies were also found to be higher than that observed under static loading conditions.

In 1978, Calcote and Kimball (5) of the Southwest Research Institute, conducted pendulum tests of posts to determine parameters for input into the computer program BARRIER VII. Both W152x12.7 (W6x8.5) steel and 152-mm x 203-mm (6-in. x 8-in.) timber posts were tested dynamically in four different soils (i.e., sandy loam, saturated clay, stiff clay, and base material) as well as concrete. It was found that guardrail systems using posts with shallow embedment or embedment in weak soils would not be able to effectively redirect vehicles after impact. Through the use of BARRIER VII computer simulation, it was determined that guardrail in test installations should have a minimum length of 45.7 m (150 ft), and that the anchor posts should be embedded in concrete so that the full strength of the posts could be developed.

In 1983, Jeyapalan, et al., (6) of the Texas Transportation Institute (TTI) conducted post tests for the Texas State Department of Highways and Public Transportation (TSDHPT). At the time, TSDHPT required that if W152x12.7 (W6x8.5) steel posts were used, then they needed to be placed in concrete footings. As a result, this made use of steel posts much more expensive than 178-mm (7-in.) diameter circular wooden posts. Through both static and dynamic testing of posts in cohesive and cohesionless soils, it was determined that steel posts without concrete footings would produce the same level of peak forces and energy absorption during a dynamic impact as that observed for wooden posts.

In 1984, Eggers, et al., (7) of TTI also conducted research for TSDHPT. At the time, when rock was encountered, 178-mm (7-in.) diameter timber posts were placed in 305-mm (12-in.) diameter holes, 457 mm (18 in.) deep and backfilled with soil or concrete as specified by the engineer. If concrete was required for backfill, then the guardrail system would become more expensive. As a result, it was necessary to determine if the soil backfill would develop the required strength for the post to perform satisfactorily. Post were placed in the center of the holes and statically loaded until post failure. Three types of soils (i.e.-sand, decayed limestone, and clay) were used for backfill as well as concrete. Peak loads and absorbed energies, both functions of a combination of backfill and post properties, were compared. It was found that the posts failed at a higher load and dissipated more energy when embedded in soil. As a result, it was determined that the use of soil for backfill was adequate for the design.

In 1986, Eggers and Hirsch (8) conducted static testing of posts to determine force-deflection characteristics of posts as a function of post type, soil type, and embedment depth. Both W152x12.7 (W6x8.5) steel and 178-mm (7-in.) diameter circular wooden posts were tested in cohesive and cohesionless soils at embedment depths of 457, 610, 762 and 965 mm (18, 24,

30, and 38 in.). They found that for a corresponding soil type and embedment depth, steel posts had slightly lower peak loads and less energy absorption than timber posts. Cohesive soils were found to dissipate more energy at shallow embedment depths, and non-cohesive soils dissipated more energy at deeper embedment depths. It was also found that decreasing the post embedment depth significantly reduced the energy absorbed from a post rotating in the soil.

In 1992, Bartlett and Kutter (9) conducted 1/8-scale vehicle crash tests on a W-beam guardrail system configured with timber posts near slopes. The intent of the research was to determine how close posts could be placed to the slope break point while conducting all testing inside a laboratory. Although the study found that modeling full-scale vehicle crash tests might have merit, a more accurate modeling of the system was needed. They did not find a simple answer to what was the optimum distance to the break point. However, one important observation was made during testing. The researchers determined that the guardrail system performed better when the soil failed instead of the post. They theorized that there was an optimum soil resistance that would mobilize the strength of the post without fracturing it. They also found that the dynamic soil resistance was greater than the static soil resistance by approximately a factor of seven.

In 1999, Safety by Design, Inc. (SDI) found through crash testing that a W-beam guardrail system with posts installed in rigid foundations would not satisfy the NCHRP Report No. 350 requirements. Test RP-1, a TL-3 full-scale vehicle crash test was conducted on a W-beam guardrail system with steel posts embedded in 203-mm (8-in.) diameter rigid holes. The test failed as the guardrail ruptured at post no. 15, the location of a rail splice. Post nos. 14 through 18 were severely twisted and bent to the ground. Sequential photographs of the test are shown in Figure 1, and damage to the guardrail system is shown in Figure 2.

In 1999, Coon conducted dynamic tests on steel posts to find parameters for use in computer simulation (10). Testing consisted of impacting posts where the failure mode of the soil was isolated. This involved restraining the post either in the front or the back in order to force soil failure to occur either in compression or shear, as shown in Figures 3 and 4, respectively. Results from testing were used in computer simulation to simulate the post and soil failure.

Figure 1. Full-Scale Vehicle Crash Test Sequentials

Figure 2. W-beam Guardrail System Damage, Test RP-1

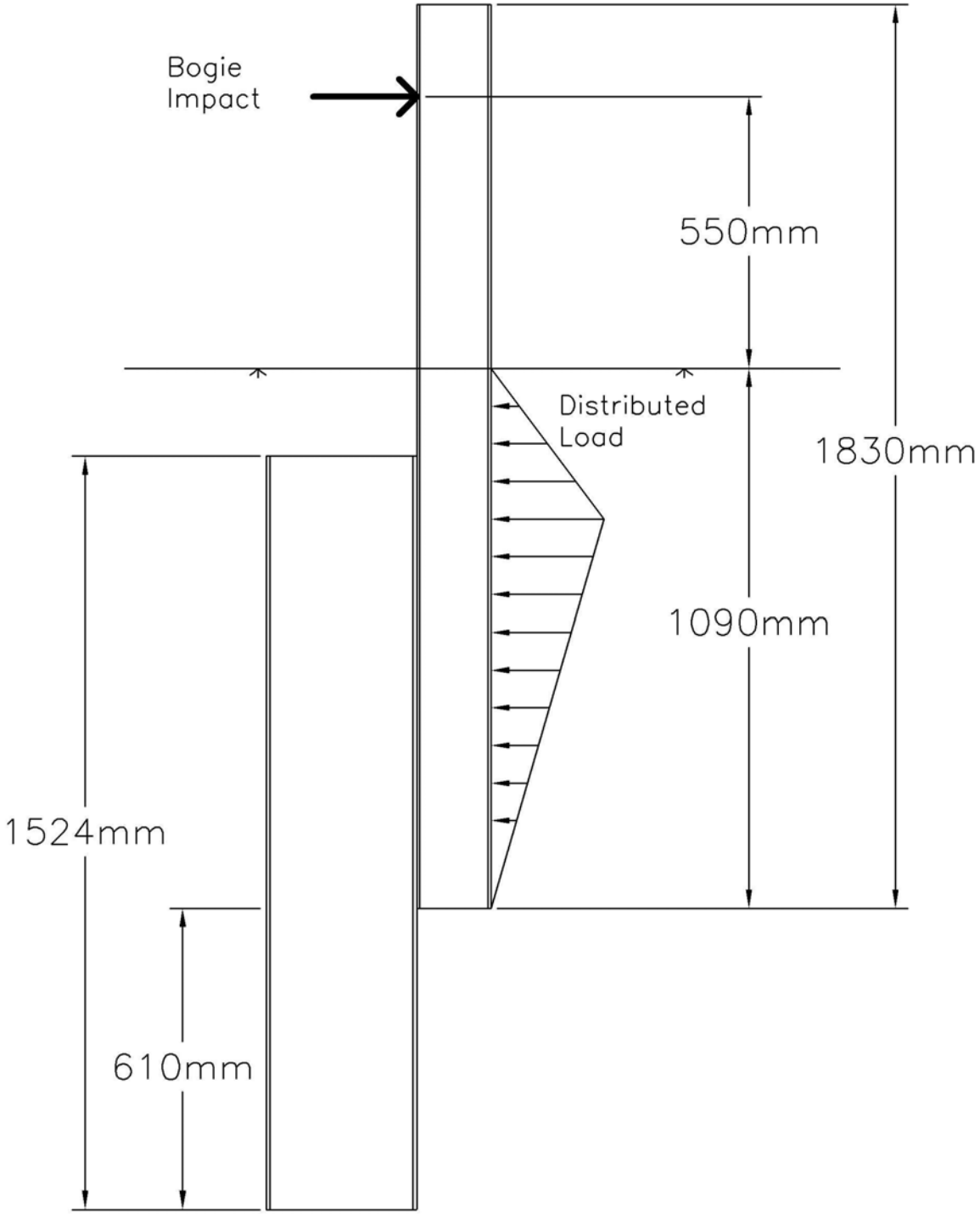

Figure 3. Side View of Post Constrained to Compressive Failure

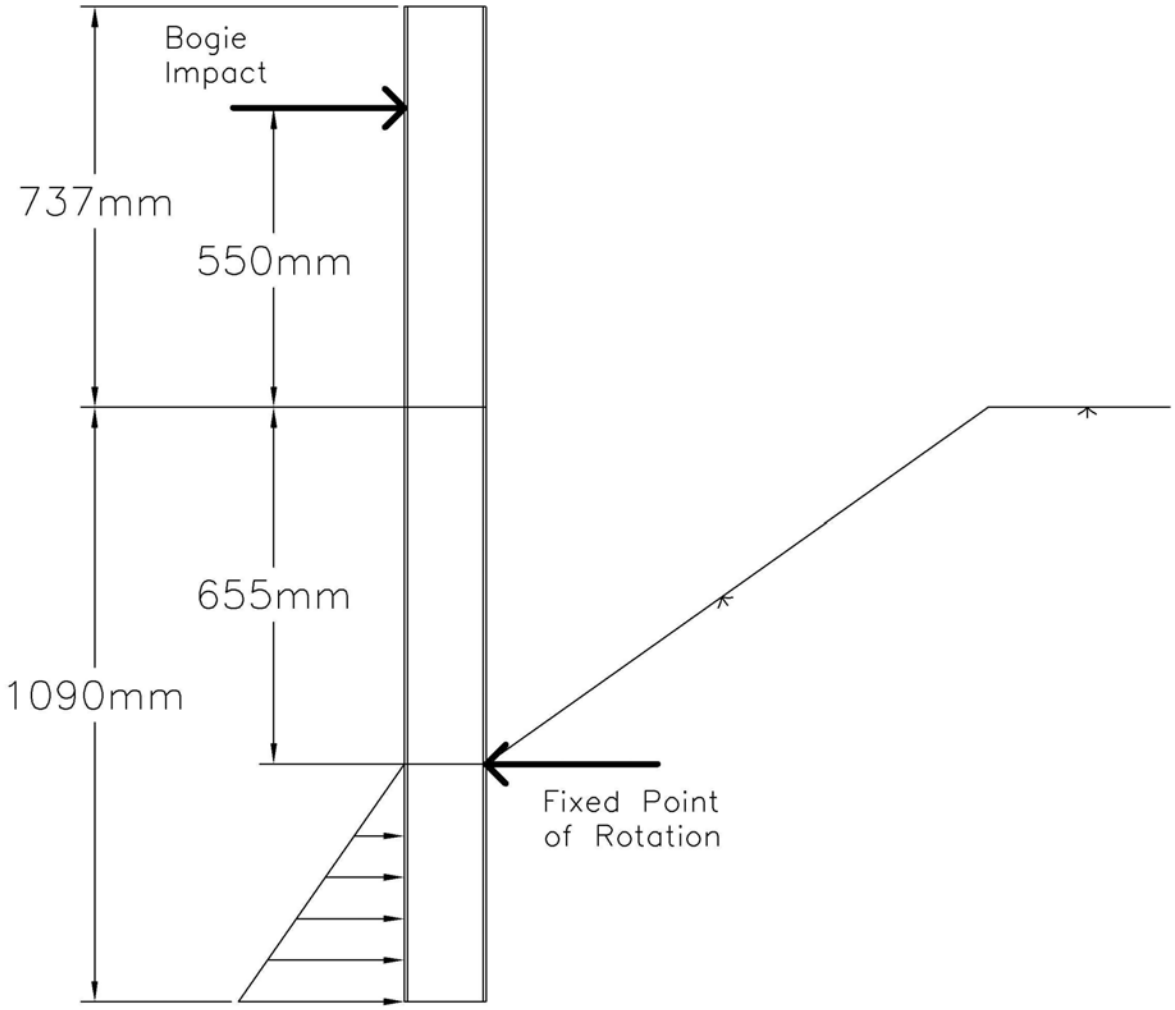

Figure 4. Side View of Post Constrained to Shear Failure

3 SYSTEM DEVELOPMENT

3.1 Introduction

Whenever there is bedrock within 1,090 mm (43 in.) of the surface, a special installation procedure for guardrail posts is warranted. Due to the lack of prior research pertaining to posts installed in rock, some initial assumptions had to be made. First, it was evident that the guardrail posts must be able to rotate in the soil and dissipate energy in order for W-beam guardrail systems to work properly. Posts installed in rigid foundations cannot fulfill these objectives, as observed in a prior crash tests conducted by SDI.

After considering a number of options, it was decided that the guardrail posts would be installed in holes drilled into the rock. The concept involved using oversized holes which gave the posts adequate distance to rotate laterally. The drilled holes would be backfilled with the proper material to adequately support the posts in the drilled holes as well as to allow for sufficient energy to be dissipated by the rotation of the posts through the backfill material.

Hole geometry, backfill material, and post type would have to be optimized in order to identify the most economical design that would provide sufficient energy dissipation at the posts to correct the problems identified in the SDI testing. As mentioned previously, rock is often found at varying depths and with varying thicknesses of overlying soil, thus resulting in the necessity for multiple post placement alternatives as the depth of soil above the rock changes. Verification of multiple post placement designs, through the use of full-scale vehicle crash testing, would be cost prohibitive. Therefore, only one post placement design would be developed for the critical condition and then verified with a full-scale vehicle crash test. Once the post placement design for the critical condition was verified, it could be correlated with

previous post testing results (10), and additional designs for rock located at varying depths could then be configured.

3.2 Determination of Critical Post Placement Condition

The critical post placement condition is a function of three general requirements for placement of guardrail posts in rock-soil foundations. These three requirements, necessary for proper performance of guardrail posts in rock-soil foundations, are as follows:

1. The posts must be allowed to rotate some minimum distance in order to provide acceptable energy dissipation.
2. The post placement design must consider the propensity for the vehicle's wheels to snag on the posts during an impact with the guardrail system.
3. The post placement design must be as economical as possible.

The depth between the soil surface and top of the bedrock is the most influential factor affecting these three requirements, and as a result, the critical post placement condition.

For rock located at the surface, the drilled hole geometry must be maximized in order to provide adequate distance for post rotation. This condition must also maximize the depth of the hole drilled into rock. These requirements, as a result, will incur the highest costs for placement of guardrail posts in rock-soil foundations.

For situations where shallow bedrock is encountered, a shorter length guardrail post (i.e., reduced embedment) could still be capable of providing an acceptable level of resistance during post rotation. This is possible since the backfill material is confined by the drilled hole, resulting in stiffer material qualities and greater resistance to post rotation. With reduced embedment depth, however, there exists a potential for increased wheel snag on the exposed portion of the posts below the W-beam rail element. For shorter posts, the point at which a post rotates in soil is closer to the soil surface. This causes the exposed portion of the post located in front of and

below the rail to be increased, resulting in increased potential for wheel snag. For rock located at the surface, the length of the post will be minimized while the potential for wheel snag will be maximized.

Therefore, it can be concluded that the critical post placement condition exists when rock is found at the surface. The critical post placement design will be dependent on the post type, drilled hole geometry, and backfill material which allows for proper performance of the W-beam guardrail system with respect to NCHRP Report No. 350 standards.

3.3 Post Type

Two post types, W152x13.4 (W6x9) steel posts and 152-mm x 203-mm (6-in. x 8-in.) timber posts, are commonly used in standard, strong-post W-beam guardrail systems found throughout the United States. Therefore, W-beam guardrail designs utilizing both post alternatives would likely be anticipated for situations where rock is found directly below grade. However, due to differences in size and material properties between the two post types, one post type may be more feasible for use in a drilled hole rock-soil foundation. Both steel and timber posts have advantages and disadvantages in this regard.

Timber posts tend to have a high ultimate load before failure compared to steel posts. However, when timber posts fail they tend to fracture abruptly, causing any load the post may be carrying to be quickly transferred to the guardrail, which could then result in rupture of the W-beam rail element. A timber post's cross-section is larger than that of a steel post. The width and depth of a wooden post are both 51 mm (2 in.) greater than that for a steel post. As a result, construction costs would be greater due to the increased size of the drilled hole necessary to allow the timber post to rotate.

When steel posts fail, they fail plastically, allowing for a somewhat more gradual transfer

of load from the post to the guardrail. However, since steel posts fail plastically and do not fracture, the vehicle's wheel may be more prone to snag on the exposed steel posts located below and in front of the W-beam rail. Past research has shown that excessive wheel snag on posts in strong-post W-beam guardrail systems has resulted in vehicle rollover. Also, when a steel posts fails, if it does not disengage from the guardrail, it could pull the guardrail down with it, leading to an increased risk for the impacting vehicle to climb, vault, or penetrate the steel-post W-beam barrier system.

While both post types have advantages and disadvantages for use in drilled hole rock-soil foundations, it is believed that construction costs should control the selection of post type. The increased costs of placing a W-beam guardrail system in rock would make any reduction in construction costs highly desirable. As a result, the W152x13.4 (W6x9) steel post option was selected for design and later evaluated by a full-scale vehicle crash test.

3.4 Drilled Hole Geometry

Cost and practical considerations for construction make smaller drilled holes in rock more advantageous. The smallest hole that would allow a W152x13.4 (W6x9) post to be installed in rock was a 203-mm (8-in.) diameter hole. However, as noted in previous testing by SDI, a single 203-mm (8-in.) diameter drilled hole was found to be too small. It should also be noted that during a vehicular impact with a guardrail system, the posts tend to rotate more laterally than longitudinally. As a result, an elongated drilled hole, that was larger in length versus width, would allow the post to rotate sufficiently.

Therefore, an elongated drilled hole was created by overlapping multiple 203-mm (8-in.) diameter drilled holes. This configuration provided an elongated hole with a width of 203 mm (8 in.), thus allowing a steel post roughly 51 mm (2 in.) of space on each side to move

longitudinally at the ground line. The required length of the elongated drilled hole must be sufficient in order to allow the post to rotate backward without contacting the back of the drilled hole until it has disengaged from the rail. Prior testing has shown that posts disengage from the center of the rail after a post has deflected between 380 mm (15 in.) and 640 mm (25 in.), even though the post may rotate much farther. Allowable post deflection at the ground surface is dependent on this disconnection distance as well as the point about which the post rotates below grade.

The rotation point of the post is dependent on two factors – post embedment depth and the location of the post within the drilled hole. If the post is placed near the front of the drilled hole, it will rotate around the base of the post, compressing the backfill material behind it. If the post is placed at the rear of the drilled hole, then the rotation point of the post will be located at the top of the drilled hole, causing the soil to shear as the base of the post rotates forward and upward. To reduce the risk of wheel snag, the rotation point of the post should be as deep as possible. This requirement would, as a result, call for the post to be placed near the front of the drilled hole.

Previous embedment depths for posts installed in rock (7) were specified at 460 mm (18 in.). However, for shorter embedment depths, if the post is allowed to rotate greater distances, the potential for the post being pulled out of the drilled hole will increase. As a result, it was determined that embedment depths of 460 mm (18 in.) and 610 mm (24 in.) would both be analyzed. The post embedment depth requirement would be found through bogie testing of posts embedded at both the 460 and 610-mm (18 and 24-in.) depths.

Since the final post embedment depth remained unknown at this stage, calculation of the required length of the drilled hole could not be determined. However, a maximum required

length could be calculated using a maximum post deflection of 640 mm (25 in.) at the rail midpoint, when the post releases from the guardrail, and a maximum embedment depth of 610 mm (24 in.). Assuming the post rotated around its bottom front edge, it was determined that the post must be allowed to deflect laterally a distance of 355 mm (14 in.) at the ground line before contacting the back of the drilled hole.

A drilled hole satisfying the above requirements could be constructed using two different methods, as shown in Figure 5. For option 1, three 203-mm (8-in.) diameter holes could be drilled adjacent to one another, overlapping on 165-mm (6.5-in.) centers. Subsequently, the sides of the drilled hole could be made smooth in order give a uniform width to the elongated drilled hole. However, under actual field conditions, if drilling holes that overlap proved undesirable, then option 2 could be implemented, where two holes would be drilled on 330-mm (13-in.) centers and the material contained between the holes chiseled out. Both options would result in an elongated drilled hole length of 530 mm (21 in.) at its centerline.

3.5 Backfill Material

The last required component for the post in rock system was the selection of the backfill material for use in the drilled hole. This selected material should fulfill two requirements. First, the material must be readily available to the State DOT's. Second, the material must possess properties that allow the post to rotate instead of yielding prematurely, be stiff enough to adequately support the post, and dissipate as much kinetic energy as possible. Computer simulation was used to aid in the determination of the optimum properties for the post force-deflection curve. This optimum force-deflection curve was then compared to force-deflection curves found from bogie testing of posts placed in different backfill materials, consisting of aggregates with common particle-size distributions. Following a comparison of the results, the

proper backfill material was chosen. The proposed final configuration of the post, blockout, drilled hole, backfill material, and guardrail for the critical post placement condition is shown in Figure 6.

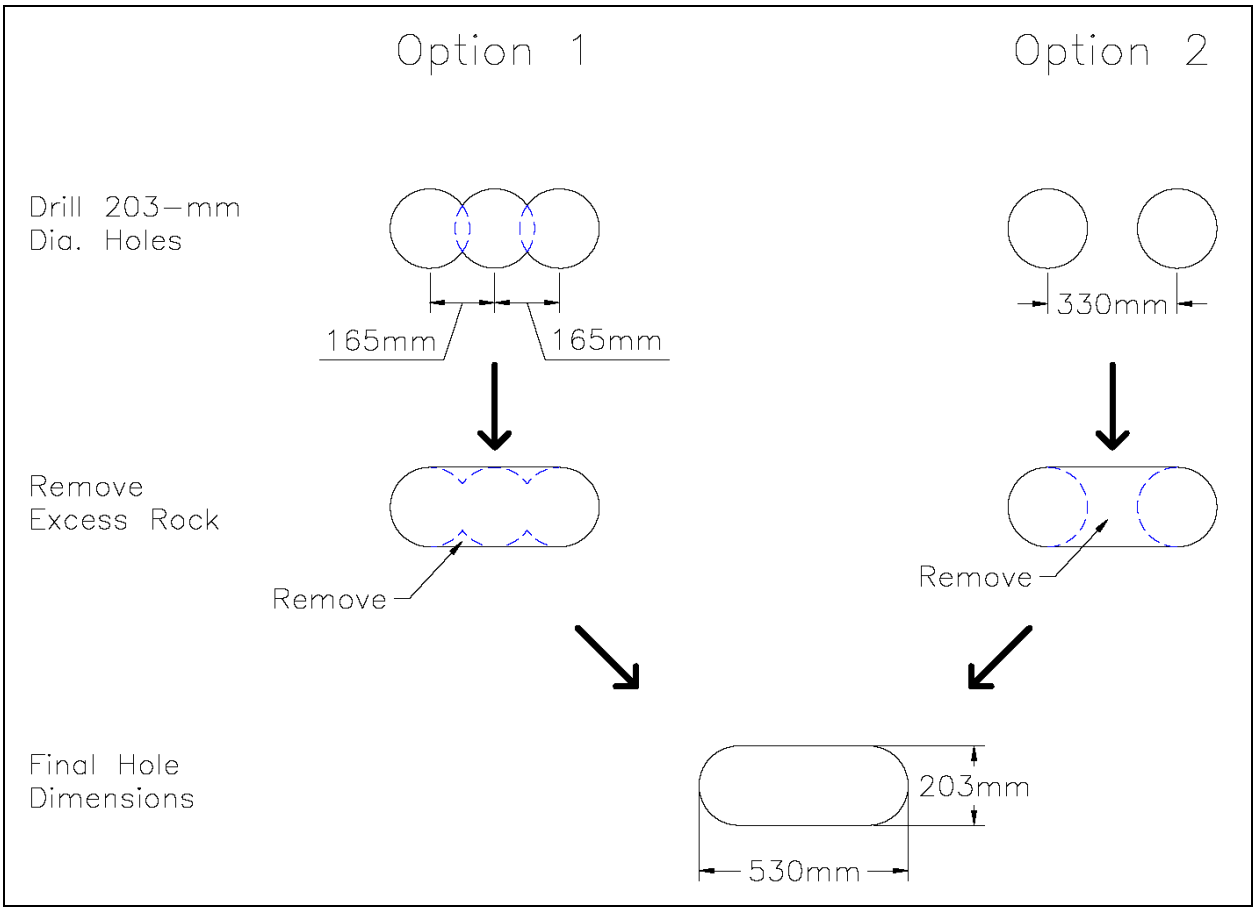

Figure 5. Drilled Hole Construction Details

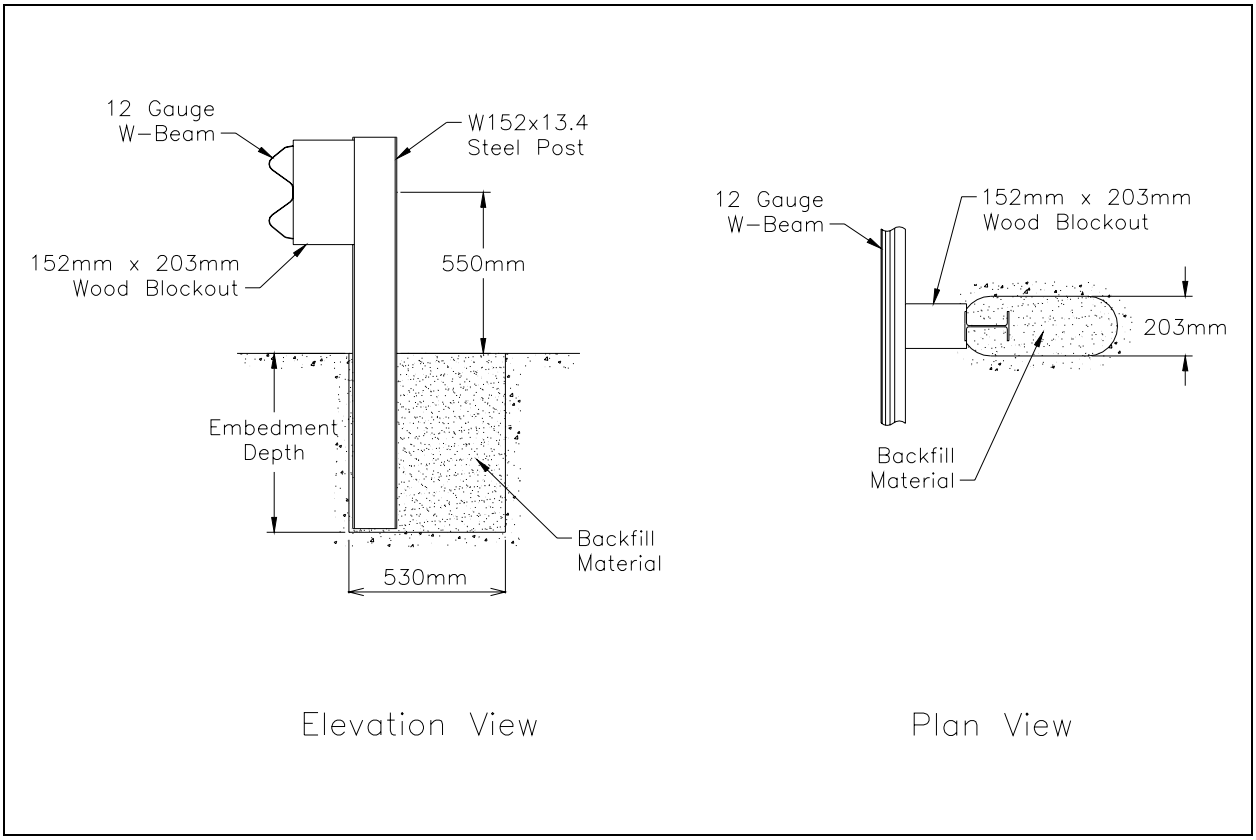

Figure 6. Post Installed in Critical Drilled Hole Configuration

4 INITIAL SIMULATION

4.1 Background

BARRIER VII, a 2-D, implicit, non-linear, finite element, computer program (11), was used to simulate vehicular impacts with a W-beam guardrail system. The W-beam guardrail section was modeled using beam elements. The vehicle was modeled as a lumped, rigid mass that is surrounded by non-linear springs. These springs simulated the crush characteristics of the vehicle shell, and the nodes at the end of the springs allowed contact to occur with the rail elements.

The post and soil response was modeled as two nodes that stayed connected in a straight line, as shown in Figure 7. Node 1 was located at the midpoint of the barrier member, whereas, node 2 was located at the ground surface and remained fixed in its position. The distance between node 1 and the base of the post was 550 mm (21.65 in.). Any forces that were applied to node 1 from barrier members were resisted by a moment located at base of the post (i.e., ground line). The resisting moment was a function of a resisting force applied at node 1 multiplied by the distance between the node 1 and the base. The resisting force was defined by a non-linear curve compromising of an elastic stiffness, yield force, and failure deflection, as shown in Figure 7. There were two functions for defining the failure criteria of the post. First, a failure deflection limit could be defined for node 1. Second, post failure could be defined as a maximum shear force at the base of the post. When the deflection or shear force at a post exceeds their associated limits, the post begins to fail and does so over 10 time steps. This staged failure prevents instabilities from occurring in the simulation. For this analysis, post failure was defined to occur by exceeding a failure deflection limit at node 1. Post parameters were defined for both the longitudinal (A) and lateral (B) axes of the post with respect to the

barrier system. The interaction of the forces between the principal axes was ignored to simplify the computational procedure.

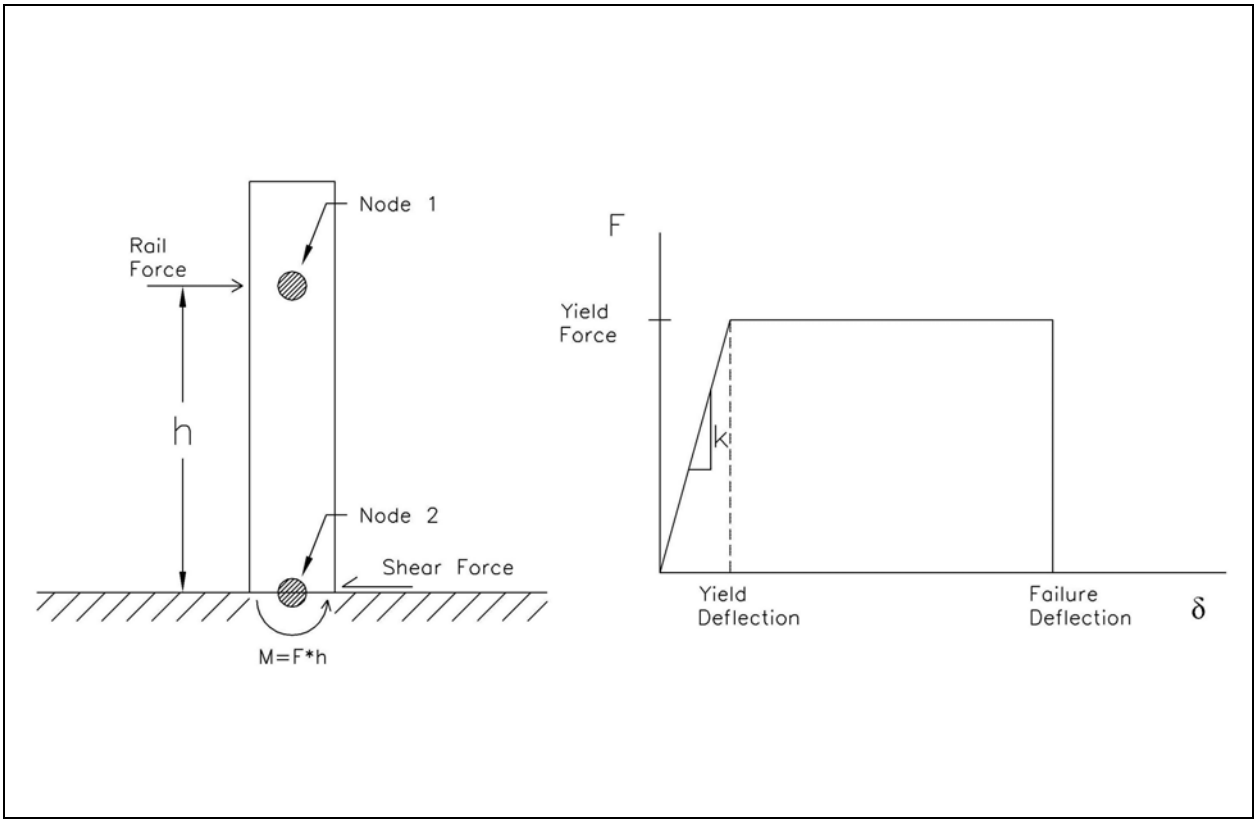

Figure 7. Conceptualization of Post Member in BARRIER VII

4.2 Application of Barrier VII

BARRIER VII was used to determine the optimum properties for the backfill material. The methodology was to model vehicular impacts into a 53.3-m (175-ft) long W-beam guardrail system supported by posts spaced on 1,905 mm (75 in.) centers. All simulations were performed with the guardrail system being impacted at post no. 13 by a vehicle with an impact speed of 100.0 km/hr (62.1 mph) and at an impact angle of 25 degrees. Details of the guardrail and

vehicle finite element model are provided in Appendix A. Parameters for the rail elements were those specified as standard properties for 12-gauge W-beam guardrail. Vehicle parameters were defined as those for a 2,000-kg (4409-lb) pickup truck. The end posts were modeled as strong anchor posts. The second post on each end of the guardrail system was modeled as a BCT post.

For all other posts in the system, material properties were set to be identical to one another. For the longitudinal rail axis or A-axis, the post was modeled as a steel post placed in a rigid foundation since the drilled hole configuration does not allow adequate clear space for the post to deflect parallel to the rail at the ground line. Weak-axis bending properties for a W152x13.4 (W6x9) steel post were used with a dynamic magnification factor of 1.5. For the axis perpendicular to the rail or B-axis, the posts were modeled as posts embedded in standard soil as specified by NCHRP Report No. 350 and meeting the AASHTO M147-65 Grading B (1990) requirements. Input parameters for the steel posts rotating about the strong axis of bending were a function of the post-soil behavior. The deflection limit at which the post failed along the B-axis was set sufficiently high so that the posts would not fail. The effective weight for the post was defined to be effectively near zero even though this parameter allows for consideration of the inertial effects of the post on the guardrail system. Instead, it was decided that the inertial effects would be considered in the dynamic force-deflection curve defined for the post. This approach was used to improve correlation between simulation and bogie testing results, since post inertial effects were incorporated in force-deflection curves obtained from testing. Maximum shear force limits were also defined for the posts but were set sufficiently high so that the shear limit would not be the controlling failure mechanism. It was assumed that the soil would fail versus the post, and as a result, the failure deflection limit was more applicable to this analysis. Values used for the rail elements, vehicle model, and posts are

defined in Table 1. An example of a standard BARRIER VII input deck is shown in Appendix B.

A number of computer simulations were completed while maintaining constant input parameters for the guardrail system except for the interior posts. The yield force defined for the posts along the B-axis was varied across a range of values. From the simulation results, as shown in Figure 8, a graphical representation was determined for the relationship between the post-soil yield force and the maximum dynamic post deflection for post nos. 14 through 16 along the B-axis. It was determined through geometry that the post could deflect roughly 600 mm (23.6 in.) at the rail midpoint height before it would contact the back of the drilled hole, as shown in Figure 9. This limitation was correlated with Figure 8, and it was determined that the post-soil response must provide a minimum yield force of 36 kN (8.1 kips) in order to keep dynamic post deflections under 600 mm (23.6 in.).

At this point, it was necessary to develop a procedure for correlating the minimum required yield force for the post response from dynamic bogie impact testing of guardrail posts. Post-soil force-deflection plots obtained from bogie testing are not composed of straight lines like those used in BARRIER VII, as shown in Figure 10. As a result, a method was developed to compare force-deflection curves between computer simulation and bogie test data. In this case, the total energy from the force-deflection curves in BARRIER VII would be compared to the total energy from force-deflection curves found through physical testing. To determine the minimum amount of energy that the rotating post needed to dissipate, a plot of the relationship between yield force and total energy, for post nos. 14 through 16 in BARRIER VII, was created, as shown in Figure 11. The total energy calculated for each post was determined by calculating the area under the force-deflection curve, with the failure deflection defined as the maximum

dynamic deflection of the post. If the post must have a minimum yield force of 36 kN (8.1 kips) to prevent the post from impacting the back of the drilled hole, then according to Figure 11, the rotating post must dissipate at least 21 kJ (186 k-in.) of energy. At this point, it was then possible to evaluate data from bogie tests of posts in drilled holes with different backfill materials and embedment depths. The energy absorbed by the post rotating in the optimum backfill material must dissipate a minimum of 21 kJ (186 k-in.) of energy before the post strikes the back of the drilled hole.

Table 1. BARRIER VII Parameters

Post Properties			
Parameter	**Anchor Post**	**2nd BCT Post**	**Standard Post**
Height of Node 2 (in.)	21.65	21.65	21.65
Stiffness along A-axis, k_A (k/in.)	4	3	30
Stiffness along B-axis, k_B (k/in.)	4	3	4
Effective Weight (lbs)	100	100	0.001
Yield Moment about B-axis (k-in.)	250	100	93.3
Yield Moment about A-axis (k-in.)	250	150	Varied
Yield Accuracy Limit	0.01	0.01	0.01
Shear Failure Limit along A-axis (kips)	100	50	5
Shear Failure Limit along B-axis (kips)	100	50	45
Deflection Failure Limit along A-axis (in.)	10	6	6
Deflection Failure Limit along B-axis (in.)	10	6	100
Beam Properties			
Parameter	**Value**		
Second Moment of Area, I ($in.^4$)	2.29		
Cross-Sectional Area, A ($in.^2$)	1.99		
Beam Length, L (in.)	Varied		
Young's Modulus, E (ksi)	30000		
Unit Weight (lb/ft)	6.92		
Yield Force, F_y (k)	99.5		
Yield Moment, M_y (k-in.)	68.5		
Yield Accuracy Limit	0.1		
Vehicle Properties			
Parameter	**Value**		
Automobile Weight (lbs)	4400		
Moment of Inertia About Vertical Axis (lb-in.-s^2)	40000		
# of Possible Contact Points	20		
# of Different Vehicle Springs Assigned to Contact Points	6		
# of Wheels	4		
Brake Code (1=on, 0=off)	0		
# of points for trajectory output	1		

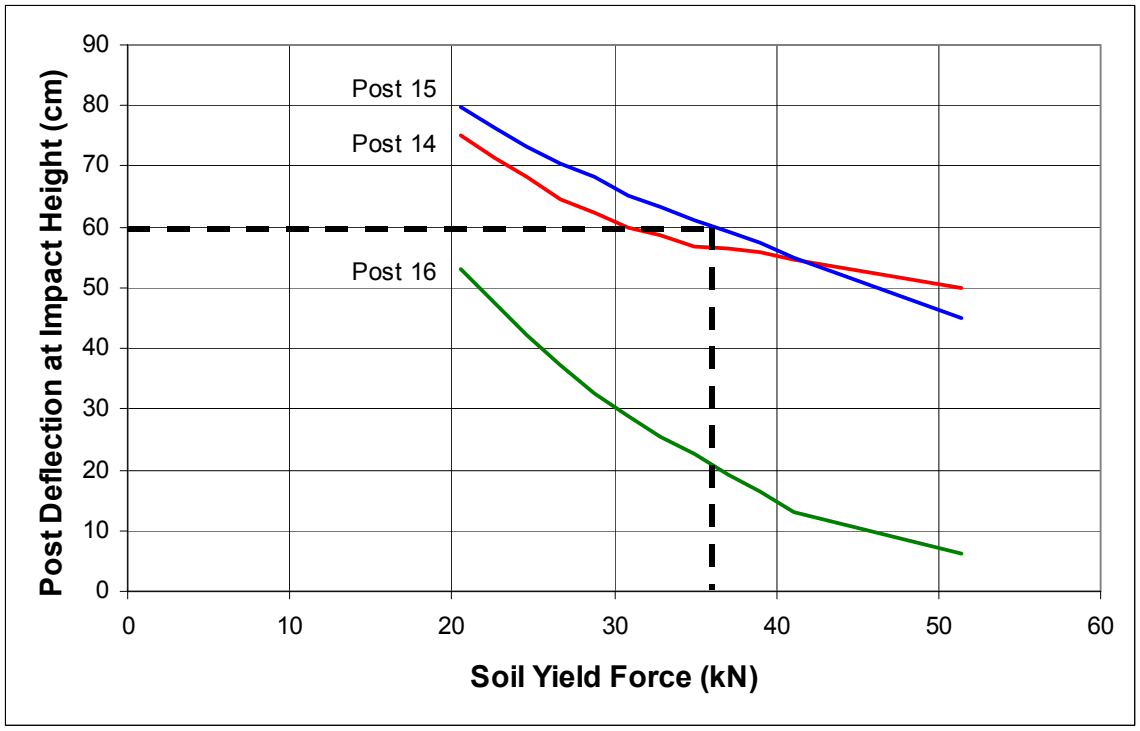

Figure 8. Post Deflection versus Yield Force

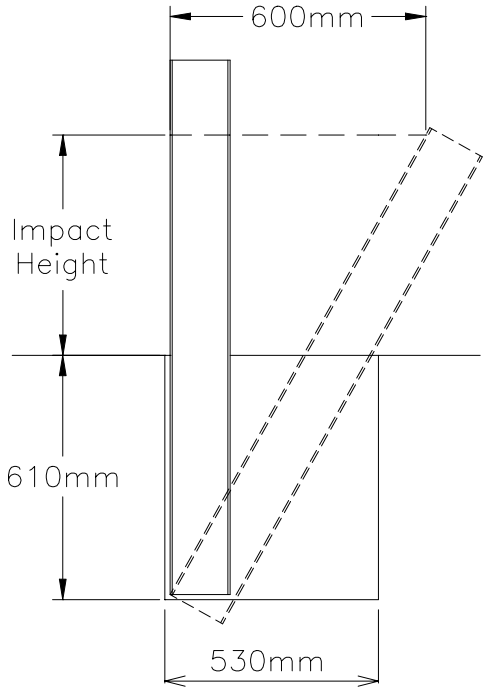

Figure 9. Determination of Allowable Deflection for Post

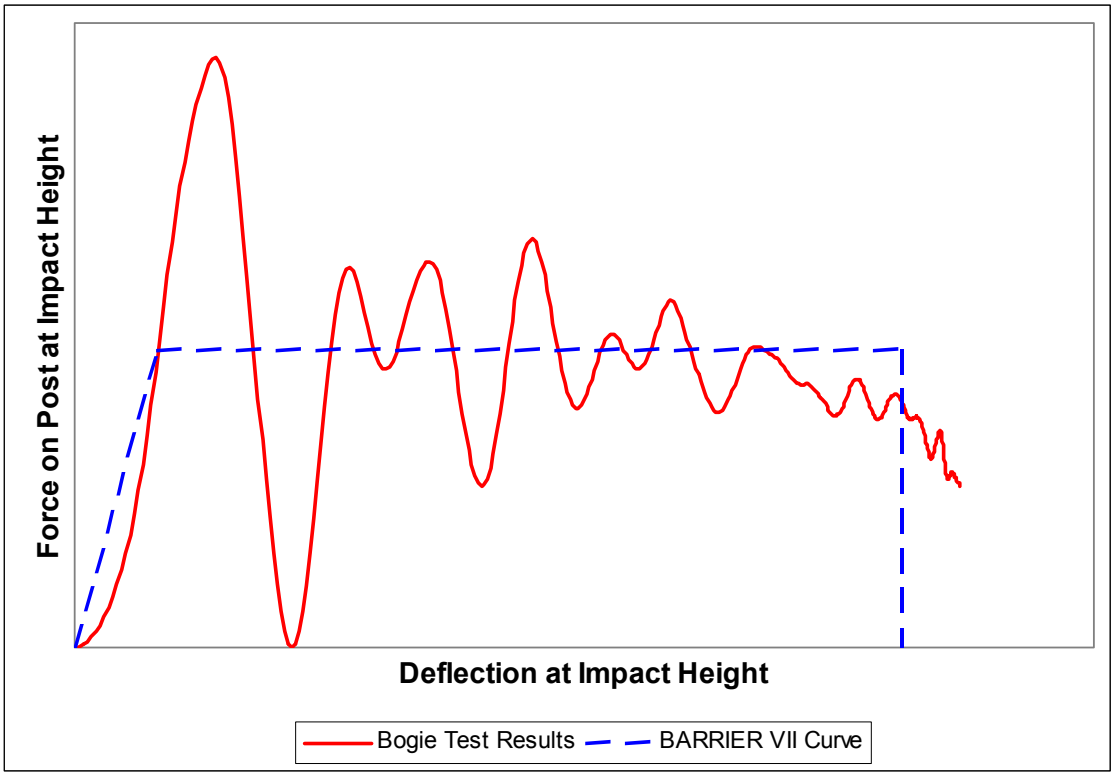

Figure 10. Correlation between Simplified BARRER VII Curve and Bogie Test Results

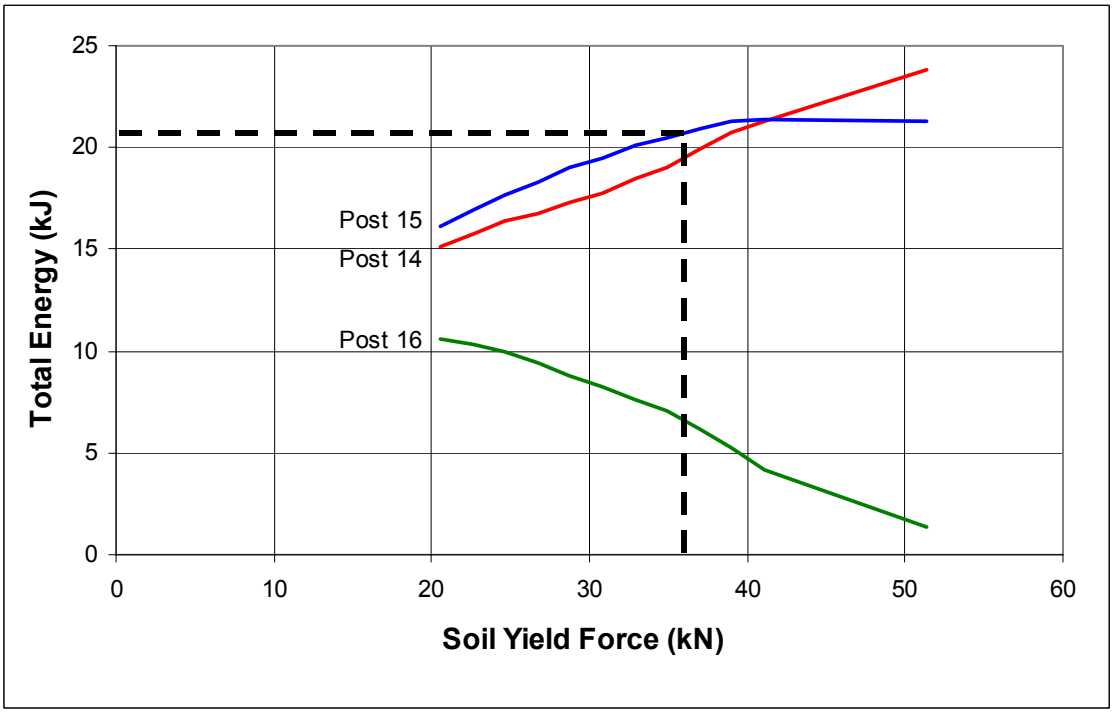

Figure 11. Total Absorbed Energy versus Yield Force

5 COMPONENT TESTING – BOGIE TESTING OF POSTS

5.1 Test Matrix

Dynamic bogie testing was conducted on posts placed in drilled holes in order to determine what type of backfill material was required to fulfill the requirements found from BARRIER VII simulation. Five tests were conducted on posts installed in the configuration shown in Figure 6. For the remaining test, test no. MPR-8, the post installed in a drilled hole was impacted by the bogie at a 10-degree angle. Analysis of previous full-scale vehicle crash tests with strong-post W-beam guardrail has shown that posts impacted by the vehicle tend to deflect approximately 10 degrees downstream instead of perpendicular to the guardrail system. Such post trajectory can cause the post to snag on the side of the drilled hole. As a result, this test was conducted in order to analyze the behavior of the post as it contacted the side of the drilled hole. Photographs of the test setup for test MPR-8 are shown in Figure 12.

The posts in all six tests were impacted at a target speed of 24.1 km/hr (15 mph) with a 964-kg (2,215-lb) bogie vehicle. It should be noted that 32.2 km/hr (20 mph) is normally considered to be the peak lateral velocity of the initial posts impacted by the vehicle. However, the average impact velocity for the posts that come into direct contact with the test vehicle is closer to 24.1 km/hr (15 mph). For all six tests, the bogie's head impacted the posts at a location of 550 mm (21.65 in.) above the ground line. Two types of steel posts and two types of backfill material were tested. Standard W152x13.4 (W6x9) guardrail posts and the stronger W152x23.8 (W6x16) posts were subjected to bogie testing. In addition, the W152x23.8 (W6x16) posts were instrumented with strain gauges in order to provide another source of data from testing. The heavier posts were chosen so that the post would not yield during testing, thereby making the instrumented post reusable. The backfill materials investigated conformed to ASTM C 33 fine

and coarse aggregate, which are typically used in concrete mix designs. As a result, these aggregate gradations should be readily available to State DOT's. The test matrix for all six bogie tests is shown in Table 2, and the associated test results are summarized in Appendix C.

It should be noted that three bogie tests, test nos. MPR-1, MPR-2, and MPR-4 are not shown nor discussed in this section. These tests were preliminary tests conducted to determine the practical aspects of evaluating posts placed in drilled holes. The tests were conducted at varying speeds in different drilled hole configurations, and as a result, the data from these tests was found to not be applicable to this study. However, the results of all three preliminary bogie tests are summarized in Appendix C.

Table 2. Test Matrix

Test Number	Post Type	Backfill Material	Embedment Depth (mm)	Impact Angle (degrees)
MPR-3	W152x23.8	Fine Aggregate	610	0
MPR-5	W152x23.8	Coarse Aggregate	610	0
MPR-6	W152x23.8	Coarse Aggregate	460	0
MPR-7	W152x13.4	Coarse Aggregate	610	0
MPR-8	W152x13.4	Coarse Aggregate	610	10
MPR-9	W152x13.4	Fine Aggregate	610	0

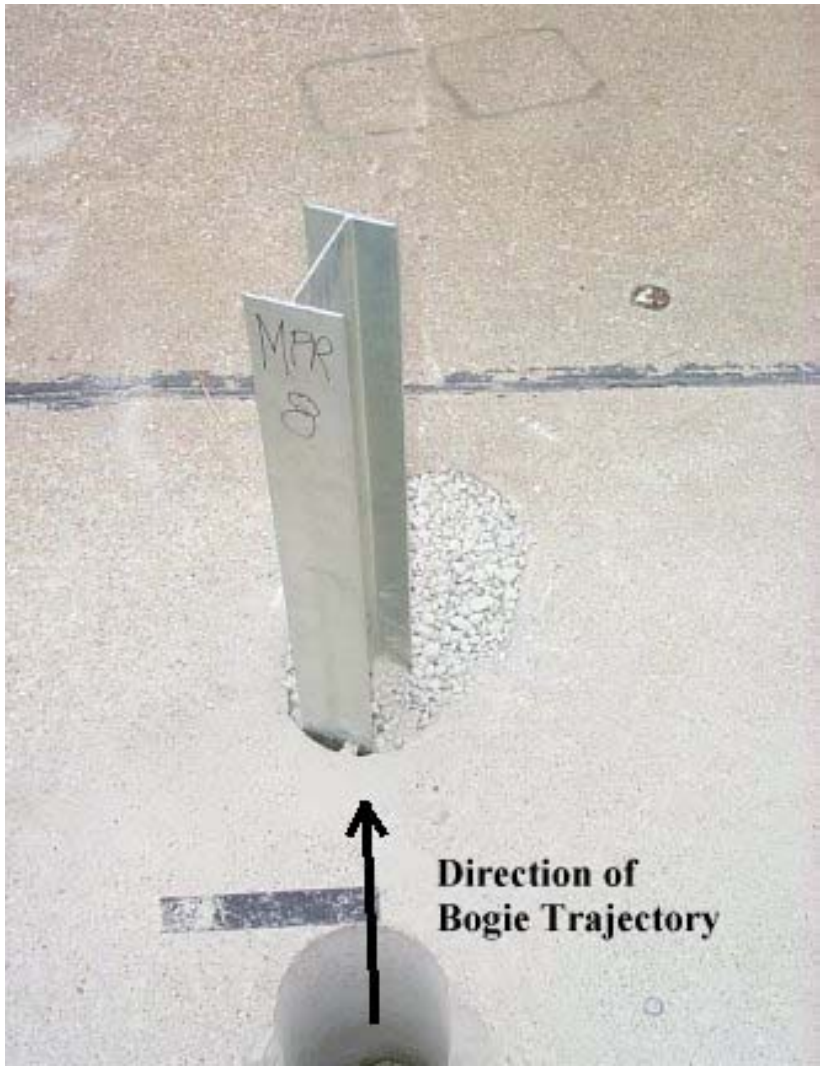

Figure 12. Test MPR-8 Configuration

5.2 Test Conditions

5.2.1 Test Facility

The testing facility is located at the Lincoln Air-Park on the northwest side of the Lincoln Municipal Airport and is approximately 8.0 km (5 mi.) northwest of the University of Nebraska-Lincoln.

5.2.2 Bogie Vehicle

A light, rigid frame bogie was used to impact the posts. This steel-framed bogie was constructed of round and rectangular steel tubing conforming to the details provided in the FHWA specifications (12). A round cylindrical impact head was attached to the bogie's front end. The cylindrical head was covered with a neoprene pad in order to properly distribute the load to the post and to reduce any sharp stress concentrations. A wooden buffer block was located between the cylindrical head and the rigid bogie frame in order to reduce the risk of damage occurring to the rigid frame in the event that the impact was too violent. Photographs of the bogie vehicle are shown in Figure 13.

5.2.3 Bogie Tow and Guidance System

Steel rollers, attached to the left side of the bogie, guided the bogie down a 30.5-m (100 ft) long guide track. The guide track consisted of a 57-mm (2.25-in.) diameter steel pipe, with a wall thickness and length of 4.76 mm (0.187 in.) and 2,965 mm (117 in.), respectively. The steel pipe was supported every 3,048 mm (10 ft) by steel stanchions. A reverse cable tow system with a 1:1 mechanical advantage was used to propel the bogie vehicle. The bogie was released from the tow cable and the bogie guide track before impact with the guardrail post, allowing the bogie vehicle to become a free projectile as it came off the bogie guide track. Photographs of the bogie guidance configuration are shown in Figure 14.

Figure 13. Rigid Bogie Vehicle

Figure 14. Bogie Tow and Guidance

In the event the post did not stop the bogie or the bogie went out of control prior to impact, the bogie vehicle was outfitted with hydraulic brakes in order to allow it to be brought to a controlled stop. An accelerometer unit was attached at the bogie's center of mass to record vehicle accelerations in all three axes.

5.2.4 Post Installation Procedure

Three holes, 203 mm (8 in.) in diameter, were drilled into the 560-mm (22-in.) thick concrete tarmac located at the Midwest Roadside Safety Facility's (MwRSF's) outdoor test site. The drilled holes were spaced on 165-mm (6.5-in.) centers and drilled to a depth of 610 mm (24 in.). The concrete left on the sides of the elongated hole was chiseled out in order to obtain a smooth-sided, elongated hole, as previously shown for Option 1 in Figure 5. The post was then placed at the front of the elongated hole, and the hole was filled with the selected backfill material in 152-mm (6-in.) lifts and hand tamped with a rod. Steel posts were cut to the proper length so that 737 mm (29 in.) of post length protruded from the drilled hole. It is noted that the rigid foundation was only 560 mm (22 in.) thick, which was less that the design post embedment depth of 610 mm (24 in.). However, it was assumed that the error resulting from this test configuration would be minor.

5.2.5 Backfill Material Properties

Both the fine and coarse aggregate used for backfill material conformed to ASTM C 33 "Standard Specification for Concrete Aggregates". The fine aggregate could be characterized as a river run gravel with particles that were fairly rounded in nature. The coarse aggregate was graded to the size number 57 specification for coarse aggregate used in concrete mix designs. In general, the coarse aggregate consisted of crushed limestone with particles that were fairly angular in shape.

5.2.6 Data Acquisition Systems

5.2.6.1 Accelerometer

A triaxial piezoresistive accelerometer system, located at the bogie's center of gravity, had a range of +200 G's and was used to measure bogie accelerations in the longitudinal direction at a sample rate of 3,200 Hz. Instrumented Sensor Technology (IST) of Okemos, Michigan, developed the environmental shock and vibration sensor/recorder system, Model EDR-3.

The EDR-3 is a self-contained, user-programmable acceleration sensor/recorder with a 74dB dynamic range. During active recording, acceleration signals are digitized to 10-bit resolution and stored in digital memory onboard the unit. The EDR-3 has a maximum cross-axis sensitivity of +3.0%.

Analog low-pass filtering was used internally in the EDR-3 to condition the input signal. A Butterworth low-pass filter with a –3dB cut-off frequency of 1,120 Hertz was use for anti-aliasing.

The EDR-3, configured with 256 KB of RAM memory, offers recording capability from three input channels simultaneously. The differential channels were used to sample internally mounted, voltage mode, piezoresistive accelerometers.

Displacement, velocity, force, and energy were found at the impact location on the post by using accelerometer and initial velocity data. It should be noted that although the acceleration data was applied to the impact location, the acceleration data came from the bogie's center of gravity. Impact force was found by multiplying the processed acceleration data by the bogie's mass. The change in velocity was found by integrating the acceleration versus time curve. Knowing the initial velocity, the actual velocity versus time curve was constructed. This

velocity versus time curve was then integrated to get the bogie displacement versus time curve. At this point, the force versus displacement curve was obtained. The dissipated energy curve was then found by integrating the force versus displacement curve.

5.2.6.2 High-Speed Photography

A high-speed Red Lake E/cam video camera, with an operating speed of 500 frames/sec, was used. The camera was positioned on the left side of the post and provided a close field of view of the post and drilled hole.

5.2.6.3 Pressure Tape Switches

Three pressure-activated tape switches, spaced at 1-m (3.28-ft) intervals, were used to determine the initial impact speed of the bogie. As the bogie's front tire passed over and activated each tape switch, an electronic timing signal was sent to the data acquisition system. By knowing the time between recorded timing signals and the distance between the switches, initial speed could be approximated.

5.2.6.4 Strain Gauges

Two strain gauges were applied to each W152x23.8 (W6x16) steel post. The gauges were placed on the inside of the front flange, one on each side of the web, 19 mm (0.75 in.) from the outside edge of the flange, and approximately 51 mm (2 in.) above the ground. Weldable strain gauges were utilized and consisted of model LWK-06-W250B-350, manufactured by Micro-Measurements Division of the Measurements Group, Incorporated, Raleigh, North Carolina. The gauges had a nominal resistance of 350±1.4 ohms and a gauge factor of 2.03. A Measurements Group Vishay Model 3210 signal-conditioning amplifier was used to power, condition, and amplify the low-level signals to high-level signals for acquisition by a Keithley-

Metrabyte DAS-1802HC data acquisition board. The computer programs ”Test Point” and “DADiSP” were used to record and analyze the data.

Strain gauge factors, used to calculate the moment in the post based on measured strain gauge voltage output, were determined through a calibration procedure. The calibration procedure consisted of a restrained post that was subjected to three-point bending, as shown in Figure 15. The load was applied to the midspan of the beam and monitored using a load cell. The moment distribution in the post was then calculated from the known load and loading configuration. A calibration factor was then determined based on the correlation between the calculated moment in the post at the strain gauge location and the measured voltage output from the strain gauge. This procedure was repeated for different loading configurations so that an average factor could be found for each strain gauge.

5.2.6.5 String Potentiometers

For bogie tests involving the use of instrumented W152x23.8 (W6x16) steel posts, post displacement was also measured using linear string potentiometers. As previously mentioned, the post was located at the front of the drilled hole, which forced it to rotate about its base on the front side. As a result, assuming the post remained essentially rigid, the displacement at any point along the length of the post could be easily calculated by knowing only one measured displacement at a given point. A schematic of the string potentiometer attached to the post is shown in Figure 16.

For testing, a UniMeasure PA-20-70120 string potentiometer (Linear Variable Displacement Transducer, LVDT) was attached to the post 305 mm (12 in.) above the ground surface. The PA-80 potentiometer has a range of 508 mm (20 in.) and a sensitivity of 19.09 mV/V/cm (48.48 mV/V/inch).

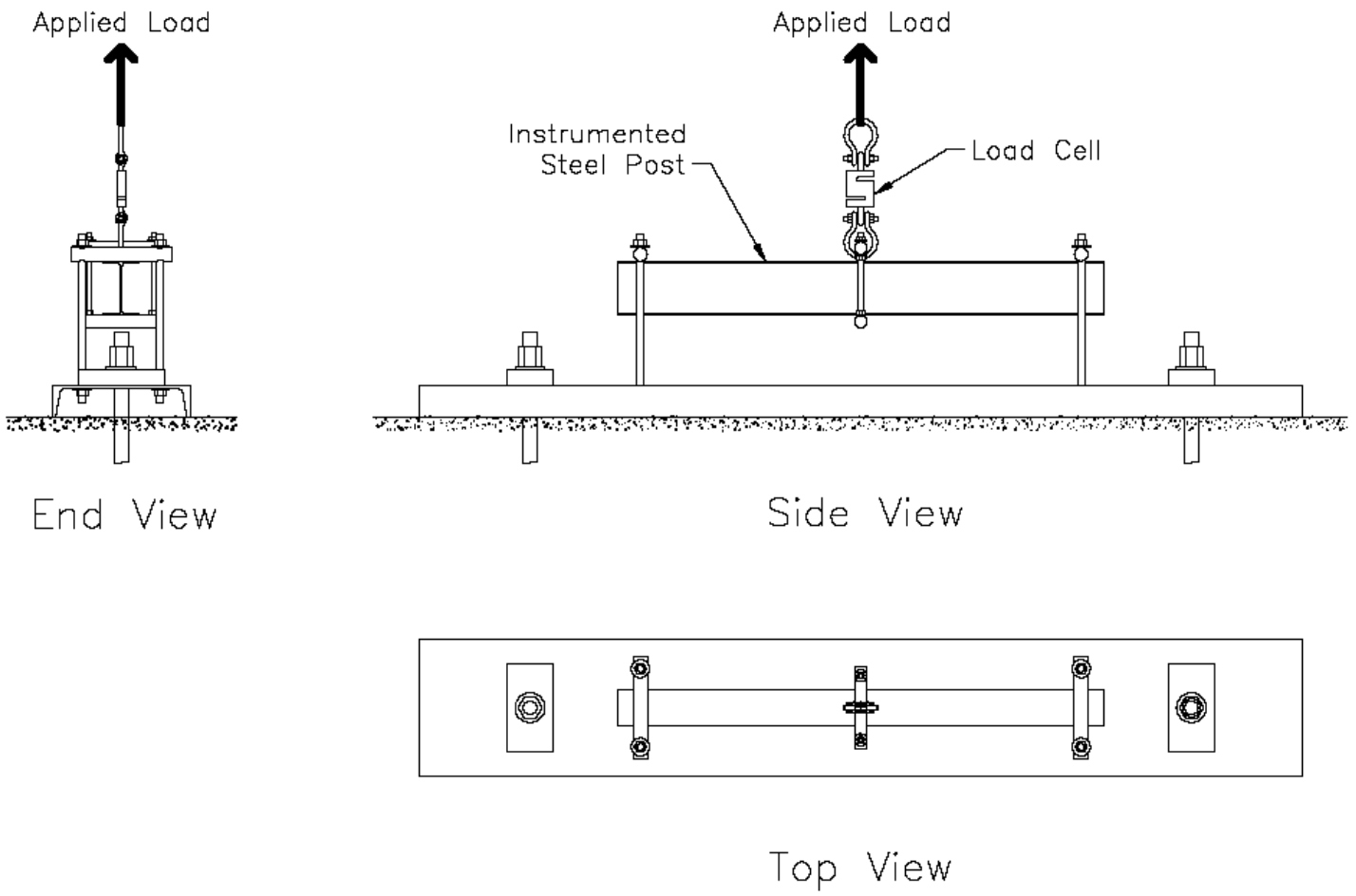

Figure 15. Calibration Setup for Instrumented Post

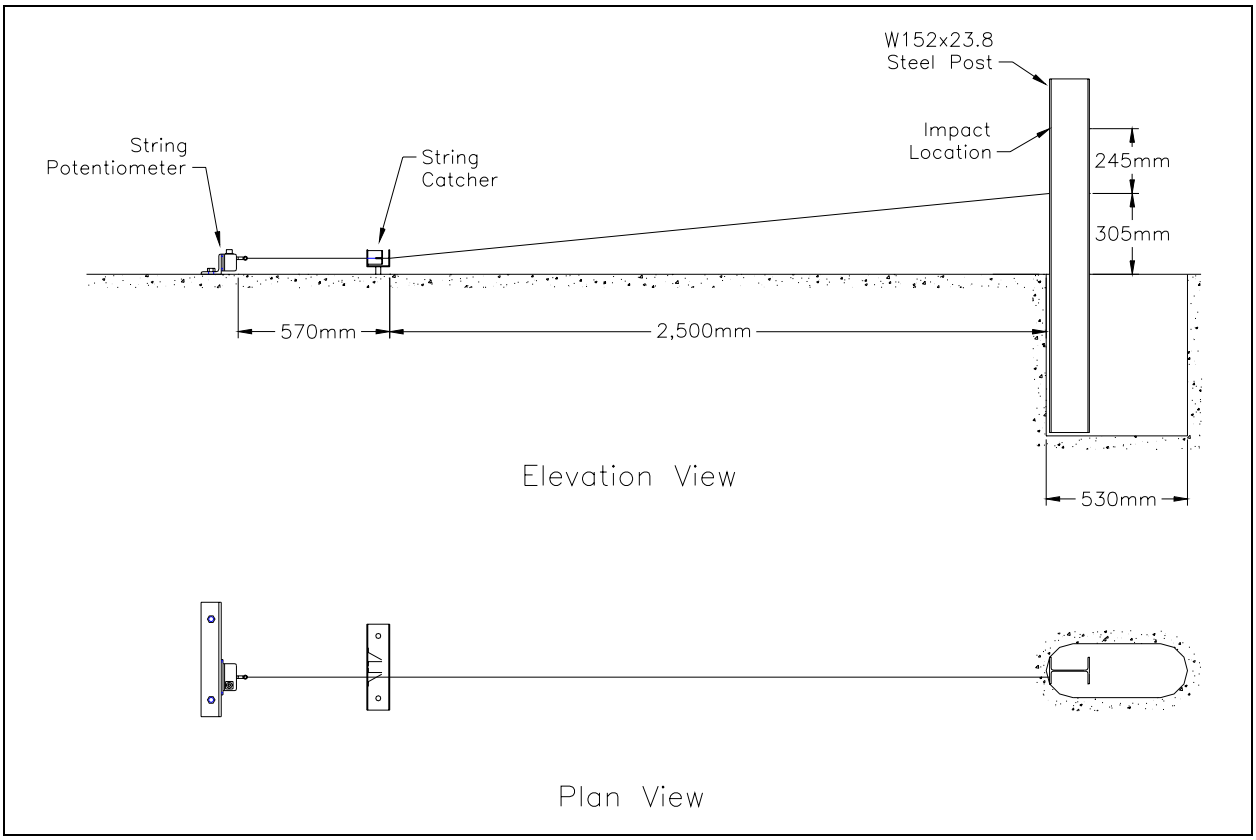

Figure 16. String Potentiometer Setup

During testing, output voltage signals from the string potentiometers were conditioned by the Vishay amplifier and then sent to a Keithley-Metrabyte DAS-1802HC data acquisition board. This signal was then acquired by the "Test Point 4.0" software package and stored on a computer hard drive.

5.3 Comparison of Data Acquisition Techniques

The objective of dynamic bogie testing was to obtain force-deflection curves, at the rail's mid-height or impact height, for posts placed in different backfill materials and at varying embedment depths. These results were then used to find total energies (the area under the force vs. deflection curve) dissipated by the backfill material so that it could be compared to the

BARRIER VII analysis. Raw data used to obtain force-deflection curves was garnered from two sources: an accelerometer unit and a strain gauge/string potentiometer configuration.

5.3.1 Application of Accelerometer Data

The first method for determining force-deflection curves was by converting raw accelerometer data, as discussed in Section 5.2.6.1. Using raw accelerometer data for analysis had both advantages and disadvantages. As previously stated, although the acceleration data was applied to the impact location on the post, the data came from the bogie's center of gravity. As a result, possible errors were incorporated into the recorded data. This was due in part to the bogie's frame not being perfectly rigid, causing there to be variations between the accelerations at the cylindrical head and those measured at the bogie center of gravity. Also, the bogie may have some pitch rotation during impact, thus instilling possibly more variation in accelerations between the cylindrical head and bogie center of gravity. While these factors may have adversely affected the accuracy of the data when applied at the bogie's cylindrical head, it was assumed that the data was not greatly influenced by them, and as a result, the data was considered useful for analysis. One advantageous aspect of using accelerometer data was that it included influences of the post inertia in the force reaction. This was important since the post's mass could possibly have an effect on a guardrail system's performance. Likewise, the force response of the post was only measured in the horizontal plane as the post rotated. This was useful when correlating test results with BARRIER VII, since the computer simulation program was only 2-dimensional and could only account for post response in the horizontal plane.

5.3.2 Application of Strain Gauge and String Potentiometer Data

The second method of obtaining force-deflection curves, was to use strain gauge data coupled with string potentiometer data. During impact, the moment in the post, 51 mm (2 in.)

above the ground surface, was determined from multiplying the recorded output voltages from the strain gauges by their calibration factors. Since the measured moment in the post was above the ground line, the moment was simply a function of the impact force on the post by the cylindrical bogie head. As a result, the force at the impact location was calculated by dividing the measured moment in the post by the distance between the strain gauge and the impact location on the post. By coupling this calculated force data with string potentiometer data, force-deflection curves were obtained at the impact location on the post.

Data acquisition using strain gauges also had certain advantages and disadvantages in analysis. Since the strain gauges had already been calibrated for known moments in the post, this method may provide more accurate data for the determination of impact forces. However, moments in the post were only a function of the applied force that resulted in bending of the post and not the acceleration of the post as it rotated. As a result, inertial effects resulting from the post's mass were not seen in the force-deflection curves. Also, the strain gauges were calibrated with a force perpendicular to the post, thus the impact force on the post was only found for the perpendicular component of the force at the impact location. This can cause some issues with accuracy as the post rotates, however, it was considered that force-deflection curves developed from strain gauges would result in greater accuracy versus those curves developed from the accelerometer data.

5.4 Test Results

Bogie testing of posts was completed in two phases. For Phase I, instrumented W152x23.8 (W6x16) posts were used. Force-deflection data was obtained from both the bogie accelerometer unit and the strain gauge/string potentiometer configuration. Analysis of Phase I results seemed to indicate that absorbed energy values for posts rotating in the fine aggregate

backfill were too low. Results from bogie impact tests with posts installed in coarse aggregate appeared to be promising with absorbed energy values in the preferred range. However, the peak loads produced by the coarse aggregate were considered to be on the high side. This fact suggested that the coarse aggregate might be too stiff for standard W152x13.4 (W6x9) steel posts, resulting in the premature failure of standard steel posts. Therefore, additional bogie tests (Phase II) were performed on standard W152x13.4 (W6x9) posts placed in both coarse and fine aggregates in order to assess the possibility of premature post failure. Force-deflection curves for Phase II of testing were only obtained from the accelerometer unit located on the bogie. Force-deflection plots for all bogie tests can be found in Appendix C.

The results from bogie testing of posts are summarized in Table 3. Absorbed energies, as determined from the accelerometer and/or strain gauge data analysis, were found at the rail's midpoint height and at a deflection of 600 mm (23.6 in.). It should be noted that for the tests involving W152x13.4 (W6x9) posts, the effects of any post deformation are included in the measured deflections and calculated absorbed energies. The final deformed state of each of the W152x13.4 (W6x9) posts is shown in Figures 17 through 19. For all tests, the soil was found to fail versus the post.

Analyses of the strain gauge and accelerometer data indicate that the absorbed energy results correlate quite closely, as shown in Table 3. Comparing the energy results, it is evident that the absorbed energy was less when calculated from strain gauge data than from accelerometer data, which is most likely attributed to post inertia. However, the difference between values is so minor that it can be ignored as being an insignificant factor in the analysis.

For test MPR-6, where the post was embedded in coarse aggregate to a depth of 460 mm (18 in.), the energy dissipated by rotation of the post in the drilled hole was found to be

insufficient. Further, the post was pulled out of the drilled hole during the bogie impact. As a result, it was determined that a minimum embedment depth of 610 mm (24 in.) was required. Based on the required amount of dissipated energy equal to 21 kJ (186 k-in.), as determined from BARRIER VII computer simulation, it was evident that the fine aggregate was not a suitable backfill material. However, it was determined that coarse aggregate backfill would allow the post to dissipate enough energy as it rotated, as shown in Table 3 for test MPR-7. The use of coarse aggregate was further supported by qualitative analysis of test MPR-8, the test where the post was placed in a drilled hole at a 10-degree angle. It was theorized that if the post did snag on the side of the drilled hole, a stiffer soil would at least slow the post to a greater extent before contact with the side occurred. This would allow the post to fail a little more gradually, thereby reducing the effect of a quick transfer of force from the post to the guardrail.

In conclusion, it was determined that for the critical post placement condition, the post should be placed at the front of an elongated drilled hole, embedded to a depth of 610 mm (24 in.), and backfilled with ASTM C 33 coarse aggregate, size number 57. This critical post placement design would then be used in the succeeding full-scale vehicle crash test with a W-beam guardrail system.

Table 3. Bogie Testing Results

Test #	Speed (km/hr)	Backfill Type	Embedment Depth (mm)	Post Type	Total Deflection (mm)	Strain Gauge Energy (kJ)	Accelerometer Energy (kJ)	Post Yield or Soil Yield	Comments
MPR-3	23.3	Fine	610	W152x23.8	570	19.4	19.9	Soil	Post hit back of hole
MPR-5	22.2	Coarse	610	W152x23.8	340	19.5	20.1	Soil	
MPR-6	24.5	Coarse	460	W152x23.8	670	7.2	7.2	Soil	Post pulled out of hole
MPR-7	24.0	Coarse	610	W152x13.4	430	NA	22.6	Soil	
MPR-8	21.7	Coarse	610	W152x13.4	610	NA	17.8	Soil	Angled impact, post hit side of hole
MPR-9	23.5	Fine	610	W152x13.4	690	NA	16.0	Soil	

Figure 17. Post Damage, Bogie Test MPR-7

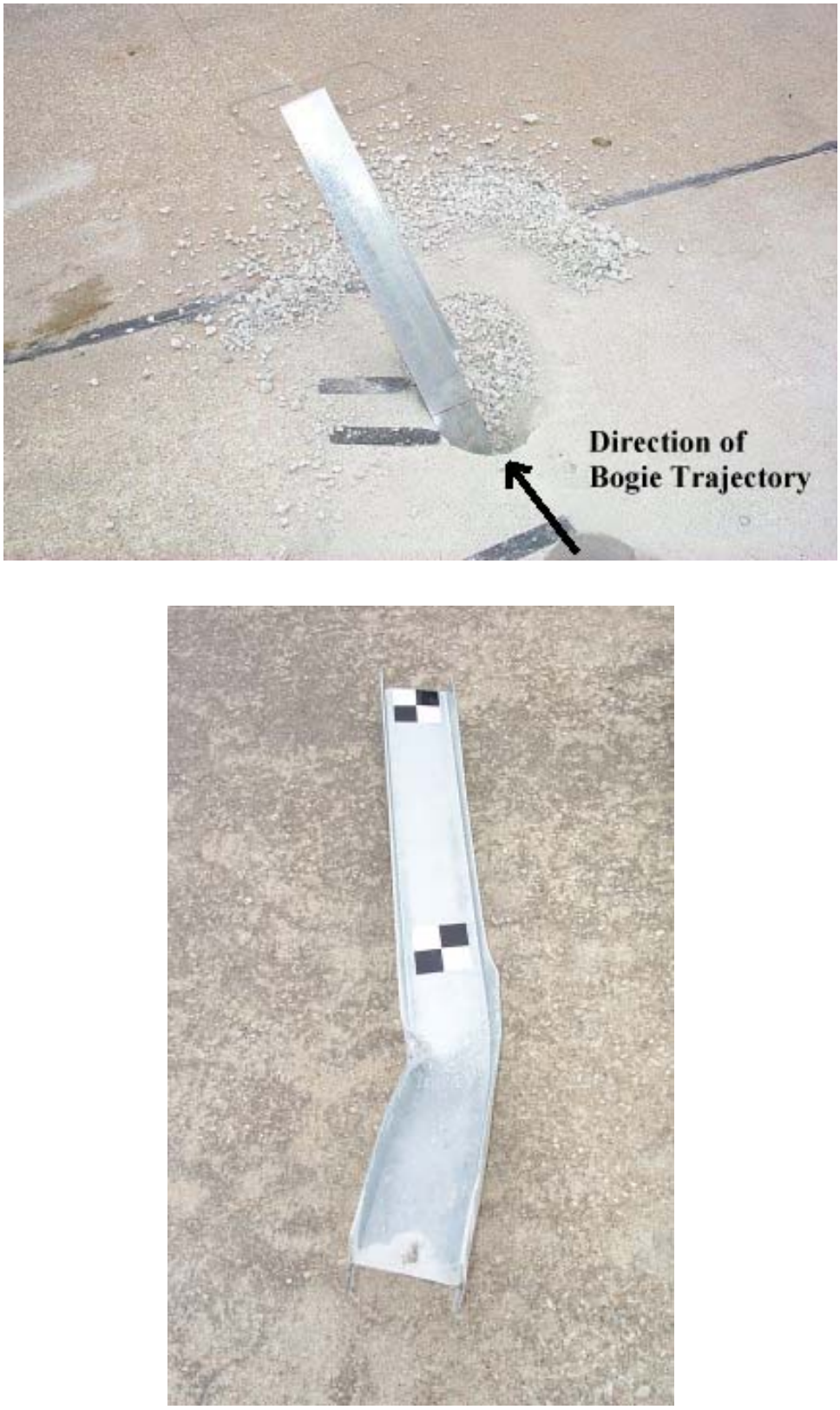

Figure 18. Post Damage, Bogie Test MPR-8

Figure 19. Post Damage, Bogie Test MPR-9

6 CRITICAL IMPACT POINT ANALYSIS

6.1 Overview

BARRIER VII (11) was used to find the critical impact point (CIP) (1,13) for a vehicle impact with W-beam guardrail. To get trustworthy results from BARRIER VII, it is best to first calibrate the model to a previously conducted full-scale vehicle crash test. However, there is one major caveat to this type of analysis: the BARRIER VII model is stiffer in behavior than in physical tests. This is a result of a number of factors, such as the fact that torsional buckling of posts cannot be simulated and a continuous structure, such as a guardrail beam, is simulated as a number of discrete elements. There are a number of ways that the finite element model can be made less stiff. However, for this study, it was decided that post parameters, obtained through physical testing for input in BARRIER VII, would be reduced in magnitude. This approach was deemed to be the most efficient way to model physical tests. As a result, it was decided that physical testing results would be factored before being inputted into BARRIER VII. The factors would be determined by comparing simulated post parameters found from calibration of full-scale crash testing to post parameters found through previous bogie testing.

6.2 Procedure

The process to find a critical impact point for a guardrail system using the critical post placement design was completed in four steps. First, the BARRIER VII model was calibrated to a previously conducted full-scale vehicle crash test. Post parameters in the model were modified until the simulation and test results correlated reasonable well. Second, the simulated post parameters found from calibration were compared to real-world post parameters obtained from bogie testing of posts installed in the same configuration as the full-scale crash test. Correlation factors were then calculated based on the difference between BARRIER VII simulation results

and bogie test results. Third, the correlation factors were applied to the post parameters found from bogie test MPR-7. These factored post parameters were then inputted into the BARRIER VII computer simulation model and used for the critical impact point (CIP) analysis. Finally, the CIP was determined for the proposed guardrail system using the critical post placement design.

6.3 Calibration of BARRIER VII Model

The BARRIER VII model was calibrated to a full-scale vehicle crash test. Test MIW-1, a full-scale vehicle crash test on Michigan's Type B (W-beam) Guardrail System (14) was used for this process. For this test, a W-beam guardrail system supported by W152x13.4 (W6x9) steel posts placed in standard, unconfined soil and at standard spacing was impacted by a 2,007-kg (4425-lb) pickup truck at a speed of 99.8 km/hr (62.0 mph) and at an angle of 25.8 degrees. Modification of the guardrail and vehicle input parameters was ignored, instead parameter calibration involved the modification of the post parameters, in particular, the post stiffness, yield force, and failure deflection about the strong axis of bending or along the B-axis. While each parameter affects the guardrail in a somewhat different way, all three post parameters affect the magnitude of dynamic deflections for both the rail and the posts.

Computer simulation modeled an initial impact at post no. 13. Maximum dynamic rail deflections were recorded at post nos. 13 through 16. These simulated deflections were compared to maximum dynamic rail deflections determined from film analysis of test MIW-1. Post parameters were repeatedly modified. New simulations were also conducted until the error between dynamic maximum deflections from the simulation and test results was minimized. The results of this analysis are shown in Table 4. Simulation "miw21" was found to have the best combination of post parameters to allow the finite element model to accurately simulate the real-world rail deflections.

Table 4. BARRIER VII Calibration Results

Simulation #	Stiffness (kN/mm)	Yield Moment (kN-mm)	Failure Deflection (mm)	Dynamic Rail Deflections (mm) [1]				Percent Error [2]				Error Range
				Post 13	Post 14	Post 15	Post 16	Post 13	Post 14	Post 15	Post 16	
Real-World	-	-	-	345	770	1001	765	-	-	-	-	-
miw1	0.350	16,948	635	340	724	881	577	-1.5	-5.9	-11.9	-24.6	23.1
miw2	0.350	16,948	508	345	737	919	699	0.0	-4.3	-8.1	-8.6	8.6
miw3	0.350	16,948	483	348	739	930	724	0.7	-4.0	-7.1	-5.3	7.8
miw4	0.350	16,948	533	340	734	914	671	-1.5	-4.6	-8.6	-12.3	10.8
miw5	0.350	16,948	584	340	726	899	622	-1.5	-5.6	-10.2	-18.6	17.1
miw6	0.350	16,948	381	356	757	965	810	2.9	-1.7	-3.6	6.0	9.5
miw7	0.350	16,948	432	348	747	953	775	0.7	-3.0	-4.8	1.3	6.2
miw8	0.525	16,948	635	335	724	861	541	-2.9	-5.9	-14.0	-29.2	26.3
miw9	0.525	16,948	584	335	729	879	569	-2.9	-5.3	-12.2	-25.6	22.6
miw10	0.525	16,948	533	335	732	892	615	-2.9	-5.0	-10.9	-19.6	16.7
miw11	0.525	16,948	508	335	734	902	645	-2.9	-4.6	-9.9	-15.6	12.7
miw12	0.525	16,948	483	333	732	909	673	-3.7	-5.0	-9.1	-12.0	8.3
miw13	0.525	16,948	432	335	742	927	724	-2.9	-3.6	-7.4	-5.3	4.4
miw14	0.525	16,948	381	340	749	950	770	-1.5	-2.6	-5.1	0.7	5.7
miw15	0.876	16,948	432	318	719	864	658	-8.1	-6.6	-13.7	-14.0	7.4
miw16	0.876	16,948	406	320	726	879	688	-7.4	-5.6	-12.2	-10.0	6.6
miw17	0.876	16,948	381	323	729	889	716	-6.6	-5.3	-11.2	-6.3	5.9
miw18	0.876	16,948	356	325	732	899	734	-5.9	-5.0	-10.2	-4.0	6.2
miw19	0.876	16,948	330	328	734	907	749	-5.1	-4.6	-9.4	-2.0	7.4
miw20	0.525	16,948	457	335	737	917	699	-2.9	-4.3	-8.4	-8.6	5.7
miw21	0.525	16,948	406	338	744	937	747	-2.2	-3.3	-6.3	-2.3	4.1
miw22	0.525	15,818	406	363	765	945	777	5.1	-0.7	-5.6	1.7	10.7
miw23	0.525	14,688	406	401	805	970	823	16.2	4.6	-3.0	7.6	19.2

[1] As measured at the top of the rail
[2] Percent error between simulated and real-world rail deflections

6.4 Comparison of BARRIER VII Model to Physical Testing

Once simulated post parameters were found through calibration, it was necessary to correlate these parameters to real-world post-soil properties. Results from bogie testing of steel posts with standard embedment (15) were analyzed to determine real-world values for stiffness and yield force. Bogie testing consisted of impacting W152x13.4 (W6x9) steel posts embedded at a standard depth of 1,090 mm (43 in.) in an unconfined soil as specified by NCHRP Report No. 350 and meeting AASHTO M147-65 Grading B (1990) requirements. Posts for test MIW-1 were embedded in the same soil in the same manner. The bogie vehicle impacted the posts at a number of different speeds. Force-deflection plots, derived from the bogie's accelerometer data and for different impact speeds, are shown in Figure 20. From this graph, the post-soil yield force and stiffness along the strong axis of the post was determined to be 50 kN (11 kips) and 1.05 kN/mm (6 k/in), respectively.

Results from test MIW-1 were used to determine a real-world failure deflection for the post bending about its strong axis. Film analysis was used to determine the post deflections over time at the guardrail midpoint height while assuming that the posts rotated about a point 1/3 of the embedment depth from the bottom of the posts. This data was then used to derive post velocities as well as a plot of post velocities versus deflection at the rail midpoint height. The post velocity versus deflection curves for the first three posts impacted by the test vehicle are shown in Figure 21. It was determined that a failure deflection of 406 mm (16 in.), as found from simulation, was considered a reasonable real-world value. At this deflection, it was obvious that the post velocities had peaked. As a result, it was suggested that after the post velocities had peak, their influence on the guardrail system was determined to be negligible, and post failure was assumed to occur.

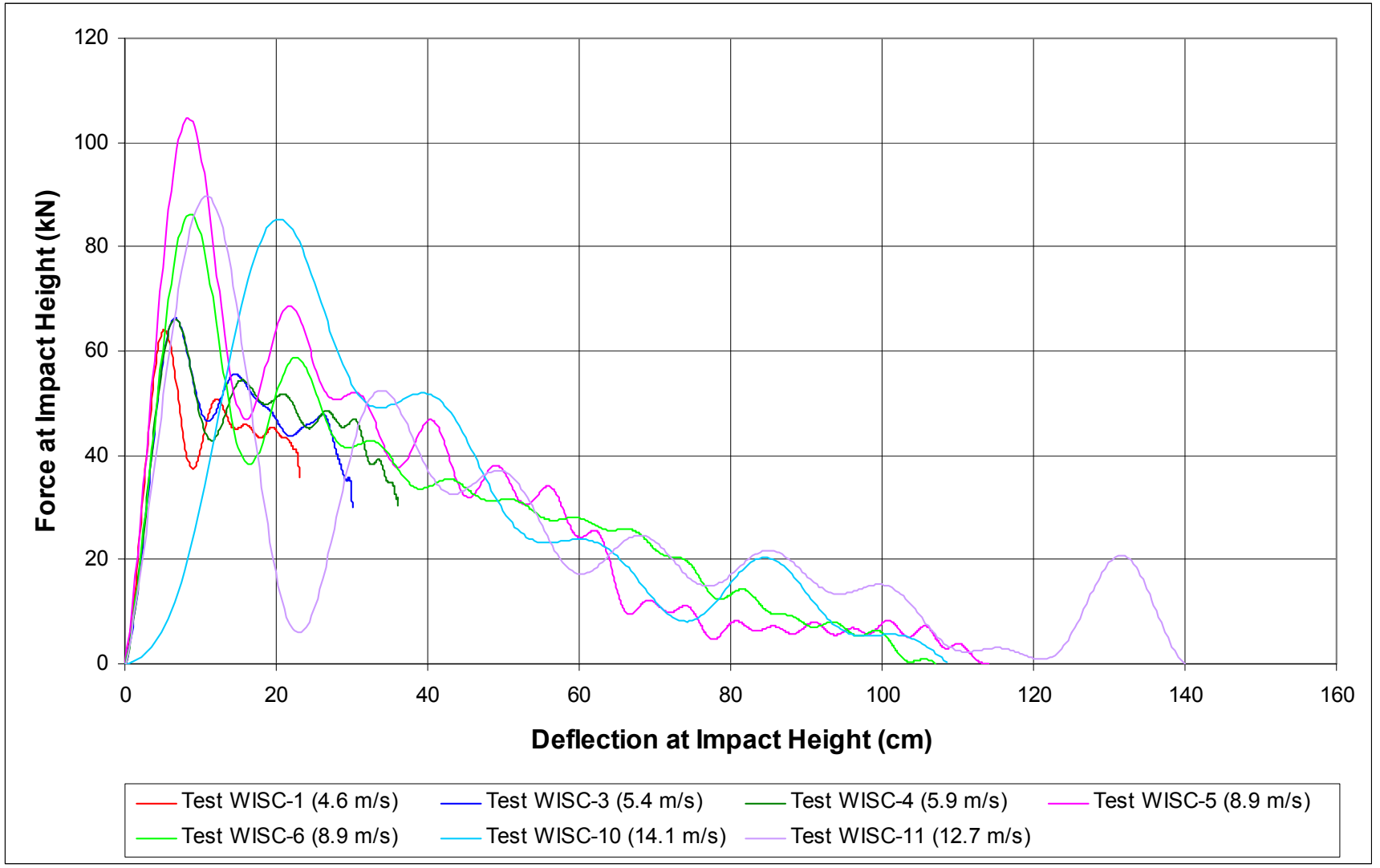

Figure 20. Force-Deflection Curves for Various Impact Speeds

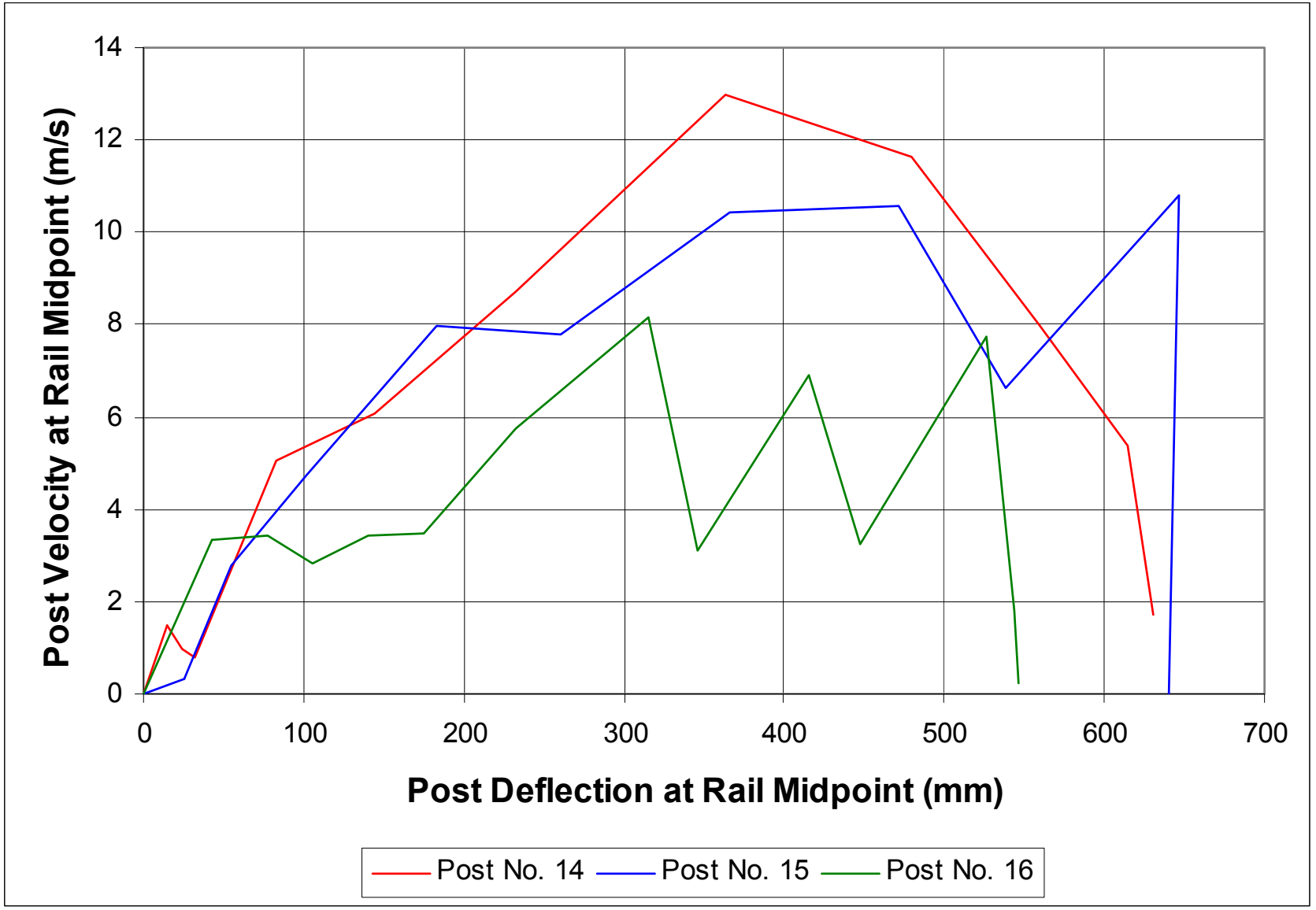

Figure 21. Post Velocity versus Deflection at Rail Midpoint Height

The post parameters for both simulation and testing are shown in Table 5. It was evident that, except for failure deflection, the parameters were not the same. As a result, correlation factors were determined for each parameter and included in Table 5. The correlation factors were calculated by dividing the BARRIER VII post parameters found from calibration by their corresponding real-world values.

Table 5. Post Parameters along B-Axis or Strong Axis of Post at Rail Midpoint Height

	Simulation	WISC Bogie Testing	Correlation Factor
Post Stiffness (kN/mm)	0.53	1.05	0.50
Yield Force (kN)	32	50	0.64
Failure Deflection (mm)	406	406	1

6.5 Derivation of BARRIER VII Post Parameters for CIP Analysis

Results from bogie test MPR-7 were chosen to get real-world post parameters for the critical post placement design. The force-deflection curve from test MPR-7 was converted to a simplified curve for input in BARRIER VII. Figure 22 shows the actual force-deflection plot as well as the simplified curve. The stiffness was fitted to the front portion of the curve and found to be 1.40 kN/mm (8 k/in.). The yield force, derived as that necessary for both the actual and simplified curves to have equal areas under the curve at a 406-mm (16-in.) deflection, was found to be 57 kN (12.8 kips). These parameters were then multiplied by the correlation factors for input into BARRIER VII. Post parameters, as determined from post bogie testing as well as the factored post parameters used in the BARRIER VII CIP analysis, are shown in Table 6.

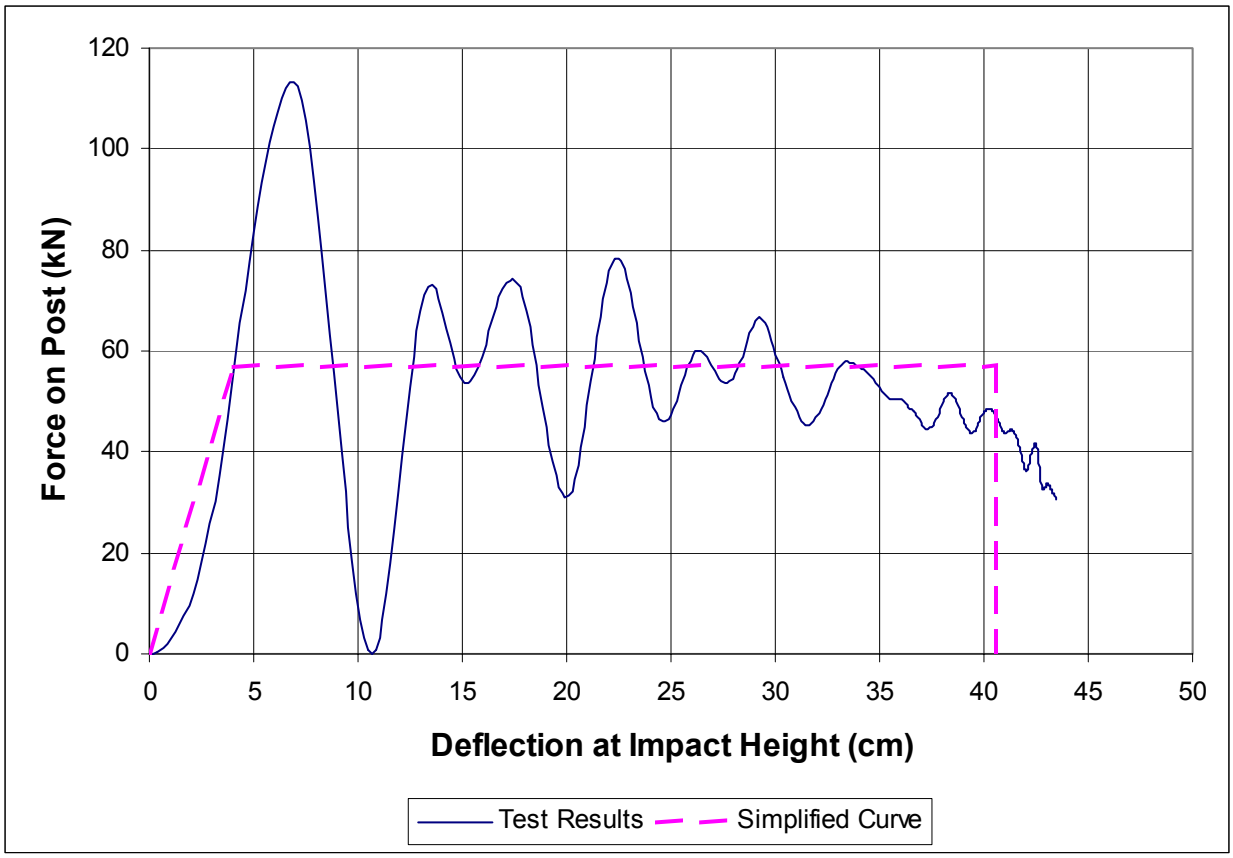

Figure 22. Force-Deflection Plot from Testing with Simplified Curve

Table 6. Bogie Testing (MPR-7) and BARRIER VII Post Parameters

Parameters	Post Stiffness (kN/mm)	Yield Force (kN)	Failure Deflection (mm)
Bogie Test MPR-7	1.40	57	406
BARRIER VII	0.70	36	406

6.6 Critical Impact Point Analysis

The CIP analysis was conducted to determine the impact point for a W-beam guardrail system supported by posts installed in the critical post placement condition. The CIP is defined

as the initial impact point on the guardrail system that will cause the greatest risk of vehicle damage, occupant risk, or barrier damage. Sources of risk include the vehicle's front wheel snagging on the guardrail posts, the vehicle pocketing in the guardrail, and guardrail rupture. For this study, it was determined that wheel snag would be the critical factor for determining the critical impact point. This was due to the reduced embedment depth that would result in a more shallow post rotation point and greater propensity for wheel snag. The BARRIER VII model was configured with a 53.3-m (175-ft) W-beam guardrail system utilizing a post spacing of 1,905 mm (75 in.). Simulations were performed with a 2000-kg (4409-lb) pickup truck impacting the barrier system at an impact speed of 100.0 km/hr (62.1 mph) and at an impact angle of 25 degrees. The post parameters inputted into the finite element model were the factored parameters found from bogie test MPR-7, as shown in Table 6. Rail and vehicle properties were the same as used in all previous simulation.

Wheel snag was determined using methods developed by Reid, et al (13). Wheel node coordinates were specified on the finite element pickup truck model and their trajectories tracked during simulation. Wheel snag was considered to occur when the front wheel's rim overlapped the post on the longitudinal axis. It was assumed that a wheel rim was configured with a radius of 203 mm (8 in.). When the front edge of the steel rim came to within 203 mm (8 in.) of the post's longitudinal coordinate, wheel snag was assumed to have occurred. Nodal trajectories for the wheel node were outputted as the node deformed with the vehicle as well as for the initial local coordinates of the wheel node with respect to the vehicle's center of gravity. As a result, snag was calculated both for a deformed wheel trajectory as well as for a wheel trajectory where the rim and tire remained rigid with respect to the vehicle.

The first simulation run was conducted with the initial impact of the vehicle at post no.

13 and with wheel snag monitored at post no. 15. Successive simulations were conducted with the initial impact point moved upstream and downstream of post no. 13 in 300-mm (12-in.) increments while continuing to monitor wheel snag at post no. 15. The analysis was stopped when it became evident that the wheel snag had peaked for a certain impact point. The results for the CIP analysis are shown in Table 7. It was found that simulation "cip13" simulated the critical impact condition for the guardrail system. The impact point of this simulation was 710 mm (28 in.) downstream of post no. 12. The input deck for simulation "cip13" is shown in Appendix B.

Table 7. Critical Impact Point Analysis Results

Barrier VII File Name	Initial Impact Location @ node	(Deformed) Wheel Snag (mm) [1]	(Rigid) Wheel Snag (mm) [2]
cip8	77	56.1	82.9
cip7	76	69.8	99.6
cip6	75	78.4	109.2
cip5	74	95.2	118.5
cip4	73	98.6	130.1
cip3	72	101.0	128.9
cip2	71	101.8	138.2
cip1	69	104.7	146.1
cip9	67	110.8	161.9
cip10	66	115.1	170.0
cip11	65	112.7	163.4
cip12	64	129.0	176.0
cip13	63	130.6	176.2
cip14	62	126.1	173.6
cip15	61	116.8	162.6
cip16	60	103.4	152.7
cip17	59	86.4	139.7
cip18	58	77.9	128.2
cip19	57	56.1	113.0

[1] Wheel snag calculated assuming wheel was allowed to deform
[2] Wheel snag calculated assuming wheel was a rigid

7 TEST REQUIREMENTS AND EVALUATION CRITERIA

7.1 Test Requirements

Longitudinal barriers, such as W-beam guardrail systems, must satisfy the requirements specified in NCHRP Report No. 350 to be approved for use on new construction projects or as a replacement for existing 3R (resurfacing, restoration, and rehabilitation) projects where designs do not meet current safety standards. For Test Level 3 (TL-3) of NCHRP Report No. 350, two full-scale vehicle crash tests must be conducted on the guardrail system involving both an 820-kg (1,808-lb) small car and a 2,000-kg (4,409-lb) pickup truck. Impact conditions for both tests are provided in Table 8.

For this project, the full-scale vehicle crash test using the small car was deemed unnecessary. Prior testing has shown that G4(1S) W-beam guardrails, when impacted by small cars, meet current safety performance standards (16-18). Under these conditions, the barrier performs as though it is essentially rigid, thus reducing the potential for vehicle pocketing, wheel snag, and/or occupant risk problems. As a result, full-scale vehicle crash testing proceeded with using only the 2,000-kg (4,409-lb) pickup truck.

7.2 Evaluation Criteria

Evaluation criteria for full-scale vehicle crash testing was based on three appraisal areas: (1) structural adequacy; (2) occupant risk; and (3) vehicle trajectory after collision. For the longitudinal barrier to be considered structurally adequate, it must either contain or redirect the vehicle, or allow the vehicle to penetrate in a controlled, predictable manner. Occupant risk was evaluated by determining to what degree the vehicle's occupant will be subjected to hazards. This would include occupant compartment intrusion, occupant impact velocities within the vehicle's interior, and accelerations applied to the occupant during collision. Vehicle trajectory

after collision was evaluated in order to determine if the vehicle's post-impact trajectory may cause secondary multi-vehicle accidents from the vehicle being redirected into other lanes of traffic. These three criteria are defined in Table 9. The full-scale vehicle crash tests were conducted and reported in accordance with the procedures provided in NCHRP Report No. 350.

Table 8. NCHRP Report No. 350 Test Level 3 Crash Test Conditions

Test Article	Test Designation	Test Vehicle	Impact Conditions		Evaluation Criteria [1]
			Speed (km/hr)	Angle (degrees)	
Longitudinal Barrier	3-10	820C	100	20	A,D,F,H,I,K,M
	3-11	2000P	100	25	A,D,F,K,L,M

[1] Evaluation criteria explained in Table 9.

Table 9. NCHRP Report No. 350 Evaluation Criteria for Crash Tests

Structural Adequacy	A.	Test article should contain and redirect the vehicle; the vehicle should not penetrate, underride, or override the installation although controlled lateral deflection of the test article is acceptable.
Occupant Risk	D.	Detached elements, fragments or other debris from the test article should not penetrate or show potential for penetrating the occupant compartment, or present an undue hazard to other traffic, pedestrians, or personnel in a work zone. Deformations of, or intrusions into, the occupant compartment that could cause serious injuries should not be permitted.
	F.	The vehicle should remain upright during and after collision although moderate roll, pitching, and yawing are acceptable.
	H.	Longitudinal and lateral occupant impact velocities should fall below the preferred value of 9 m/s, or at least below the maximum allowable value of 12 m/s.
	I.	Longitudinal and lateral occupant ridedown accelerations should fall below the preferred value of 15 g's, or at least below the maximum allowable value of 20 g's.
Vehicle Trajectory	K.	After collision it is preferable that the vehicle's trajectory not intrude into adjacent traffic lanes.
	L.	The occupant impact velocity in the longitudinal direction should not exceed 12 m/sec, and the occupant ridedown acceleration in the longitudinal direction should not exceed 20 G's.
	M.	The exit angle from the test article preferably should be less than 60 percent of test impact angle measured at time of vehicle loss of contact with test device.

8 TEST CONDITIONS

8.1 Test Facility

The testing facility is located at the Lincoln Air-Park on the northwest side of the Lincoln Municipal Airport and is approximately 8.0 km (5 mi.) northwest of the University of Nebraska-Lincoln.

8.2 Vehicle Tow and Guidance System

A reverse cable tow system with a 1:2 mechanical advantage was used to propel the test vehicle. The distance traveled and the speed of the tow vehicle were one-half that of the test vehicle. The test vehicle was released from the tow cable before impact with the guardrail system. A digital speedometer was located on the tow vehicle to increase the accuracy of the test vehicle impact speed.

A vehicle guidance system developed by Hinch (19) was used to steer the test vehicle. A guide-flag, attached to the front-right wheel and the guide cable, was sheared off before impact with the guardrail system. This allowed the vehicle to be completely unrestrained at impact. The 9.5-mm (3/8-in.) diameter guide cable was tensioned to approximately 13.3 kN (3 kips), and supported laterally and vertically every 30.48 m (100 ft) by hinged stanchions. The hinged stanchions stood upright while holding up the guide cable, but as the vehicle was towed down the line, the guide-flag struck and knocked each stanchion to the ground. For test PR-1, the vehicle guidance system was 218-m (715-ft) long.

8.3 Test Vehicle

For test PR-1, a 1996 Chevrolet 2500 3/4-ton pickup truck was used as the test vehicle. The test inertial and gross static weights were 1,994 kg (4,396 lbs). The test vehicle is shown in Figure 23, and vehicle dimensions are shown in Figure 24. The longitudinal component of the

Figure 23. Test Vehicle, Test PR-1

Date: 6/20/02 Test Number: PR-1 Model: 2500

Make: Chevrolet Vehicle I.D.#: 1GCFC24MOT2178386

Tire Size: 1J 225/75 R16 Year: 1996 Odometer: 165742

*(All Measurements Refer to Impacting Side)

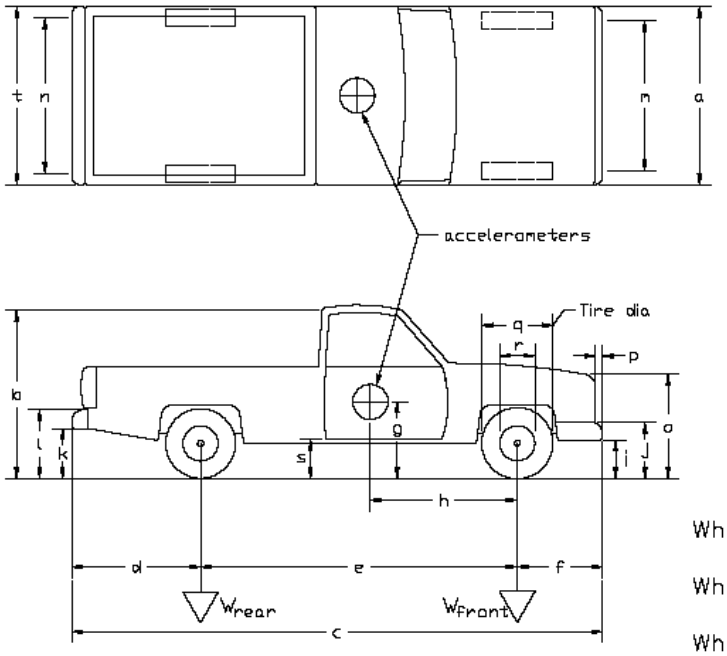

Vehicle Geometry – mm

a	1892	b	1775
c	5537	d	1295
e	3353	f	889
g	667	h	1499
i	378	j	629
k	527	l	718
m	1575	n	1607
o	968	p	83
q	730	r	445
s	403	t	1835

Wheel Center Height Front 349

Wheel Center Height Rear 356

Wheel Well Clearance (FR) 835

Wheel Well Clearance (RR) 873

Engine Type 8 CYL. GAS

Engine Size 5.7 L 350 CID

Transmission Type:

(Automatic) or Manual

FWD or (RWD) or 4WD

Weights – kg

	Curb	Test Inertial	Gross Static
W_{front}	1007	1104	1104
W_{rear}	746	890	890
W_{total}	1753	1994	1994

Note any damage prior to test: none

Figure 24. Vehicle Dimensions, Test PR-1

center of gravity was determined using the measured axle weights. The location of the final center of gravity is shown in Figure 24.

Square, black and white, checkered targets were placed on the vehicle to aid in the analysis of high-speed film and E/cam video, as shown in Figure 25. One target was placed directly above each wheel on the test vehicle. Five targets were also placed on the top of the vehicle with one on the hood and two in the bed of the pickup positioned along its longitudinal centerline. Two additional targets were placed on the windshield. Round targets were placed on the both doors as well as the roof of the vehicle to display the center of gravity location.

The front wheels of the test vehicle were aligned for camber, caster, and toe-in values of zero so that the vehicle would track properly along the guide cable. Two 5B flash bulbs were mounted on both the hood and roof of the vehicle to pinpoint the time of impact with the guardrail on the high-speed film and E/cam video. The flash bulbs were fired by a pressure tape switch mounted on the front face of the bumper and on the driver-side corner. A remote-controlled brake system was installed in the test vehicle so the vehicle could be brought safely to a stop after the test.

8.4 Data Acquisition Systems

8.4.1 Accelerometers

Two triaxial piezoresistive accelerometer systems, located at the vehicle's center of gravity, were used to measure vehicle accelerations. The primary accelerometer unit had a range of ±200 G's and was used to measure the acceleration in the longitudinal, lateral, and vertical directions at a sample rate of 10,000 Hz. The environmental shock and vibration sensor/recorder system, Model EDR-4M6, was developed by Instrumented Sensor Technology (IST) of Okemos,

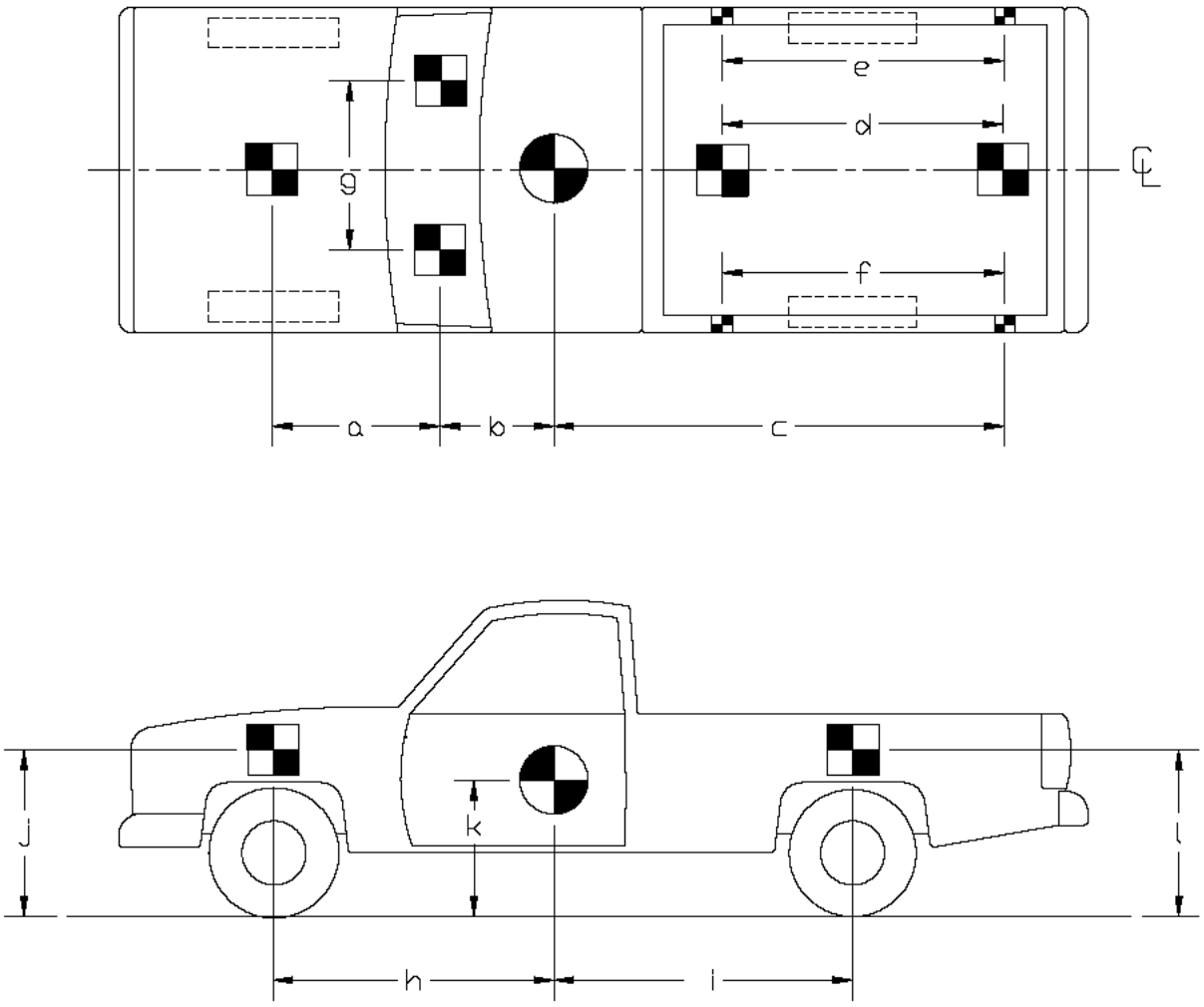

TEST #: PR-1

TARGET GEOMETRY (mm)

a	845	d	1607	g	1080	j	937
b	794	e	2153	h	1499	k	667
c	2604	f	2158	i	1854	l	975

Figure 25. Vehicle Target Locations, Test PR-1

Michigan. The EDR-4 is a self-contained, user-programmable acceleration sensor/recorder with a 74dB dynamic range. During active recording, acceleration signals are digitized to 12-bit resolution and stored in digital memory onboard the unit. The EDR-4 has a maximum sampling rate of 10,000 Hz and maximum cross-axis sensitivity of ±3.0%. The EDR-4 was configured with 6 MB of RAM memory and offers recording capability from six input channels simultaneously. Three differential channels are connected to internally mounted, voltage-mode, piezoresistive accelerometers. The remaining three channels are connected to a Humphrey 3-axis rate transducer. Analog low-pass filtering was used internally in the EDR-4 to condition the analog input signal. A 4-pole Besel low-pass filter with a –3dB cut-off frequency of 1,500 Hz was used. Computer software, "DynaMax 1 (DM-1)" and "DADiSP", was used to analyze, filter, and plot the accelerometer data.

The secondary accelerometer unit was used as a backup should the data from the EDR-4 be lost or corrupted. This accelerometer with a range of ±200 G's also measured the acceleration in the longitudinal, lateral, and vertical directions at a sample rate of 3,200 Hz. Instrumental Sensor Technology (IST) of Okemos, Michigan, developed the environmental shock and vibration sensor/recorder system, Model EDR-3. The EDR-3 is a self-contained, user-programmable acceleration sensor/recorder with a 74dB dynamic range. During active recording, acceleration signals are digitized to 10-bit resolution and stored in digital memory onboard the unit. The EDR-3 has a maximum cross-axis sensitivity of ±3.0%. The EDR-3, configured with 256 KB of RAM memory, offers recording capability from three input channels simultaneously. The differential channels were used to sample internally mounted, voltage-mode, piezoresistive accelerometers. Analog low-pass filtering was used internally in the EDR-3 to condition the analog input signal. A Butterworth low-pass filter with a –3dB cut-off

frequency of 1,120 Hz was used for anti-aliasing. Computer Software, "DynaMax 1 (DM-1)" and "DADiSP", was used to analyze, filter, and plot the accelerometer data.

8.4.2 Rate Transducers

Test vehicle angular rates of motion were measured using a Humphrey 3-axis rate transducer with a range of 360 deg/sec in each of the three directions (roll, pitch, and yaw). The rate transducer was rigidly attached to the vehicle near the test vehicle's center of gravity. Rate transducer signals, excited by a 28-volt DC power supply, were received through the three single-ended channels located externally on the EDR-4M6 and stored in the internal memory. The raw data was then downloaded for analysis and plotted. Computer software, "DynaMax 1 (DM-1)" and "DADiSP", was used to analyze and plot the rate transducer data.

8.4.3 High-Speed Photography

For test PR-1, two high-speed 16-mm Red Lake Locam cameras, five high-speed Red Lake E/cam video cameras, and five Canon digital video (DV) cameras were used to film the crash test. The Locams had operating speeds of approximately 500 frames/sec, the E/cam cameras had operating speeds of 500 frames/sec, the DV cameras had a standard operating speed of 29.97 frames/sec. A Locam, with a wide-angle 12.5-mm lens, and two E/cams were placed overhead of the initial impact point on the barrier, providing a perpendicular view of the barrier with respect to the ground. Downstream from the barrier, a Locam and a DV camera were place to give a field of view parallel to the barrier. An E/cam and DV camera were placed behind the barrier downstream of the initial impact point. Another E/cam and DV camera were also placed behind the barrier upstream of the initial impact point. At the upstream end of the barrier, another E/cam and DV camera were placed to give a slightly overhead, parallel field of view of the barrier. One DV camera was placed on the traffic side of the barrier, giving a field of view

perpendicular to the barrier and parallel to the ground. A schematic of all twelve camera locations for test PR-1 is shown in Figure 26. The Locam film and E/cam video was analyzed using the Vanguard Motion Analyzer and the Redlake Motion Scope software, respectively. Actual camera speed and camera divergence factors were considered in the analysis of the high-speed film.

8.4.4 Pressure Tape Switches

For test PR-1, five pressure-activated tape switches, spaced at 2-m (6.56-ft) intervals, were used to determine the initial impact speed of the vehicle. As the left-front tire of the test vehicle contacted each tape switch, a strobe light was fired which sent an electronic timing signal to the data acquisition system. The data acquisition system was connected to a computer where the signal was recorded using the "Test Point" software. Test vehicle speed was then determined by comparing the time between electronic signals and the distance between tape switches. Strobe lights and high-speed film analysis were used only as a backup in the event that vehicle speed could not be determined from the electronic data.

8.4.5 Strain Gauges

Two strain gauges were placed on the back side of the guardrail and located on the vertical neutral axis, one on each side of the center hump, at the midspan between post nos. 10 and 11, as shown in Figure 27. These gauges were used to measure the dynamic axial rail strains. Two strain gauges were also applied to each post for post nos. 13 through 16, as shown in Figure 28. The gauges were placed on the inside of the front flange, one on each side of the web, 19 mm (0.75 in.) from the outside edge of the flange, and approximately 51 mm (2 in.) above the ground. Weldable strain gauges, consisting of model LWK-06-W250B-350, manufactured by Micro-Measurements Division of the Measurements Group, Incorporated, in

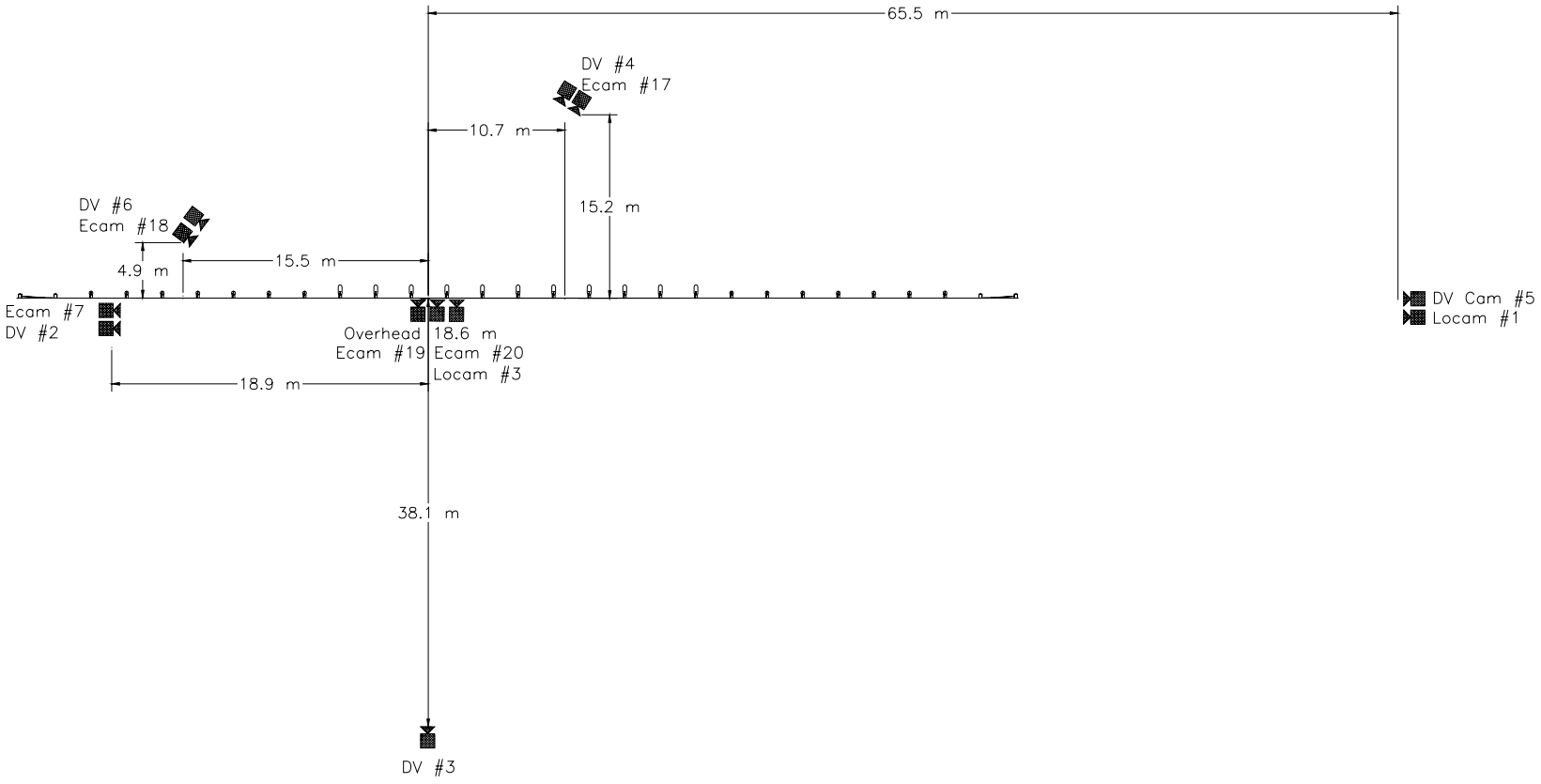

Figure 26. Location of High-Speed Cameras, Test PR-1

Raleigh, North Carolina, were used. The gauges had a nominal resistance of 350±1.4 ohms and a gauge factor of 2.03. A Measurements Group Vishay Model 3210 signal-conditioning amplifier was used to power, condition, and amplify the low-level signals to high-level signals for acquisition by a Keithley-Metrabyte DAS-1802HC data acquisition board. The computer programs ”Test Point” and “DADiSP” were used to record and analyze the data.

Figure 27. Location of Strain Gauges on Guardrail

Figure 28. Location of Strain Gauges on Post No. 15

8.4.6 Load Cell

A load cell was attached to the upstream anchor cable in order to measure the load transferred from the guardrail to the anchor post. The load cell consisted of a steel cylinder with two weldable strain gauges attached to the outside and on opposite sides from one another, as shown in Figure 29. The attachment of the load cell to the anchor cable is shown in Figure 30. The load cell was calibrated on a hydraulic press from a range of 0 to 111 kN (25 kips).

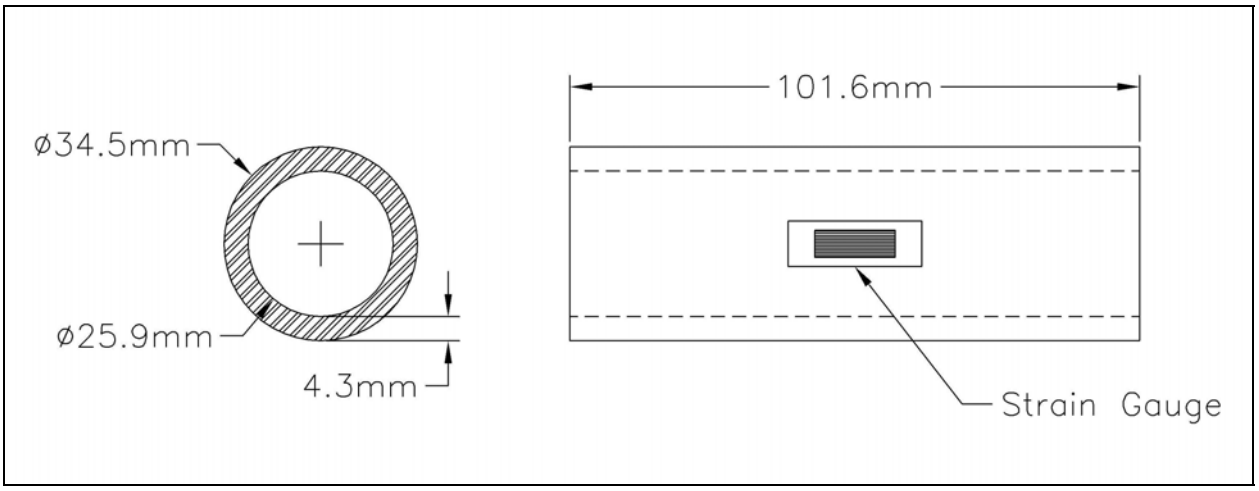

Figure 29. Load Cell Dimensions

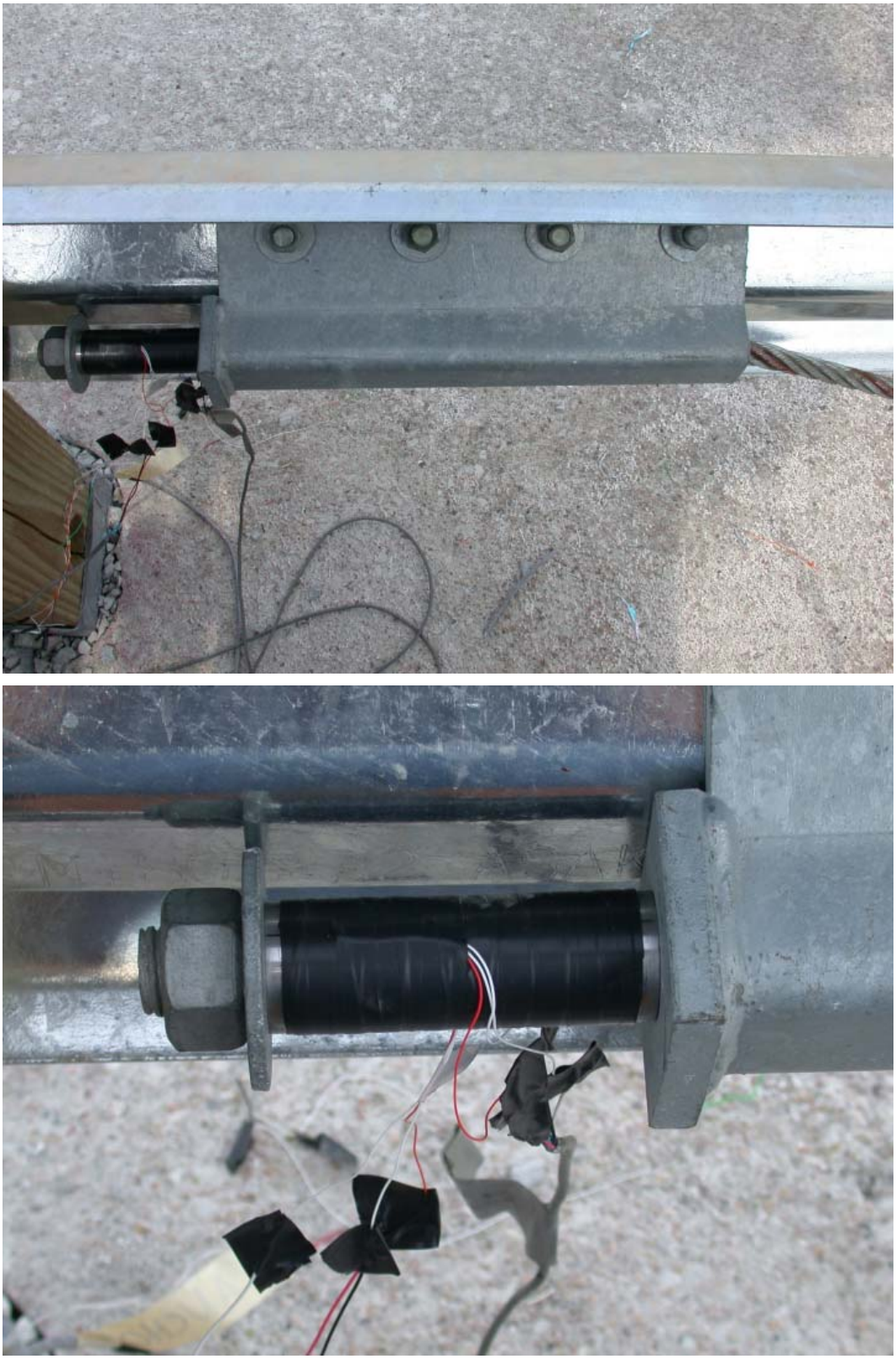

Figure 30. Attachment of Load Cell to Guardrail Anchor Cable

9 POST-IN-ROCK GUARDRAIL DESIGN DETAILS

The test installation consisted of 53.34 m (175 ft) of standard 2.66-mm (12-gauge) thick W-beam guardrail supported by steel posts, as shown in Figure 31. Anchorage systems, similar to those used on tangent guardrail terminals, were utilized on both the upstream and downstream ends of the guardrail system. Photographs of the test installation are shown in Figures 32 through 35.

The entire system was constructed using 25 steel and 4 timber guardrail posts, spaced on 1,905-mm (75-in.) centers. Post nos. 3 through 27 were W152x13.4 (W6x9) galvanized ASTM A36 steel posts, measuring 1,346 mm (53 in.) in length. Post nos. 1, 2, 28, and 29 were timber posts measuring 140-mm (5.5-in.) wide x 190-mm (7.5-in.) deep x 1,090-mm (43-in.) long and were placed in steel foundation tubes installed in 203-mm (8-in.) diameter drilled holes. The timber posts and foundation tubes were part of anchor systems designed to replicate the capacity of a tangent guardrail terminal.

Post nos. 3 through 9 and 21 through 27 were embedded 610 mm (24 in.) into 203-mm (8-in.) diameter holes cored into the concrete tarmac and backfilled with ASTM C33 coarse aggregate. Post nos. 10 through 20 were embedded 610 mm (24 in.) into the front of elongated drilled holes and backfilled with ASTM C33 coarse aggregate, as shown in Figures 31 and 34. It was determined from simulation that deflections for posts nos. 3 through 9 and 21 through 27 would be small, making installation of the posts in an elongated hole unnecessary. Post nos. 3 through 27 used 152-mm (6-in.) wide x 203-mm (8-in.) deep x 356-mm (14-in.) long, routed wood spacer blocks to block the rail away from the posts, as shown in Figures 32 through 34.

One standard 2.66-mm (12-gauge) thick W-beam rail measuring 7,620 mm (300 in.) long was placed between post nos. 1 and 5, as shown in Figure 31. Ten standard 2.66-mm (12-guage)

thick W-beam rails, each measuring 3,810 mm (150 in.) in length, were placed between post nos. 5 and 25. One standard 2.66-mm (12-gauge) thick W-beam rail measuring 7,260 mm (300 in.) long was place between post nos. 25 and 29. The top mounting height of the W-beam rail was 706 mm (27.8 in.). All lap-splice connections between the rail sections were overlapped downstream to reduce vehicle snagging at the splice during the crash test.

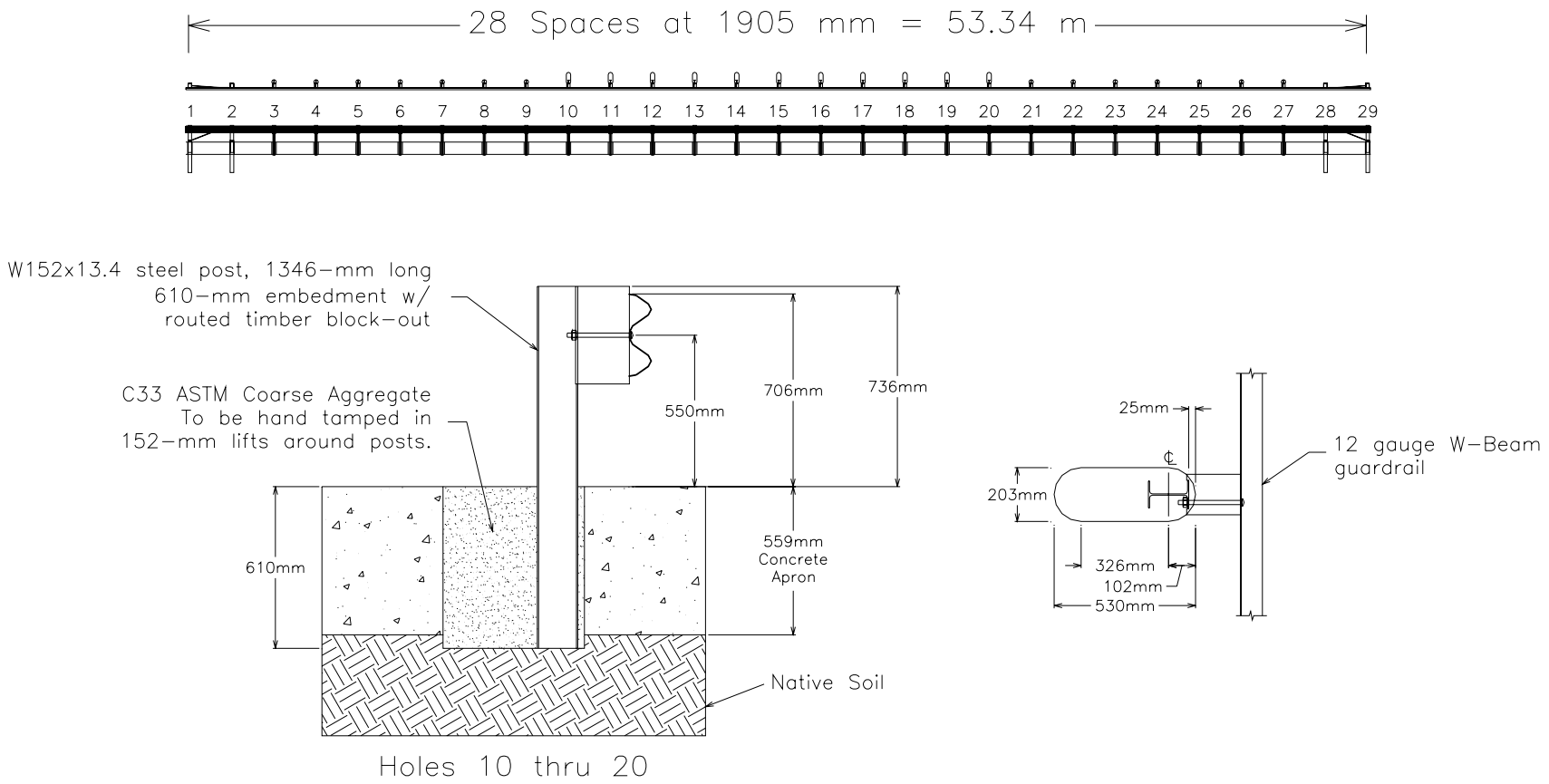

Figure 31. W-beam Guardrail Attached to Posts in Rock

Figure 32. W-beam Guardrail Attached to Posts in Rock

Figure 33. W-beam Guardrail Attached to Posts in Rock

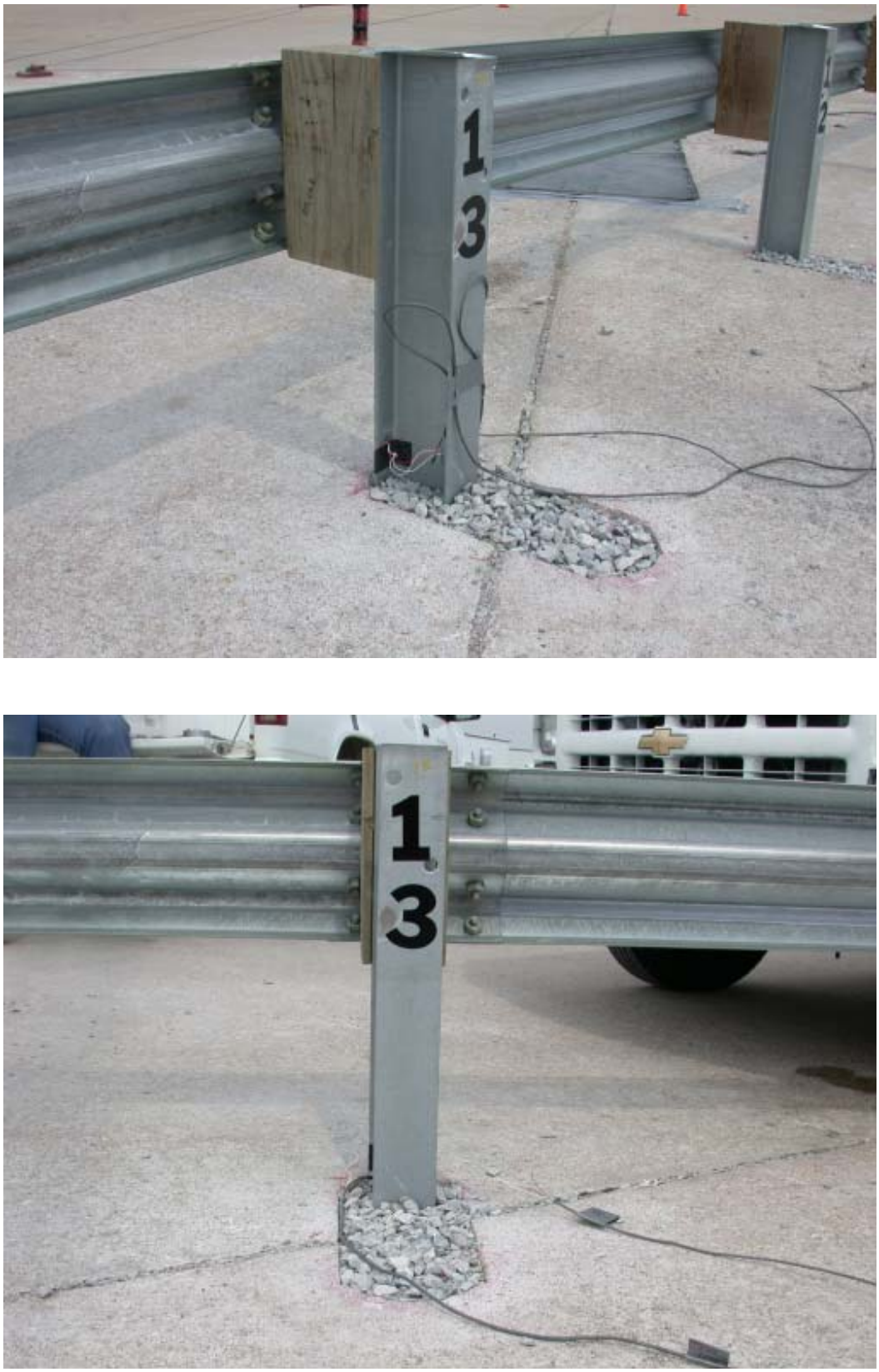

Figure 34. Typical Post Installed in Elongated Drilled Hole

Figure 35. End Anchorage System

10 CRASH TEST PR-1

10.1 Test PR-1

The 1,994-kg (4,396-lb) pickup truck impacted the W-beam guardrail at a speed of 98.9 km/hr (61.5 mph) and at an angle of 25.4 degrees. A summary of the test results and the sequential photographs are shown in Figure 36. Additional sequential photographs are shown in Figures 37 through 39. Documentary photographs of the crash test are shown in Figures 40 through 41.

10.2 Test Description

Initial impact occurred between post nos. 12 and 13, 800 mm (31.5 in.) downstream of post no. 12, as shown in Figure 42. At 0.230 sec, the guardrail achieved a maximum dynamic rail deflection of 980 mm (38.6 in.). The vehicle was parallel to the barrier and began to pitch forward at 0.297 sec with a resultant velocity of 75.9 km/hr (47.2 mph). At 0.675 sec, the vehicle lost contact with and exited the guardrail system with a resultant velocity of 74.2 km/hr (46.1 mph) and at a vehicle heading angle of approximately 18.0 degrees. At 1.070 sec, the vehicle was once again level with all four tires contacting the ground. The vehicle came to a stop 12.2 m (40.0 ft) downstream from the end of the guardrail system and 33.5 m (109.9 ft) laterally away from the traffic-side face of the guardrail, as shown in Figure 43. Times of tires leaving and touching back down are shown in Table 10. Times for significant post events are shown in Table 11.

10.3 Barrier Damage

Damage to the W-beam guardrail system was moderate, as shown in Figures 44 through 50. Barrier damage consisted mostly of deformations to the W-beam rail, contact marks on the rail, steel post deformations, and fracture of timber blockouts.

The W-beam rail was deformed and flattened between post nos. 12 and 17 as well as the rail being buckled at post no. 12. Rail contact marks were observed between post nos. 13 and 17. The W-beam had disconnected from the posts between post nos. 14 and 16. There was no significant damage to the rail upstream of post no. 12 or downstream of post no. 17.

Post no. 12 was rotated back slightly with a maximum dynamic deflection of 200 mm (7.9 in.) and a permanent set deflection of 150 mm (5.9 in.) at rail midpoint height. No deformation on the post was observed above the ground line, and there was no contact with the side of the drilled hole. Post no. 13 was rotated back with a dynamic deflection of 420 mm (16.5 in.) and a permanent set deflection of 300 mm (11.8 in.). No significant post deformation above the ground line was observed, and the post did not contact the side of the drilled hole. A small contact mark from the vehicle tire was present on the front face of the post, near the ground line. Post nos. 14 and 15 were buckled and bent downstream, touching the downstream sides of the drilled holes at the ground line. Contact marks from the vehicle wheels were evident on both posts. Post no. 16 was deflected and rotated backwards and downstream, touching the downstream side of the drilled hole at the ground line. The post did not buckle, but both lateral and rotational deformation of the post was evident above the ground line. A dynamic lateral deflection of 470 mm (18.5 in.) was observed for post no. 16 at center height of the rail. Contact marks were observed on the upstream edge of the front flange of the post. Post no. 17 was slightly deflected laterally backward. No plastic deformation of the post was observed, and the post did not contact the side of the drilled hole. No significant post deflection or deformation was observed for post nos. 1 through 11 and 18 through 29. The upstream and downstream anchorage systems showed no significant amount of damage or movement. Post deflections were obtained from analysis of the overhead Locam high-speed film and were measured at the

top of the post. Post deflections at the rail midpoint height were calculated from geometry and assumed that the post remained straight and rotated around its front bottom flange.

The wooden blockouts on post nos. 14 and 15 disengaged from the posts and landed behind and downstream of the guardrail. The blockout at post no. 16 disengaged from the rail but remained attached to the post. Slight splintering of the blockout was evident. The blockouts at post nos. 1 through 13 and 17 through 29 remained attached to the W-beam rail, and no significant evidence of damage was observed.

The permanent set deflections for the guardrail posts are shown in Figures 44 through 50. The maximum lateral permanent set rail deflection was 670 mm (26.3 in.) at the centerline of post no. 15. The maximum lateral dynamic rail deflection was 980 mm (38.6 in.) at the midspan between post nos. 14 and 15, as determined from high-speed film.

10.4 Vehicle Damage

Exterior vehicle damage was moderate, as shown in Figures 51 through 54. Vehicle damage was localized to the left side of the front bumper and grill, the left-front quarter panel, and left-front suspension and wheel. Only minor damage was observed on the left-side door and box. No occupant compartment deformations were apparent. The left side and rear of the vehicle were undamaged. The vehicle's hood, roof, and window glass were also undamaged.

Contact marks were visible along the lower left side of the vehicle. Most of the vehicle deformation was found at the left-front quarter panel and on the left side of the front bumper. The front bumper was buckled in the center, and the left side of the bumper was deformed inward and was contacting the vehicle's steel frame rail. The left side of the front grill was broken, and the left headlight was detached from the vehicle. The left-front quarter panel was deformed inward toward the engine compartment. The upper and lower control arms and tie rod

on the left-front side suspension were deformed but remained attached to the wheel. The left-front tire was deflated with small holes visible in the sidewall. The left-front rim was deformed, and contact marks were apparent. The left door had minor deformations near the front and minor contact marks were visible. The left door remained fully functional. There were minor deformations in the box near the left side of the rear bumper. Contact marks were visible on the left-rear tire but without damage to the rim or tire.

10.5 Occupant Risk Values

The longitudinal and lateral occupant impact velocities (OIV's) were determined to be 5.09 m/s (16.70 ft/s) and 4.74 m/s (15.55 ft/s), respectively. The maximum 0.010-sec average occupant ridedown decelerations (ORD's) in the longitudinal and lateral directions were 8.04 g's and 7.11 g's, respectively. The longitudinal and lateral OIV and ORD were within the preferred limits of NCHRP Report No. 350. The results of the occupant risk, determined from the accelerometer data, are summarized in Figure 36. Results are shown graphically in Appendix D. The results from the rate transducer are shown graphically in Appendix E, however, pitch data was lost during testing and is not included.

10.6 Strain Gauge Results

Plots of strain versus time, as measured from the gauges applied to posts, are shown in Figure 55. It should be noted that the data plots for each individual gauge have been adjusted to all begin at time zero as opposed to showing the actual time lags. For post nos. 13, 14, and 16, only one of the two strain gauges applied to each post was found to provide acceptable data. However, both gauges provided acceptable data for post no. 15. It is assumed that a standard steel post will yield between 250 to 290 MPa (36 to 42 ksi), with the associated strain at yield ranging between 0.00124 to 0.00145. Analysis of Figure 55 indicates that the posts yielded at

each strain gauge location, likely due to the posts being subjected to bending moments about both axes as well as torsional loading. As a result, impact loads on the posts could not be determined from only one or two strain gauge readings on each post.

For the strain gauges located on the guardrail and the anchor cable's load cell, the maximum measured strains were all under the calculated yield strains. As a result, this recorded data was considered useful. Plots of the calculated tensile load in the guardrail and anchor cable are shown in Figures 56 and 57, respectively. The tensile loads were calculated based on measured strains in both elements using Hooke's law. It should be noted that the data plots for each individual gauge have been adjusted to all begin at time zero as opposed to showing the actual time lags.

10.7 Discussion

Analysis of test results for test PR-1 verified that the W-beam guardrail with the critical post installation design adequately contained and redirected the vehicle with controlled lateral displacements of the guardrail. No detached guardrail system elements or fragments posed any risk of penetrating the occupant compartment nor created any undue hazard to other traffic. There were no deformations of or intrusions into the occupant compartment. The test vehicle did not override nor penetrate the W-beam guardrail and remained upright during and after collision. Vehicle roll, pitch, and yaw angular displacements did not adversely influence occupant risk safety criteria nor caused vehicle rollover and were, as a result, deemed acceptable. The vehicle's exit angle of 18.0 degrees (heading angle)was greater than 60 percent of the impact angle of 25.4 degrees. Since this evaluation criteria is only preferred and not required, the exit angle was deemed acceptable. Therefore, test PR-1 conducted on W-beam guardrail using the

critical post installation design was determined to be acceptable according to the TL-3 safety performance criteria found in NCHRP Report No. 350.

0.000 sec

0.100 sec

0.198 sec

0.300 sec

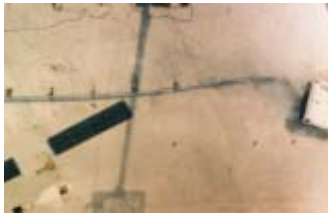

0.587 sec

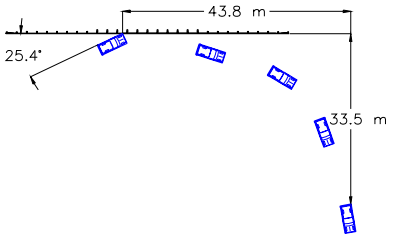

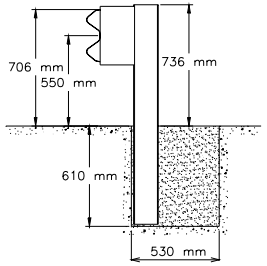

- Test Number PR-1
- Date 6/20/02
- Appurtenance ..... W-beam guardrail with posts installed in rock
- Total Length ..... 53.34 m
- Steel W-beam
  - Thickness ..... 2.66 mm
  - Top Mounting Height ..... 706 mm
- Steel Posts
  - Post Nos. 3 – 27 ..... W152x13.4 by 1,346-mm long
- Wood Posts
  - Post Nos. 1 – 2, 28 – 29 (BCT) ..... 140 mm x 190 mm by 1,080-mm long
- Wood Spacer Blocks
  - Post Nos. 3 – 27 ..... 152 mm x 203 mm by 356-mm long
- Soil Type ..... ASTM C33 Coarse Aggregate Size # - 57
- Vehicle Model
  - Curb ..... 1,753 kg
  - Test Inertial ..... 1,994 kg
  - Gross Static ..... 1,994 kg
- Vehicle Speed
  - Impact ..... 98.9 km/hr
  - Exit (resultant) ..... 60.0 km/hr
- Vehicle Angle
  - Impact (trajectory) ..... 25.4 deg
  - Exit (heading only) ..... 18.0 deg
- Vehicle Snagging ..... Minor on post nos. 14 and 15
- Vehicle Pocketing ..... None
- Vehicle Stability ..... Satisfactory
- Occupant Ridedown Deceleration (10 msec avg.)
  - Longitudinal ..... 8.04 < 20 G's
  - Lateral (Not Required) 7.11
- Occupant Impact Velocity
  - Longitudinal ..... 5.09 < 12 m/s
  - Lateral (Not Required) 4.74
- Vehicle Damage ..... Moderate
  - TAD[20] 11-LFQ-4
  - SAE[21] 11-LFEE5
- Vehicle Stopping Distance ..... 43.8 m downstream 33.5 m traffic-side face
- Barrier Damage ..... Moderate
- Maximum Rail Deflections
  - Permanent Set ..... 670 mm
  - Dynamic ..... 980 mm
- Working Width ..... 1010 mm

Figure 36. Summary of Test Results and Sequential Photographs, Test PR-1


0.000 sec

0.000 sec


0.133 sec

0.100 sec


0.267 sec

0.234 sec


0.501 sec

0.334 sec


0.667 sec

0.467 sec


0.901 sec

0.634 sec

Figure 37. Additional Sequential Photographs, Test PR-1


0.000 sec


0.000 sec


0.133 sec


0.032 sec


0.267 sec


0.112 sec


0.434 sec


0.224 sec


0.634 sec


0.310 sec


0.868 sec


0.502 sec

Figure 38. Additional Sequential Photographs, Test PR-1

0.000 sec

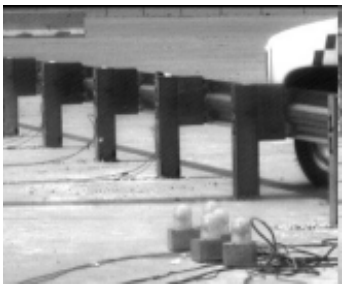

0.000 sec

0.100 sec

0.056 sec

0.200 sec

0.070 sec

0.300 sec

0.100 sec

0.434 sec

0.118 sec

Figure 39. Additional Sequential Photographs, Test PR-1

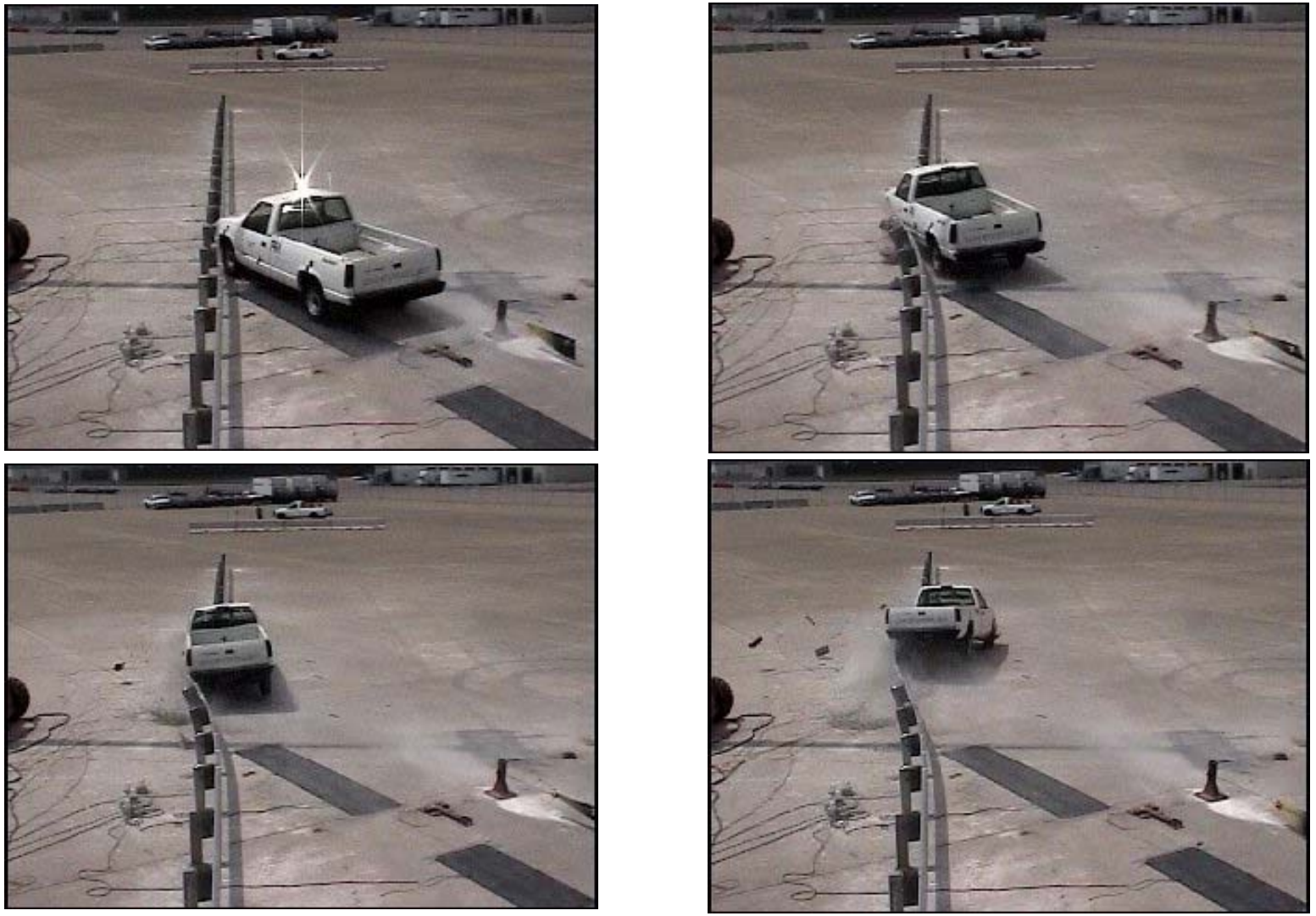

Figure 40. Documentary Photographs, Test PR-1

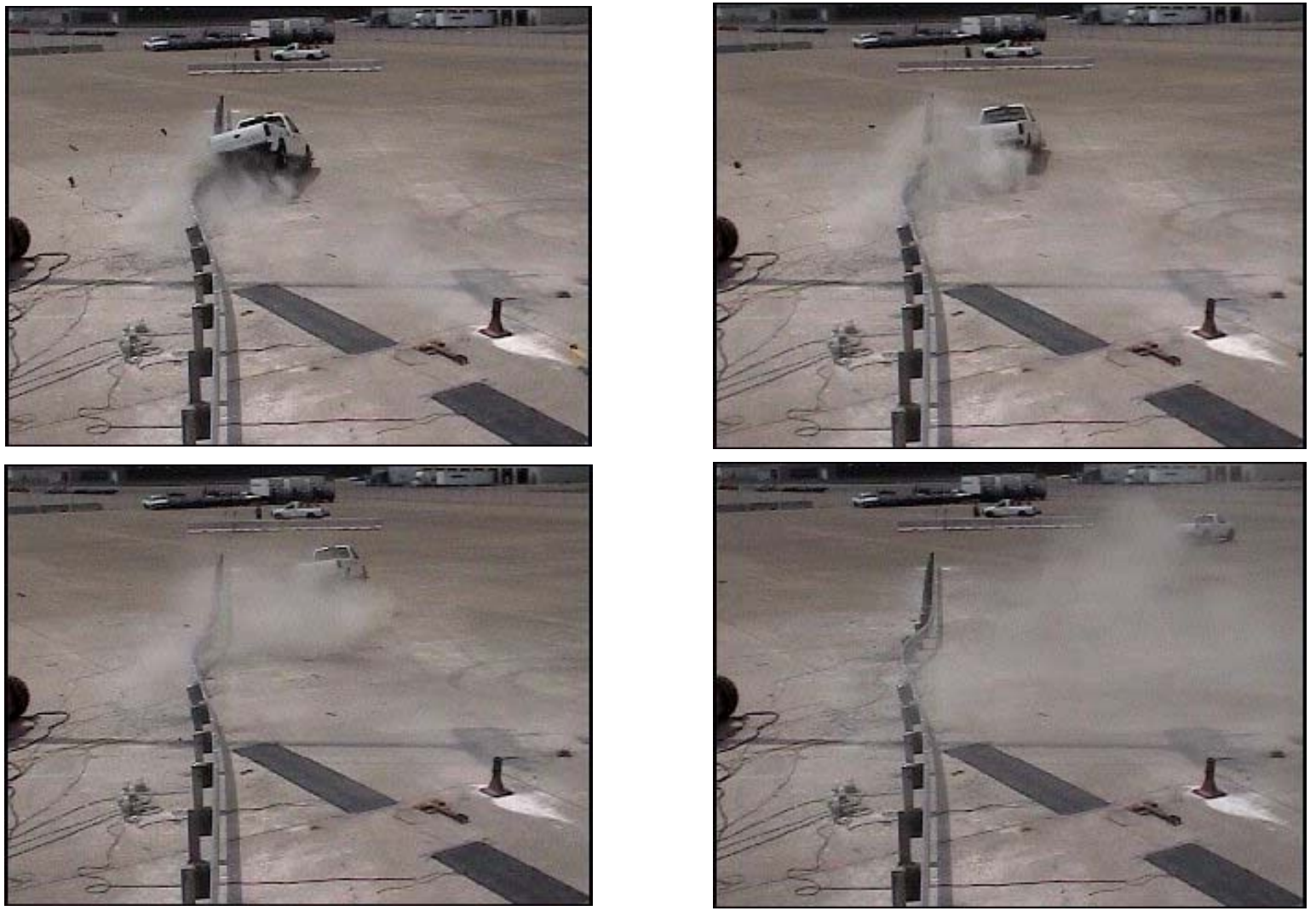

Figure 41. Documentary Photographs, Test PR-1

Figure 42. Impact Location, Test PR-1

Figure 43. Vehicle Final Position

Table 10. Tire Contact Times

Tire Location	Time Tire Leaves Ground (sec)	Time Tire Touches Back Down (sec)
Right Front	0.199	0.333
Left Front	No Loss of Contact	-
Right Rear	0.240	1.070
Left Rear	0.330	1.020

Table 11. Significant Post Events

Post No.	Time at Which Vehicle Component Contacted Post (sec)		Time of Post Event (sec)		
	Front Corner of Vehicle	Center of Left Front Wheel	Beginning of Deflection	Disconnection From Rail	Post Failure
11	No Contact	No Contact	0.028	No Disconnection	No Failure
12	No Contact	No Contact	0.005	No Disconnection	No Failure
13	0.045	0.074	0.007	No Disconnection	No Failure
14	0.122	0.158	0.031	0.110	0.130
15	0.202	0.236	0.056	0.170	0.240
16	0.298	0.322	0.115	0.325	No Failure

Figure 44. W-beam Guardrail System Damage, Test PR-1

Figure 45. W-beam Guardrail System Damage, Test PR-1

Figure 46. W-beam Guardrail System Damage, Test PR-1

Figure 47. W-beam Guardrail System Damage, Test PR-1

Figure 48. Post Nos. 12 and 13 Damage, Test PR-1

Figure 49. Post Nos. 14 and 15 Damage, Test PR-1

Figure 50. Post Nos. 16 and 17 Damage, Test PR-1

Figure 51. Vehicle Damage, Test PR-1

Figure 52. Vehicle's Left-Side Damage, Test PR-1

Figure 53. Vehicle Undercarriage Damage, Test PR-1

Figure 54. Occupant Compartment Deformations, Test PR-1

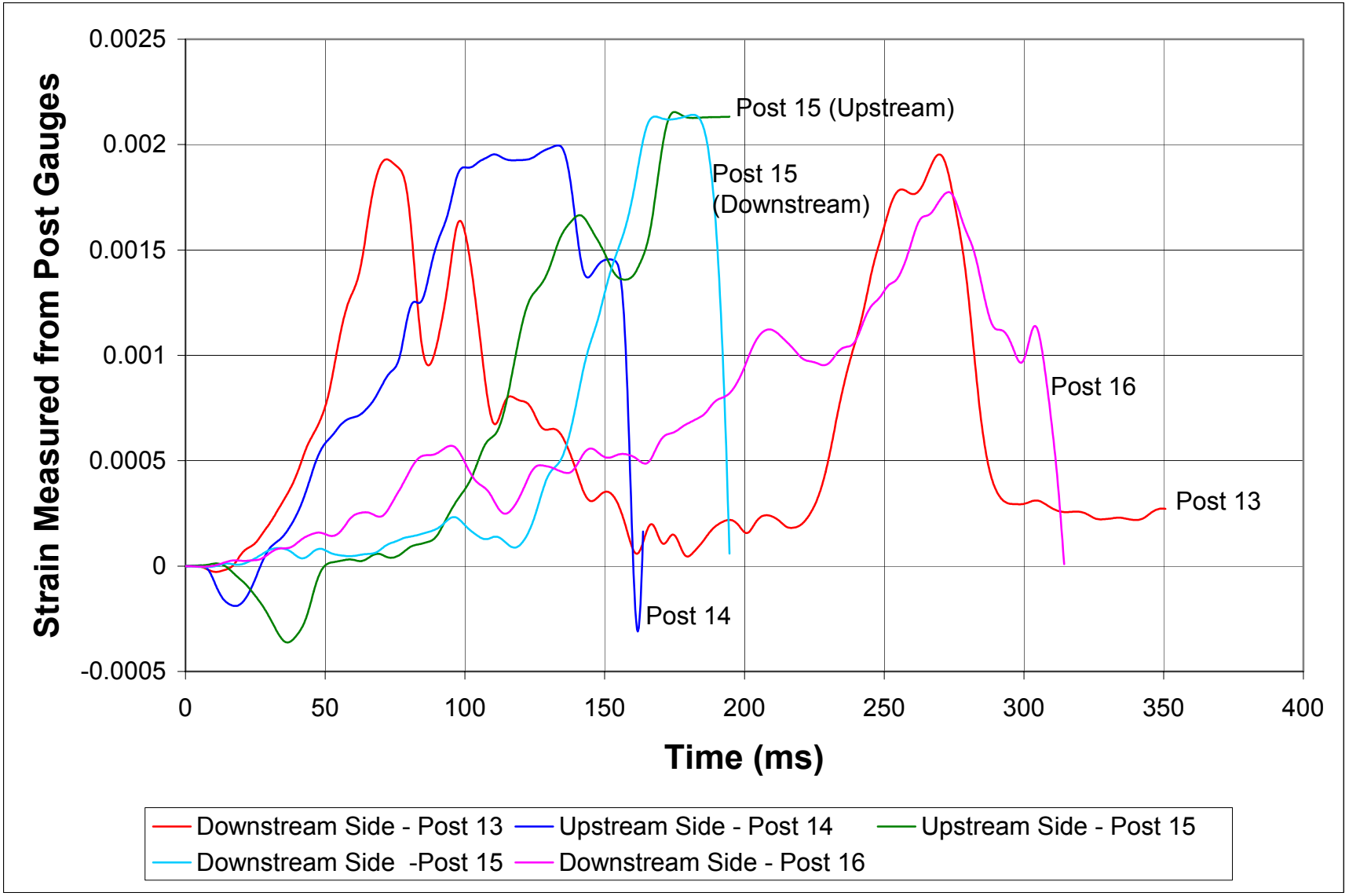

Figure 55. Measured Strain in Post Strain Gauges

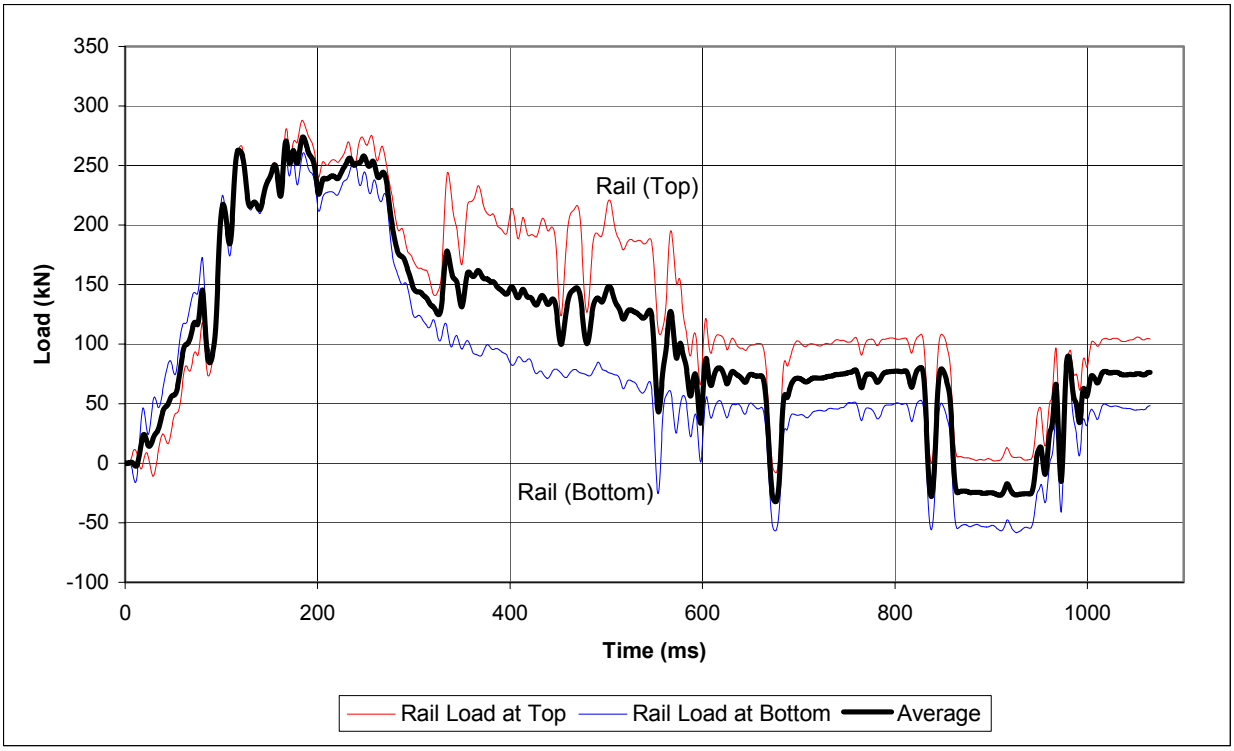

Figure 56. Tensile Load in Guardrail Determined from Strain Gauges

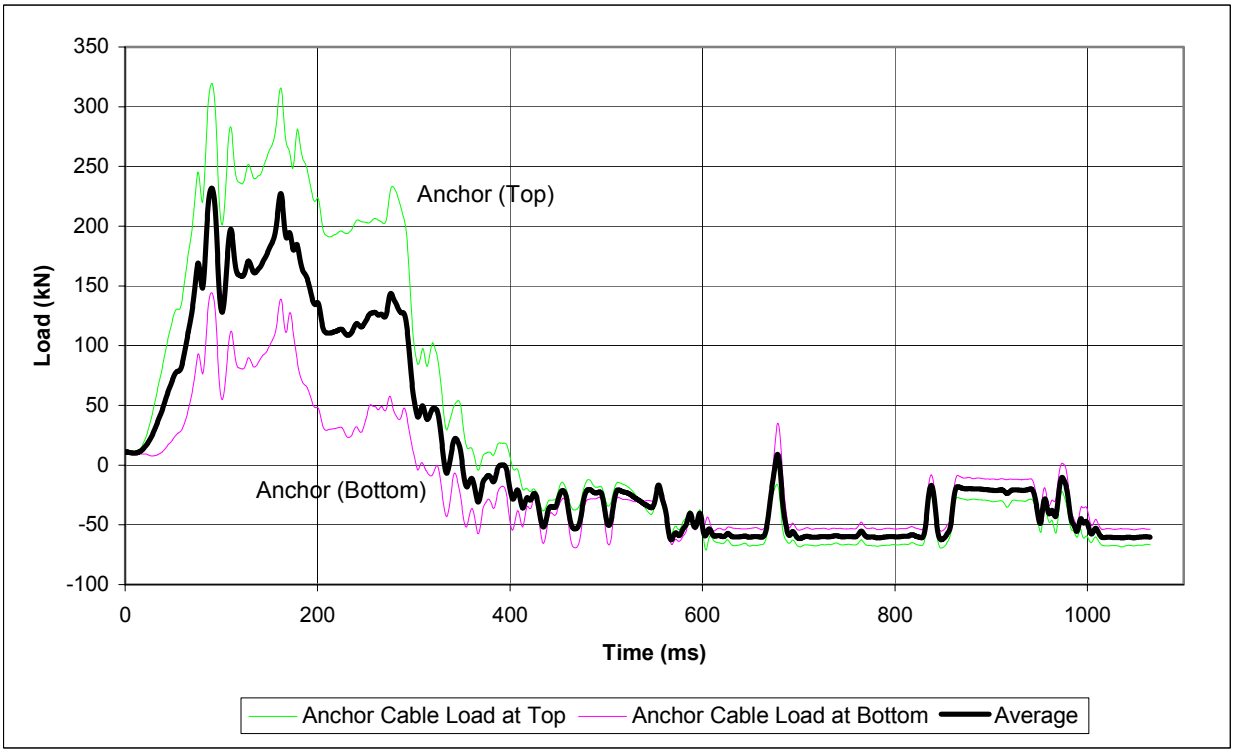

Figure 57. Tensile Load in Anchor Cable Determined from Strain Gauges

11 VALIDATION OF BARRIER VII MODEL

The BARRIER VII finite element model, used for simulation and validation of the full-scale vehicle test crash with posts installed in the critical post placement condition, was simulation no. "cip13". The validity of the model was assessed in four different ways. First, tensile loads in the rail obtained from strain gauges located on the guardrail as well as axial loads determined from a strain-gauge based load cell on the anchor cable, as shown in Figures 56 and 57, were compared to simulated maximum tensile loads in the rail elements. Second, velocity and trajectory of the test vehicle during the full-scale crash test was compared to that outputted from simulation. Third, maximum dynamic rail deflections measured from high-speed film were compared to those obtained from the simulation results. Finally, the distance that the posts deflected at the time of disengagement from the guardrail was obtained from the high-speed film analysis and compared to the BARRIER VII input for the post failure deflection limit.

The tensile load in the guardrail was measured with strain gauges attached to the rail as well as with a load cell attached to the anchor cable, as shown in Figure 56 and 57. It was assumed that the tensile load in the anchor cable was directly related to the guardrail tension at the start of the cable. Maximum average load seen in the anchor cable during the full-scale crash test was 232 kN (52.2 kips). Maximum average tensile load seen in the guardrail during the full-scale crash test was 274 kN (61.6 kips). The results from simulation show a maximum rail tensile load of 258 kN (58.0 kips). This is within acceptable levels of error and verified that our Barrier VII model had outputted reasonably accurate results.

Test vehicle velocity and trajectory over time compared well between simulation and full-scale testing. Simulation showed that the vehicle was parallel to the barrier system at 0.265 sec with a resultant speed of 77.6 km/hr (48.2 mph). Full-scale test results indicated that the test

vehicle was parallel to the barrier at 0.297 sec with a resultant speed of 75.9 km/hr (47.2 mph). For simulation, the vehicle lost contact with the barrier system at 0.399 sec with a resultant speed of 64.3 km/hr (40.0 mph) and a vehicle heading angle of 8.3 degrees. Testing showed that the test vehicle had a resultant speed of 74.0 km/hr (46.0 mph) and a vehicle heading angle of 8.5 degrees at 0.399 sec after impact. However, it was determined from analysis of high-speed film that the test vehicle exited the barrier system at approximately 0.675 sec with a resultant speed of 74.2 km/hr (46.1 mph) and a vehicle heading angle of 18.0 degrees.

Maximum dynamic deflections for the guardrail system, measured at the top of the rail, for both simulation and testing are shown in Figure 58. The BARRIER VII model predicted the maximum rail deflection roughly 15% lower than the maximum rail deflection obtained from the full-scale test. This was within the margin of error considered acceptable for simulation results. However, the location of the maximum rail deflection for simulation was closer to the impact point than that observed during testing. If further simulation work were required, recalibration of the model would be advantageous.

Post-guardrail disengagement times were compared with the high-speed film analysis results to determine how far the post had deflected at the rail midpoint height when it disengaged from the guardrail. Times for post disengagement from the guardrail for the full-scale crash test are shown in Table 11. The deflection versus time data for the posts at the rail midpoint height, obtained from the high-speed film analysis, is shown in Figure 59. Combining post disengagement times with deflection data, it was determined that the three posts that disconnected from the rail, disconnected at approximately 460 mm (18 in.) of deflection, which was greater than the failure deflection limit of 406 mm (16 in.) inputted into BARRIER VII. Since the model was stiffer than that seen in testing, increasing the failure deflection of the posts

to 460 mm (18 in.) would make the model even stiffer. However, this would also move the location of the simulated maximum dynamic rail deflection further down on the rail, making it closer to the crash tested deformed barrier shape, as shown by the modified simulation curve provided in Figure 58.

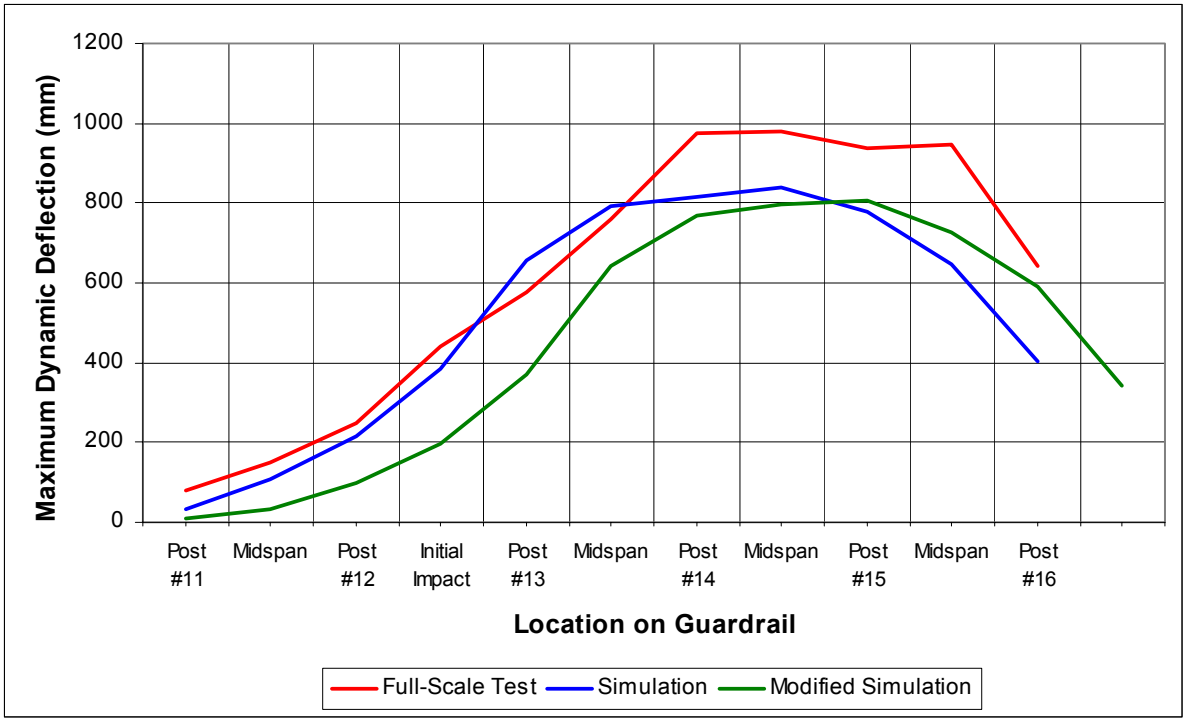

Figure 58. Comparison of Maximum Dynamic Rail Deflections

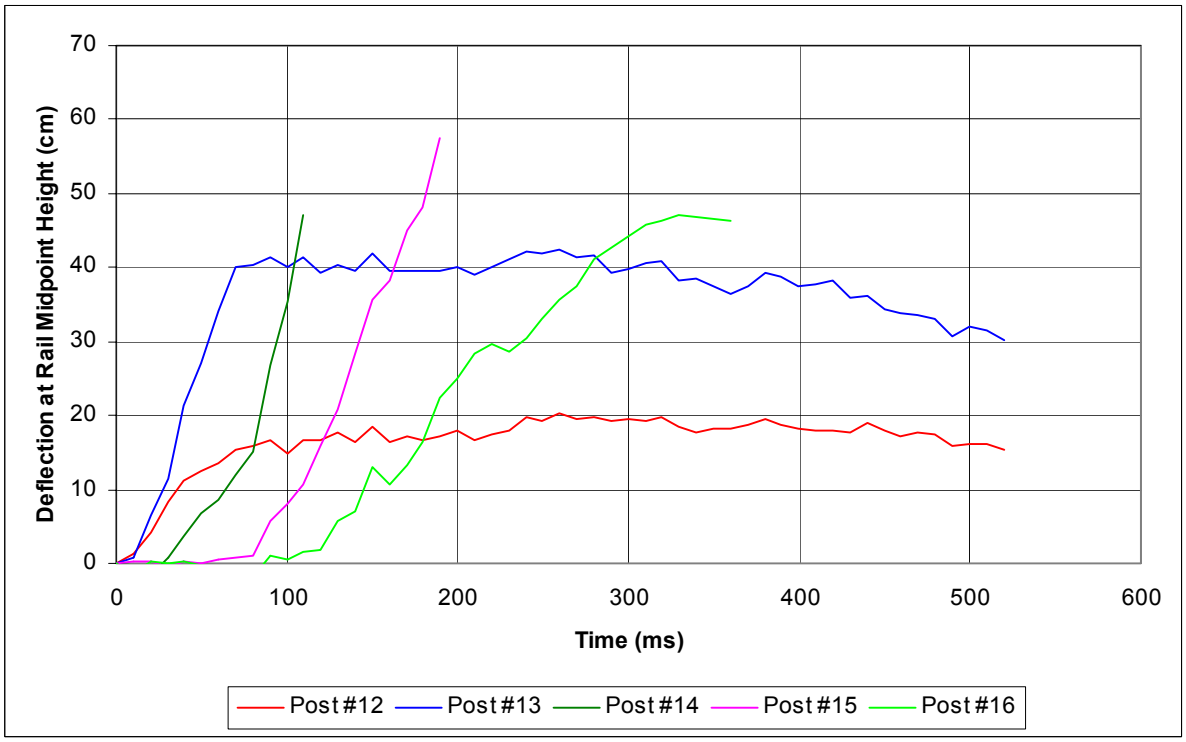

Figure 59. Post Deflection versus Time at Rail Midpoint Height

12 FINAL DESIGN

12.1 Overview

In the field, bedrock or rock formations can be found at various depths. When the rock is located at the surface, post installation procedures used in test PR-1 will allow the W-beam guardrail system to satisfy safety performance standards found in NCHRP Report No. 350. However, a problem exists if rock is found below the surface, covered by any significant amount of soil, and the post is installed in a drilled hole as tested in test PR-1, as shown in Figure 60. The additional force applied to the post as it rotates through this overlying soil will affect performance of the post, possibly causing the post to fail prematurely. As a result, further development of post installation procedures for rock located below the surface was required.

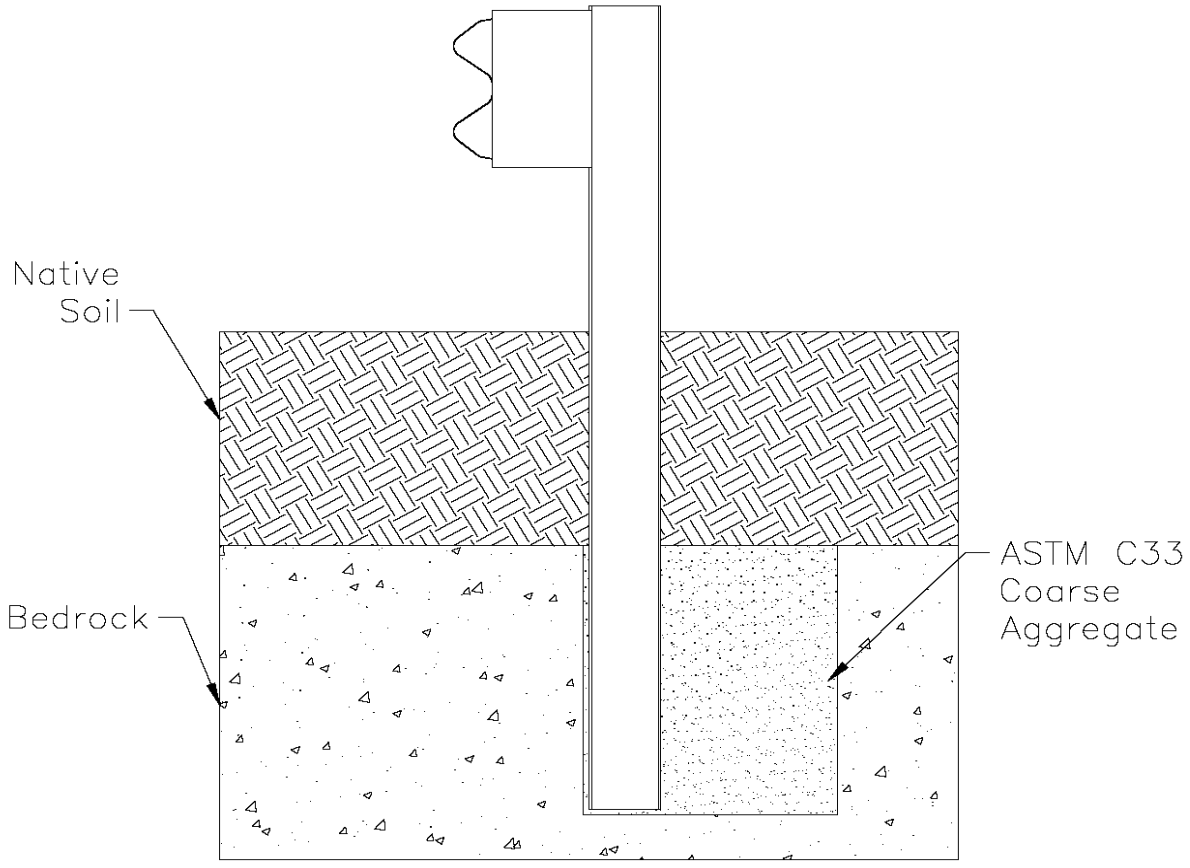

Figure 60. Post Installed in Field Conditions

12.2 Initial Development

All further post installation designs should be economical, promote ease of installation, and allow the post to dissipate the required amount of energy. The energy dissipated by the post is the most significant factor effecting guardrail system performance. As a result, post installation procedures were based on a balance of absorbed energy. From bogie test MPR-7, it was determined that the rotating post needed to dissipate at least 23 kJ (203 k-in.) of energy before post failure or post-rail disengagement occurred. Analysis of high-speed film from test PR-1 indicated that the post would disengage from the guardrail at 460 mm (18 in.) of deflection at the rail midpoint height. As result, it was determined that the sum of energy dissipated from the overlying soil, backfill material in the drilled hole, and post deformation, must fulfill these requirements for all post placement designs.

As the overlying soil thickness increases, more energy will be dissipated by the soil during post rotation, requiring the confined backfill material in the drilled hole in rock to absorb less energy. This allows for smaller drilled hole geometries in the rock, which should decrease costs of installation and make post installation easier. All designs would continue to use ASTM C33 coarse aggregate for backfill in the drilled hole, and the post would continue to be installed in the front of the drilled hole to reduce the risk of wheel snag. The post placement designs, as required by the post placement conditions, would only differ by the number of 203-mm (8-in.) diameter holes drilled on 165-mm (6.5-in.) centers and the depth to which they were drilled.

Post installation conditions were divided into four cases. The first case is the critical condition where rock is located at or near the surface. The case 1 condition, as tested in test PR-1, requires a steel post be embedded 610 mm (24 in.) into a drilled hole consisting of three 203-mm (8-in.) diameter holes drilled 165 mm (6.5 in.) on center. Case 2 conditions consist of a

certain range of overlying soil thicknesses that allow the post to be embedded 460 mm (18 in.) in a drilled hole consisting of two 203-mm (8-in.) diameter holes drilled 165 mm (6.5 in.) on center into the rock. The case 3 conditions would allow the post to be embedded 305 mm (12 in.) in a single 203-mm (8-in.) diameter drilled hole in rock. In this stage, the energy absorbed by the backfilled material is ignored and replaced by the energy absorbed from yielding of the post at the top of the drilled hole. The final case 4 condition would require the post to still be installed in a single 203-mm (8-in.) diameter hole drilled into the rock. However, the depth of drilled hole would be limited by a maximum overall post embedment depth of 1090 mm (43 in.).

12.3 Post Testing

As previously discussed, the design for the case 1 condition was completed. For cases 2 and 3, further bogie testing of posts was deemed necessary to determine the magnitude of absorbed energies resulting from a post rotating in backfill material confined in smaller drill hole geometries and from post deformation. Three new bogie tests were conducted for this phase of design, tests MPR-10, MPR-11, and PRH-1. All tests used the same test conditions and data acquisition systems as used for previous bogie testing of posts, as discussed in Section 5. The post placement configuration in test MPR-10 was found to be too stiff for use in the following analysis and was not considered in this study. However, the results for test MPR-10, as well as for all other bogie tests of posts, can be found in Appendix C. In the end, four bogie tests of posts were used to determine proper post placement designs. Test descriptions and configurations for these four tests are shown in Table 12 and Figure 61, respectively.

Test MPR-7 provided the energy dissipated by the backfill material in a 530-mm (21-in.) long hole with 610 mm (24 in.) of embedment depth in rock, as tested in test PR-1. Test MPR-11 provided the energy dissipated by the backfill material in a 370-mm (14.6-in.) long hole with

460 mm (18 in.) of embedment in rock, which was the hole geometry chosen for the case 2 condition. Test PRH-1 provided the energy of the post yielding around its strong axis in bending. Finally, test SSF-9 provided the energy dissipated by the overlying soil. The energy plots for all four bogie tests are shown in Figure 62.

The component of energy dissipation from the overlying soil at any thickness was determined from data obtained from test SSF-9, originally conducted by Coon (10). This bogie test used an instrumented W152x23.8 (W6x16) steel post with 10 strain gauges attached to the inside of the front flange to measure tensile strains in the post, as shown in Figure 64. These gauges were calibrated and correlated to known moments in the post. This allowed for the determination of the moment distribution throughout the post during impact with the bogie. From this moment distribution, the shape and magnitude of the force distribution on the post from soil resistance was obtained as was previously shown in Figure 3. This was achieved by conducting a number of iterations where the force distribution on the post was changed until the resulting moment distribution in the post matched that obtained from testing. At this point, resultant forces were computed for each strain gauge location below the surface over time. Deflections at any point on the post versus time were obtained from a string potentiometer attached to the post. Knowing the resultant force and deflection at each strain gauge, absorbed energy could be calculated. The absorbed energy determined for each gauge location was correlated with the total absorbed energy from the post rotating in soil in percent. At this point, the percent of total energy dissipated by the post was correlated with embedment depth. The results of this analysis are shown in Figure 63. Using this graph, the component of absorbed energy for any thickness of overlying soil was determined.

Table 12. Bogie Test Descriptions

Test Number	Description
MPR-7	Steel post embedded 610 mm into drilled hole and backfilled with ASTM C33 coarse aggregate. Impact speed was 6.7 m/s. Drilled hole consisted of three 203-mm diameter holes drilled on 165-mm centers. Drilled hole geometry used for Stage 1.
MPR-11	Steel post embedded 460 mm into drilled hole and backfilled with ASTM C33 coarse aggregate. Impact speed was 7.1 m/s. Drilled hole consisted of two 203-mm diameter holes drilled on 165-mm centers. Drilled hole geometry used for Stage 2.
SSF-9	Test simulates post with full embedment in native soil. Steel post is embedded 1090 mm into AASHTO M147 Grade B soil. Post is restrained at its lower front edge so that it can only rotate backwards in the same manner as the MPR tests. Impact Speed was 9.3 m/s.
PRH-1	Steel post embedded 1090 mm in rigid hole. Impact Speed was 6.7 m/s.

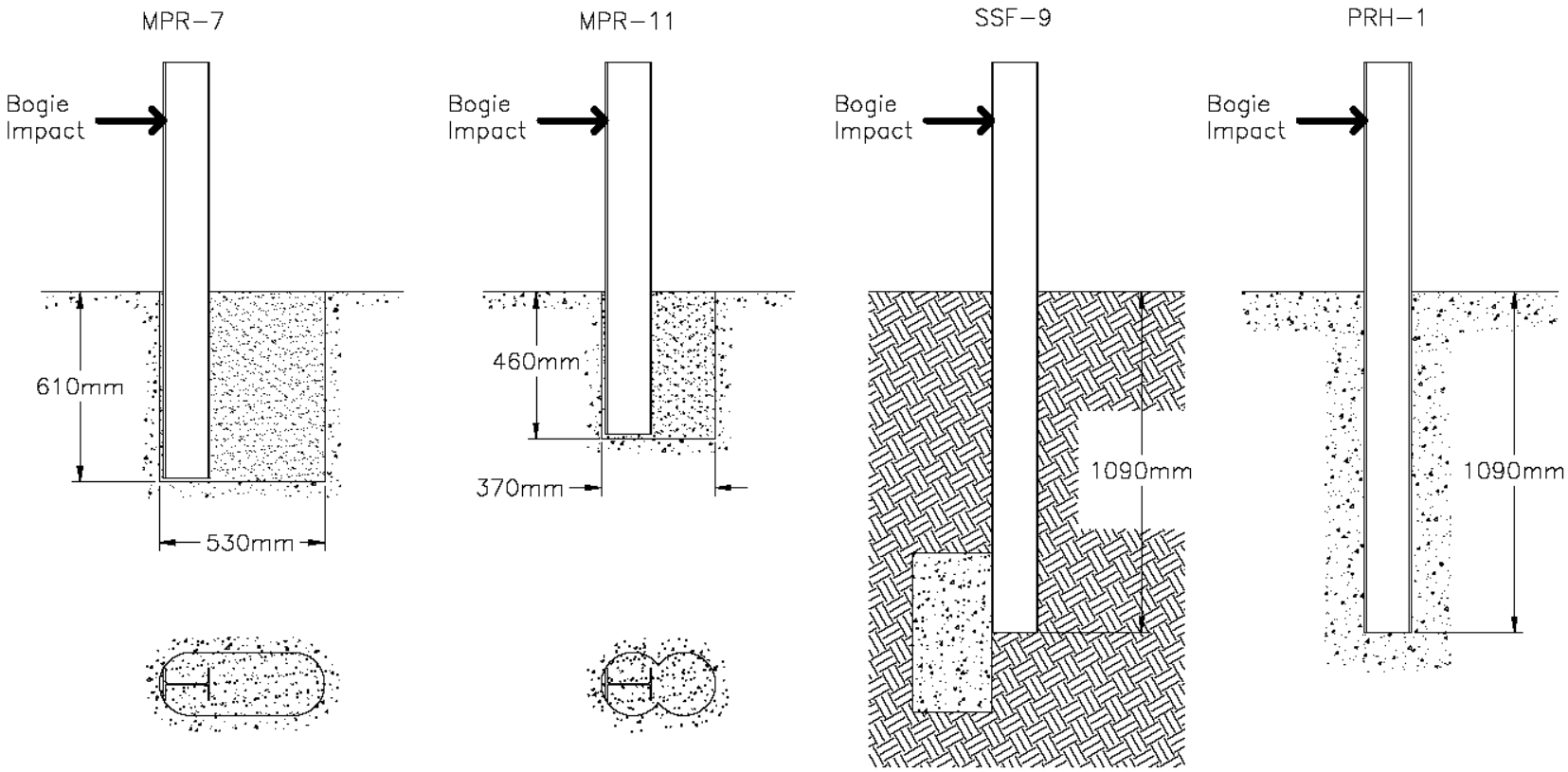

Figure 61. Configurations for Post Bogie Testing

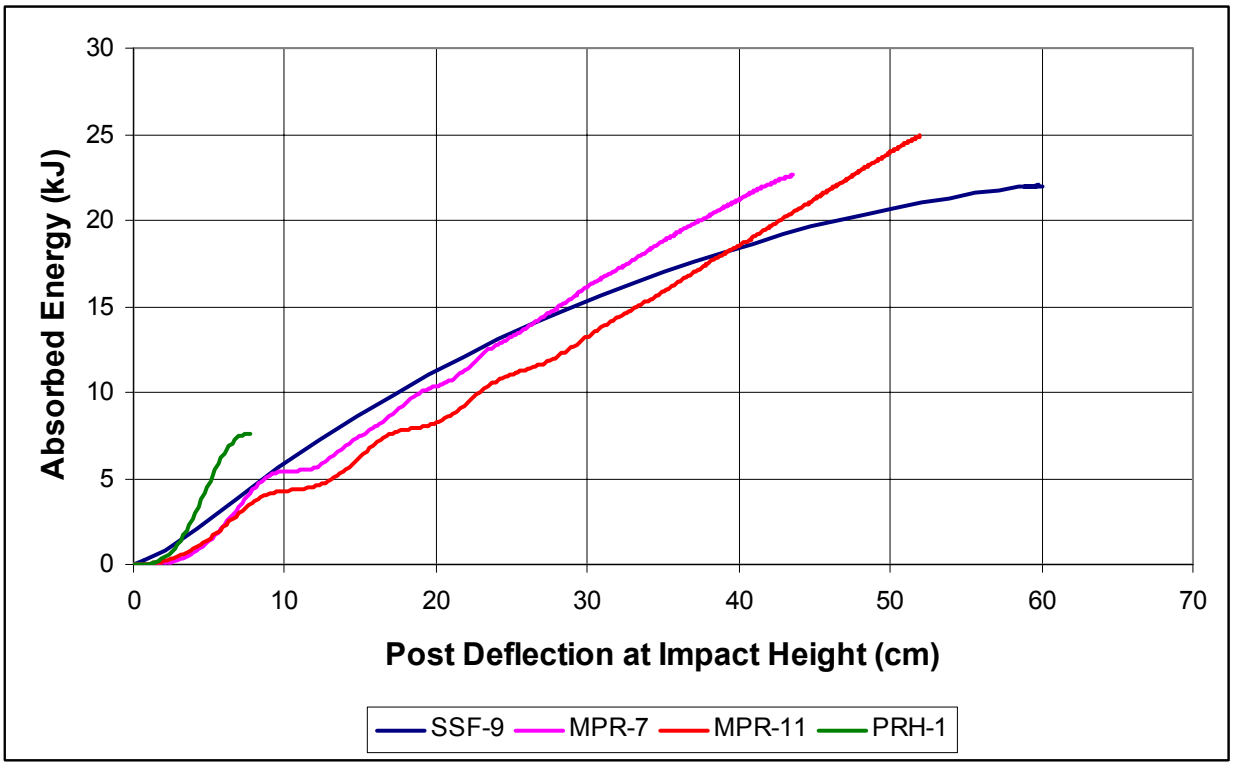

Figure 62. Absorbed Energy Plots from Bogie Testing

Figure 63. Percentage of Absorbed Energy versus Embedment Depth in Soil, Test SSF-9

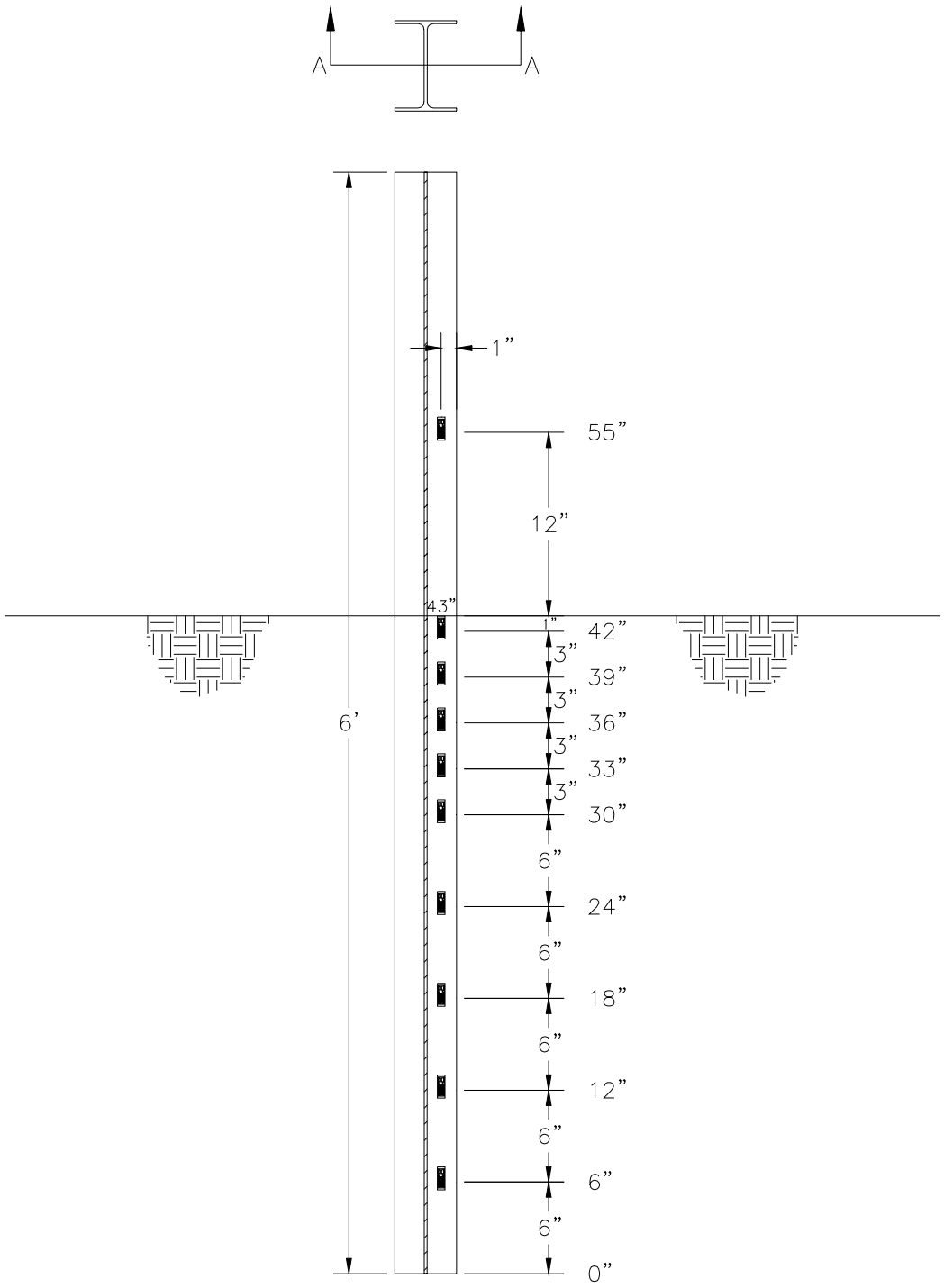

Figure 64. Strain Gauge Locations on Post, Test SSF-9

12.4 Case Condition Design

12.4.1 Case 1

Case 1 conditions consisted of rock located at or near the surface. A post placement design was determined and its performance, when installed in a W-beam guardrail system, was found to fulfill the requirements of NCHRP Report No. 350.

12.4.2 Case 2

For Case 2, it was necessary to determine a minimum depth of overlying soil that would fulfill the total energy requirement of 23 kJ (203 k-in.). For this case condition, the total energy requirement was fulfilled by a sum of the energy dissipated by the post rotating through the overlying soil, the post compressing the backfill material in the drilled hole, and post deformation, over 460 mm (18 in.) of post deflection at the rail midpoint height. Determination of the minimum thickness of overlying soil was as follows from Table 13. First, the post deflection of 460 mm (18 in.) at rail midpoint height was converted to deflections of the post at the ground line and at the top of the drilled hole in rock for varying thickness of overlying soil, as shown in the columns 4 and 5 of Table 13. Bogie post testing took place with the top of the Case 2 drilled hole at the surface, and data was based off deflections at the rail midpoint height of 550 mm (21.65 in.). When the top of the drilled hole is below the surface, the correlation between the deflections at rail midpoint height and at the top of the drilled hole will change. As a result, to allow data from testing to be applied to conditions where the top of the drilled hole in rock was some depth below the surface, the deflections at the rail midpoint height were recalculated to correlate to the deflection at the top of the drilled hole, as shown in column 6 of Table 13. Using this equivalent deflection at the rail midpoint height, the amount of energy dissipated from backfill compression and post deformation was found from the results of test

MPR-11, as shown in column 7 of Table 13. Subtracting this energy from the required amount of total energy (23 kJ), produced the energy required from the overlying soil, as shown in column 8 of Table 13. By comparing this required energy to the total dissipated energy (22.7 kJ) at 460 mm (18 in.) of deflection from test SSF-9, the percentage of energy needed from test SSF-9 was calculated, as shown in column 9 of Table 13. Finally, this value was correlated with Figure 63 and the minimum thickness of overlying soil was obtained, as shown in column 10 of Table 13. By plotting columns 3 and 10 of Table 13, a graphical determination of the minimum overlying soil for Case 2 was obtained, as shown in Figure 65. From this analysis, it was determined that a minimum thickness of 160 mm (6 in.) of overlying soil was needed to allow for the implementation of a Case 2 drilled hole geometry.

12.4.3 Case 3

For this case, energy dissipation was a combination of post rotation through the overlying soil and post yielding around its strong axis. From test PRH-1, 7.6 kJ (67.3 k-in.) of energy was dissipated by the post yielding which required that the overlying soil provide 15.4 kJ (135.7 k-in.) of energy. The overlying soil component of energy was determined to be 67.8% of the total energy from test SSF-9. Using Figure 63, it was determined that a minimum overlying soil thickness of 460 mm (18 in.) was required to allow implementation of the Case 3 drilled hole geometry.

12.4.4 Case 4

Standard post embedment depth in unconfined soils is 1,090 mm (43 in.). As a result, overall embedment depth of the post installed in a drilled hole in rock should not exceed this standard embedment depth. If the post is placed in a 203-mm (8-in.) diameter hole drilled 305 mm (12 in.) into rock when the overlying soil thickness is greater than 785 mm (31 in.), the

overall embedment depth will exceed the standard embedment depth of 1,090 mm (43 in.). As a result, Case 4 conditions are those where the overlying soil thickness is greater than 785 mm (31 in.). It was determined that the drilled hole in rock would continue to be a 203 mm (8 in.) in diameter, but would only be drilled to a depth which would allow for a total post embedment depth of 1,090 mm (43 in.)

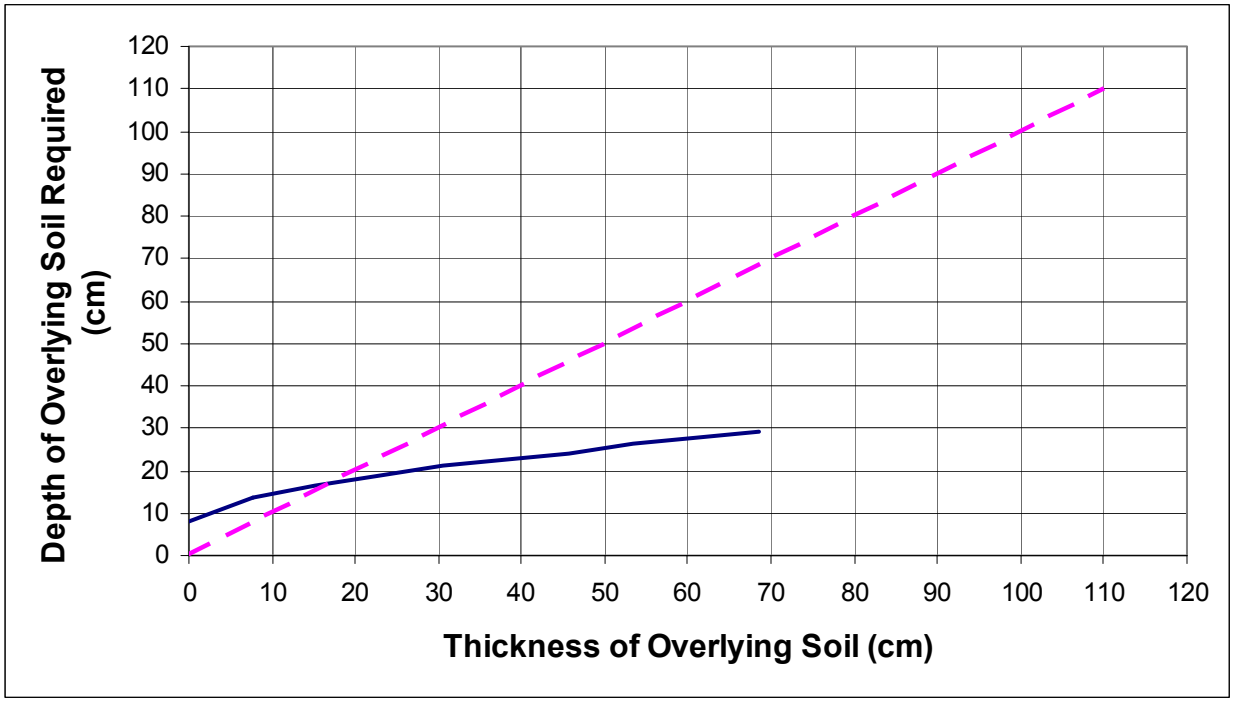

Figure 65. Determination of Minimum Soil Overlay for Case 2

Table 13. Stage 2 Analysis for 460-mm Embedment in Rock

Deflection at Impact Ht. (cm)	Embedment Depth (in rock) (cm)	Thickness of Overlying Soil (cm)	Deflection at Ground Line (cm)	Deflection at Rock Surface (cm)	Equiv. Defl. at Rail Midpoint Ht. (cm)	From MPR-11 Energy for Equiv. Defl. (kJ)	Needed Energy (kJ)	% Energy of Test SSF-9	Emb. Depth from Figure 63 (cm)
46	46	0.0	20.95	20.95	45.7	21.63	1.37	6.0	8.1
46	46	7.6	22.70	19.48	42.9	19.90	3.10	13.7	13.5
46	46	15.2	24.23	18.21	40.1	18.38	4.62	20.4	16.5
46	46	22.9	25.58	17.08	37.6	17.07	5.93	26.1	18.8
46	46	30.5	26.76	16.09	35.4	15.90	7.10	31.3	21.1
46	46	38.1	27.81	15.21	33.5	14.90	8.10	35.7	22.6
46	46	45.7	28.75	14.42	31.8	14.05	8.95	39.4	24.1
46	46	53.3	29.60	13.71	30.2	13.20	9.80	43.2	26.2
46	46	61.0	30.38	13.06	28.8	12.35	10.65	46.9	27.7
46	46	68.6	31.08	12.48	27.5	11.74	11.26	49.6	29.0

12.5 Discussion

Plans for all four stages are shown in Figure 66. Post placement designs were designed for a minimum thickness of overlying soil. However, when posts are installed in conditions where the lower limit design is used or maximum thickness of overlying soil exists, the additional force on the post as it rotates through the soil may cause it to fail prematurely. As a result, it was necessary to predict how much energy would be dissipated for each case condition when the lower limit post placement design was implemented. It was determined from previous post bogie testing (15), where posts were placed in unconfined soil as specified by NCHRP Report No. 350 and meeting AASHTO M147-65 Grading B (1990) requirements, that a W152x13.4 (W6x9) steel post could dissipate as much as 30.1 kJ (266 k-in.) of energy as it deflected 460 mm (18 in.) at the rail midpoint height. The yield load at the rail midpoint height for a W152x13.4 (W6x9) steel post was assumed to be approximately 70 kN (15.5 kips) if a dynamic magnification factor of 1.5 was applied to the strong axis plastic yield moment. As a result, it was decided that for the lower limit post placement design, the total dissipated energy should be less than 30 kJ (266 k-in.) and average force levels should be below 70 kN (15.5 kips). Dissipated energies and average forces for lower limit post placement designs at each case condition are shown in Table 14. Further evidence of actual peak loads on a steel post installed at the lower limit for case 4, where the lower front edge of the post is still fixed, is shown in Figure 67. As can be seen, the peak load of 67 kN (15.0 kips) from the strain gauge data is under the assumed post yield load of 70 kN (15.5 kips).

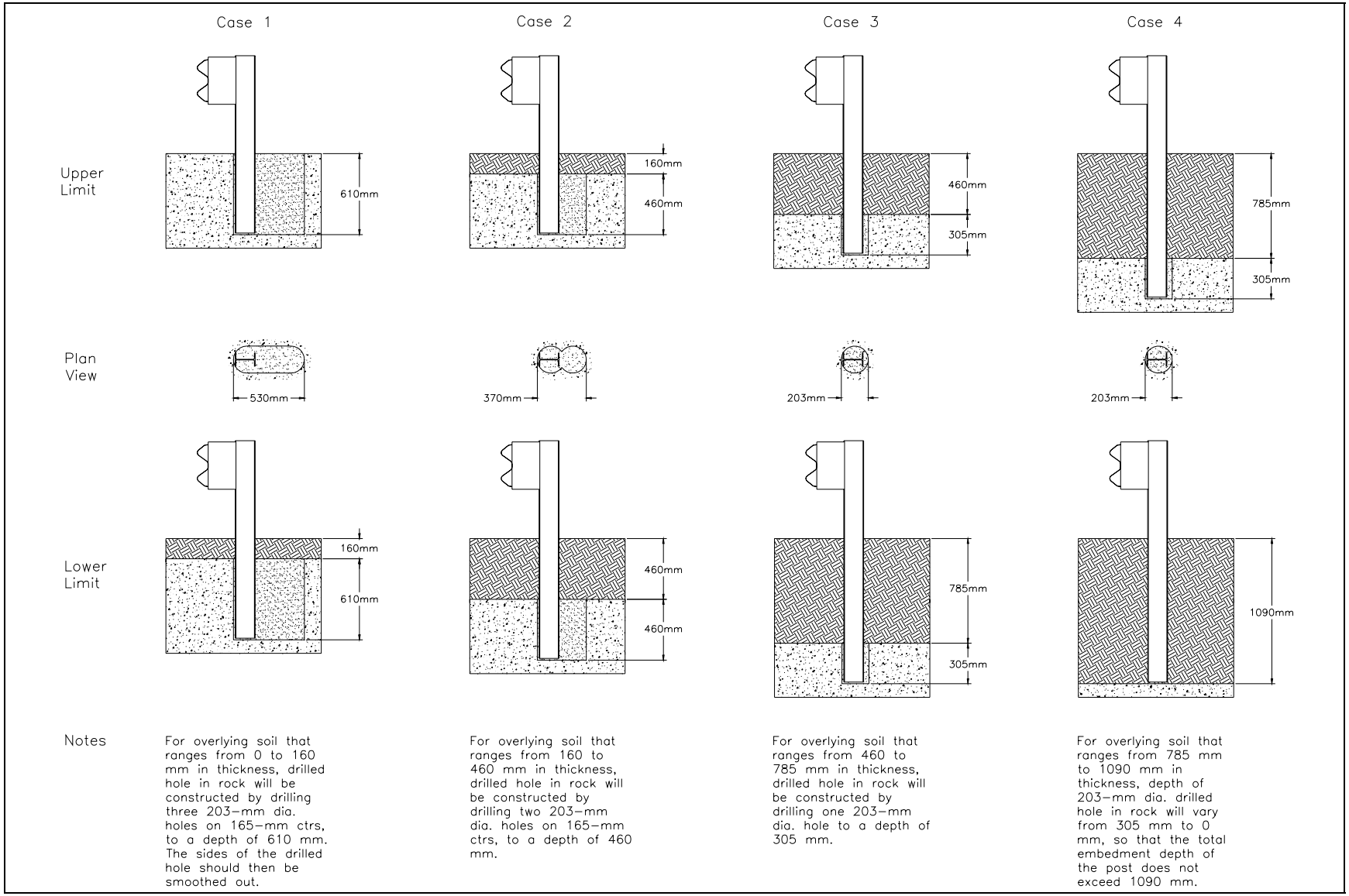

Figure 66. Post in Drilled Hole Configuration for all Stages

Table 14. Lower Limit Post Placement Design Analysis

Case Condition	Lower Limit Dissipated Energies (kJ)			Average Force (kN) [1]	Lower Limit Design OK?
	Backfill & Post Deformation	Overlying Soil	Total		
1	21.3	4.1	25.4	55.2	Yes
2	14.1	16.8	30.9	67.2	Yes
3	7.6	22.0	29.6	64.3	Yes
4 [2]	0	22.7	22.7	49.3	Yes

[1] Average Force is the total energy divided by a deflection of 460 mm
[2] Post was assumed to be fixed at the lower front edge

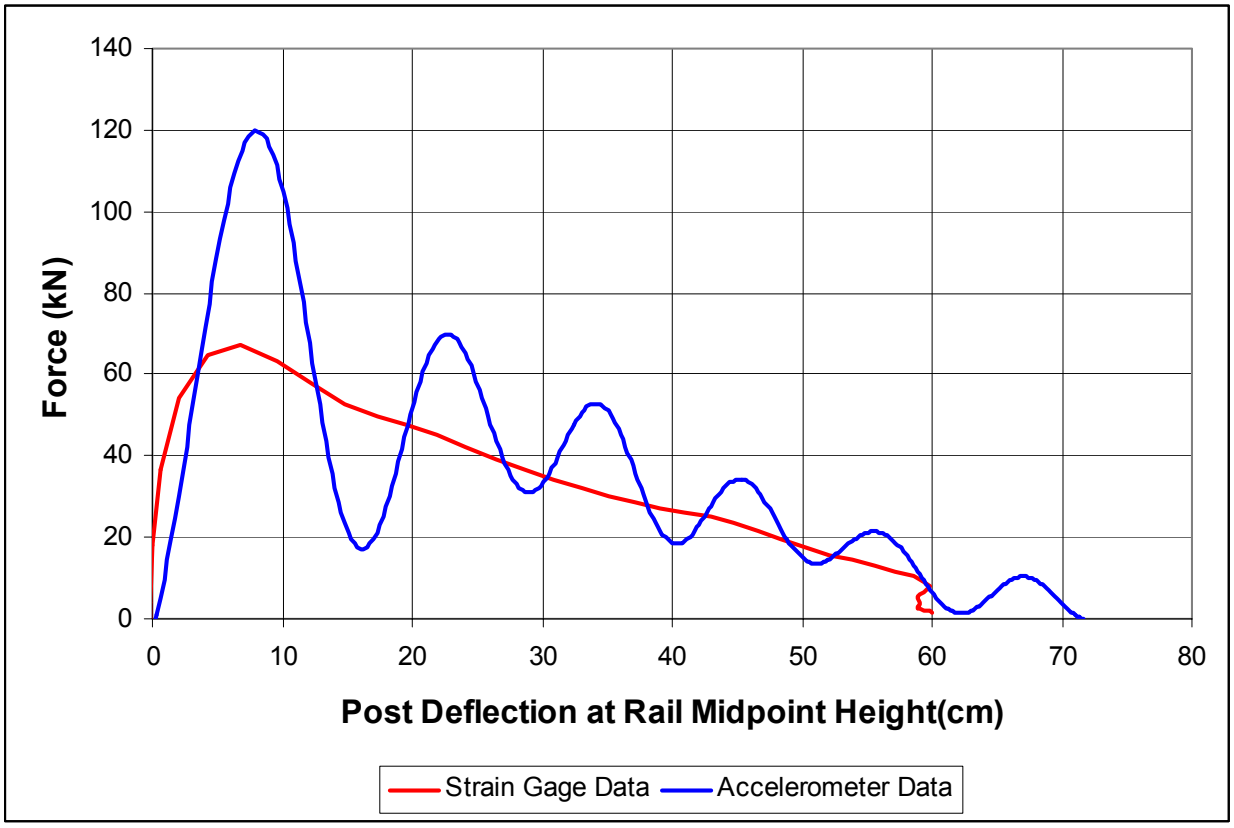

Figure 67. Force-Deflection Curves from Test SSF-9

12.5.1 Construction Considerations

Certain practices are recommended during installation to optimize the performance of the W-beam guardrail systems using the post-in-rock post placement designs. For Case 1 and 2, it is recommended that the sides of the elongated drilled hole should be smoothed out to minimize snagging of the post on the side of the rigid hole when the overlying soil thickness is less than 305 mm (12 in.). To guarantee that backfill material will be stiff enough, the backfill should be placed in the drilled hole in 150-mm thick lifts and compacted. To simplify construction, it is considered acceptable to backfill to the surface of the drilled hole above the rock, with the backfill material used in the drilled hole in rock. This should also offer some degree of verification to the inspector or engineer that the posts were placed properly in the ground.

These post installation procedures should only be used in competent rock. The post-in-rock post placement designs should not be used in conditions where cobbles or boulders impede installation of posts into the ground. Doing so will not allow the backfill material to be compressed properly during impact, leading to reduced absorbed energies and possible guardrail failure.

13 SUMMARY AND CONCLUSIONS

Computer simulation and physical testing of posts and guardrail installations was performed to develop procedures for the installation of a W-beam guardrail system in areas where rock is encountered at or below grade. System design was based primarily on an energy balance and a required energy absorption from post rotation.

First, a critical post placement design was developed for situations where rock was located at the surface. Most aspects of the design were developed through a simple rational analysis of the problem based on cost considerations and potential for wheel snag on posts. Other aspects of the design, such as backfill material used in the drilled hole and post embedment depth, required further analysis through testing and simulation. BARRIER VII computer simulation was used to determine a minimum absorbed energy requirement for a post rotating in a selected backfill material. Bogie testing of posts was then conducted to determine the proper backfill material and embedment depth that would fulfill the minimum absorbed energy requirement. A full-scale vehicle crash test, performed according to the TL-3 criteria specified in NCHRP Report No. 350, was conducted to verify that the post placement design for the critical condition would work in a W-beam guardrail system. A summary of the safety performance of the guardrail is shown in Table 15. Finally, additional post placement designs were developed for conditions were rock was encountered below grade. In total, four post placement designs for four corresponding depths to bedrock were developed, as shown in Figure 66.

Table 15. Summary of Safety Performance Evaluation Results

Evaluation Factors	Evaluation Criteria		Test PR-1
Structural Adequacy	A.	Test article should contain and redirect the vehicle; the vehicle should not penetrate, underride, or override the installation although controlled lateral deflection of the test article is acceptable.	Satisfactory
Occupant Risk	D.	Detached elements, fragments or other debris from the test article should not penetrate or show potential for penetrating the occupant compartment, or present an undue hazard to other traffic, pedestrians, or personnel in a work zone. Deformations of, or intrusions into, the occupant compartment that could cause serious injuries should not be permitted.	Satisfactory
	F.	The vehicle should remain upright during and after collision although moderate roll, pitching, and yawing are acceptable.	Satisfactory
Vehicle Trajectory	K.	After collision it is preferable that the vehicle's trajectory not intrude into adjacent traffic lanes.	Satisfactory
	L.	The occupant impact velocity in the longitudinal direction should not exceed 12 m/sec, and the occupant ridedown acceleration in the longitudinal direction should not exceed 20 G's.	Satisfactory
	M.	The exit angle from the test article preferably should be less than 60 percent of test impact angle measured at time of vehicle loss of contact with test device.	Marginal

14 RECOMMENDATIONS

14.1 General

A W-beam guardrail system with posts installed in drilled holes in rock, where the rock is located at the surface, was successfully tested according to TL-3 criteria found in NCHRP Report No. 350. Test results indicate that this design is suitable for use on Federal-aid highways. Further designs with posts installed in rock at varied depths below the surface have been developed based on an energy-balance analysis. This analysis is considered to be conservative and should offer satisfactorily performance for guardrail systems that encounter rock within 1,090 mm (43 in.) of the surface.

This guardrail system was tested with the entire length installed tangent. However, in actual field conditions, one or two flared end sections can be installed. For locations were flared sections will be used, the flare rates should follow the recommended guidelines provided in AASHTO's *Roadside Design Guide* (22).

14.2 Further Testing

The post placement design for Case 4 was developed to take into consideration conditions where rock impedes full embedment depth of 1,090 mm (43 in.). However, it may be possible for the post to be embedded to slightly shallower depths and still adequately support the W-beam guardrail system during impact. As a result, further research into shallower embedment depths may be warranted, allowing for changes to be made to the Case 3 and 4 post placement designs. If future W-beam guardrail systems are approved with shallower post embedment depth, redesign of post placement designs or Cases 3 and 4 would be warranted.

14.3 BARRIER VII Calibration Procedures

For this study, post parameters gained from testing were factored before input into

BARRIER VII for the critical impact point analysis, as discussed in Section 6. Validation of the simulation results in Section 11, indicate that this analysis improved the accuracy of the finite element model. As a result, if parameters used for input into BARRIER VII are obtained from physical testing, it may be advantageous to compare them to parameters found from calibration to a similar, previously conducted, test. If significant discrepancies exist, a BARRIER VII analysis, as conducted for this study, may be warranted.

14.4 Further Post Placement Designs for Posts Installed in Pavement

If guardrail posts are to be installed in pavement, such as in shoulders alongside the roadway, it would be possible to blockout a portion of the pavement so that the post would have room to rotate backwards. This could be done for both W152x13.4 (W6x9) steel and 152-mm x 203-mm (6-in. x 8-in.) timber posts. The size of the blocked out portion of the pavement for the post could be determined by assuming the post would rotate around a point two-thirds the depth of full embedment, and the post would be allowed to deflect backwards 460 mm (18 in.) at the rail midpoint height before contact with the pavement. Figure 68 shows possible geometries for blockout portions of pavement. Backfill with confined compression properties similar to ASTM C33 coarse aggregate, size no. 57, would possibly be acceptable for this application, but further testing should be conducted.

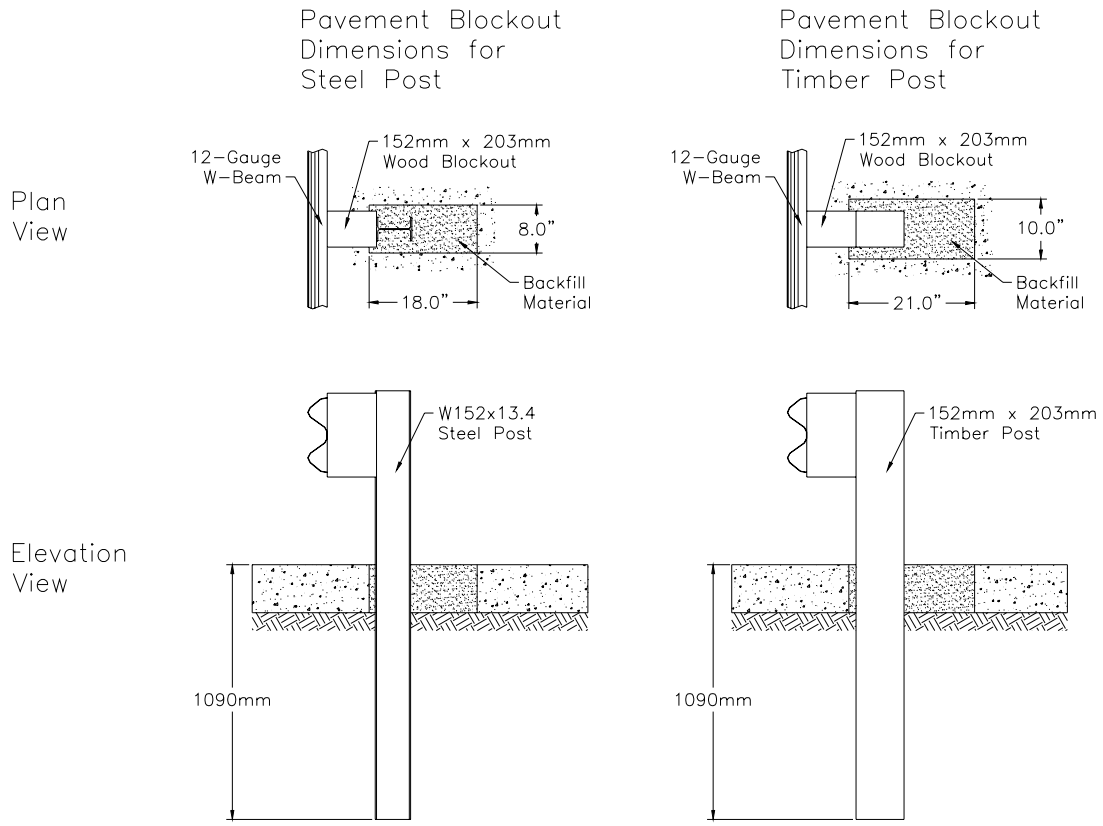

Figure 68. Details for Blocking Out Concrete for Guardrail Posts

15 REFERENCES

1. Ross, H.E., Sicking, D.L., Zimmer, R.A., and Michie, J.D., Recommended Procedures for the Safety Performance Evaluation of Highway Features, National Cooperative Research Program (NCHRP) Report No. 350, Transportation Research Board, Washington, D.C., 1993.

2. Cichowski, G., Skeels, P.C., and Hawkins, W.R., "Appraisal of Guardrail Installations by Car Impact and Laboratory Tests," Highway Research Board Proceedings, Vol. 40, 1961.

3. Graham, D., et al., "New Highway Barriers: The Practical Application of Theoretical Design," Highway Research Record, Vol. 174, 1967.

4. Michie, J.D., Response of Guardrail Posts During Impact, Southwest Research Institute Report No. 03-9051, San Antonio, Texas, October 1970.

5. Calcote, L.R., and Kimball, C.E., "Properties of Guardrail Posts for Various Soil Types," Transportation Research Record, Vol. 679, 1978.

6. Jeyapalan, J.K., Dewey, J.F., Hirsch, T.J., Ross, H.E., and Crooner, H., "Soil-Foundation Interaction Behavior of Highway Guardrail Posts," Transportation Research Record, Vol. 970, 1983.

7. Eggers, W., Hirsch, T.J., and Ross, H.E., Jr., Strength of Guardrail Post in Rock, Federal Highway Administration Report No. FHWA/TX-85/42+343-1(Suppl.), September 1984.

8. Eggers, W. and Hirsch, T.J., The Effects of Embedment Depth, Soil Properties, and Post Type on the Performance of Highway Guardrail Posts, Federal Highway Administration Report No. FHWA/TX-86/64+405-1, August 1986.

9. Bartlett, R. and Kutter, B.L., Lateral Load Capacity of Posts and Footings for Metal Beam Guardrails Located Close to Slopes, Federal Highway Administration Report No. FHWA/CA/TL 93-02, September 1992.

10. Coon, B., *D*ynamic Impact Testing and Simulation of Guardrail Posts Embedded in Soil, Thesis, University of Nebraska – Lincoln, December 1999.

11. Powell, G.H., BARRIER VII: A Computer Program For Evaluation of Automobile Barrier Systems, Federal Highway Administration Report No. FHWA RD-73-51, April 1973.

12. Hargrave, M.W., and Hansen, A.G., "Federal Outdoor Impact Laboratory - A New Facility For Evaluating Roadside Safety Hardware," Transportation Research Record, Vol. 1198, 1988.

13. Reid, J.D., Sicking, D.L., and Bligh, R., "Critical Impact Point for Longitudinal Barriers," ASCE Journal of Transportation Engineering, Vol. 124, No. 1, pp. 65-72, Jan./Feb, 1998.

14. Polivka, K.A., Crash Testing of Michigan's Type B (W-beam) Guardrail System, Midwest Roadside Safety Facility Report TRP-03-90-99, Lincoln, Nebraska, November 1999.

15. Coon, B.A., Reid, J.D., and Rohde, J.R., Dynamic Impact Testing of Guardrail Posts Embedded in Soil, Midwest Roadside Safety Facility Report TRP-03-77-98, Lincoln, Nebraska, July 1999.

16. Buth, C.E., Campise, W.L., Griffin, III, L.I., Love, M.L., and Sicking, D.L., Performance Limits of Longitudinal Barrier Systems - Volume I - Summary Report, Federal Highway Administration Report No. FHWA/RD-86/153, May 1986.

17. Ivy, D.L., Robertson, R., and Buth, C.E., *Test and Evaluation of W-beam and Thrie-Beam Guardrails*, Federal Highway Administration Report No. FHWA/RD-82/071, March 1986.

18. Ross, Jr., H.E., Perera, H.S., Sicking, D.L., and Bligh, R.P., *Roadside Safety Design for Small Vehicles*, National Cooperative Highway Research Program (NCHRP) Report No. 318, Transportation Research Board, Washington, D.C., May 1989

19. Hinch, J., Yang, T.L., and Owings, R., Guidance Systems for Vehicle Testing, ENSCO, Inc., Springfield, VA 1986.

20. Vehicle Damage Scale for Traffic Investigators, Second Edition, Technical Bulletin No. 1, Traffic Accident Data (TAD) Project, National Safety Council, Chicago, Illinois, 1971.

21. Collision Deformation Classification - Recommended Practice J224 March 1980, Handbook Volume 4, Society of Automotive Engineers (SAE), Warrendale, Pennsylvania, 1985.

22. Roadside Design Guide, American Association of State Highway and Transportation Officials (AASHTO), Washington, D.C., January 1996.

16 APPENDICES

APPENDIX A

BARRIER VII Computer Model

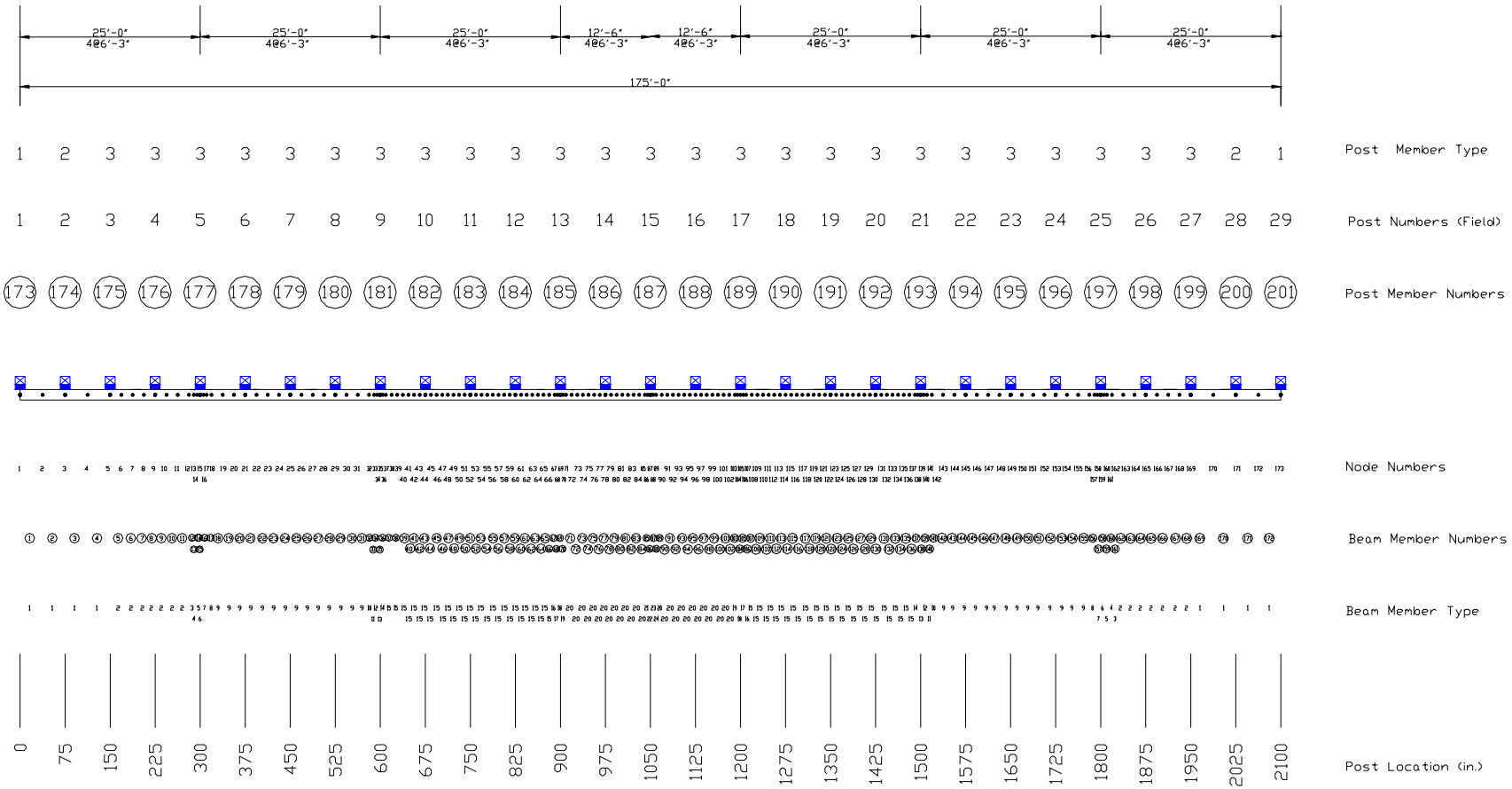

Figure A-1. Model of the Post-in-Rock Guardrail System

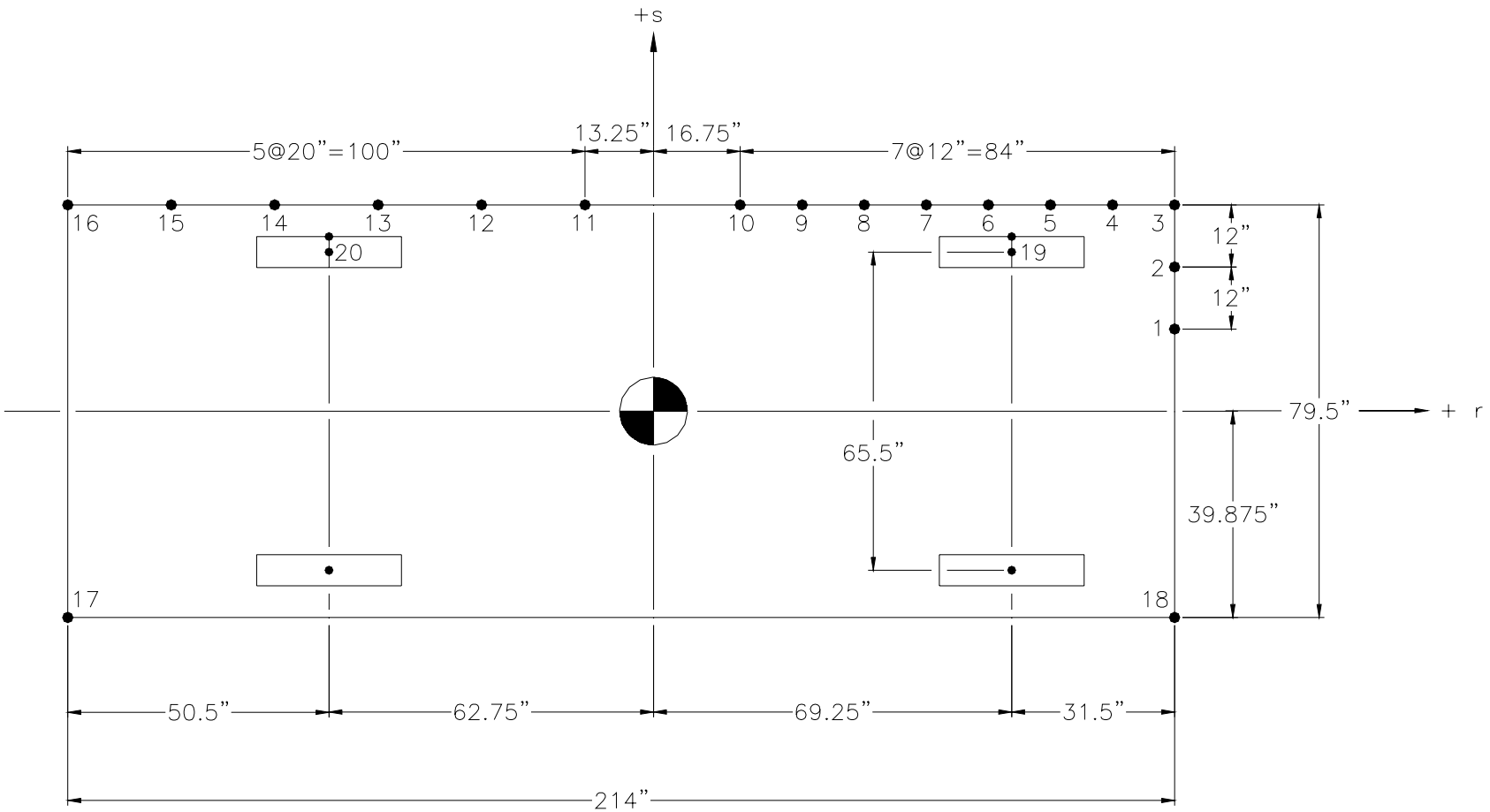

Figure A-2. Idealized Finite Element, 2 Dimensional Vehicle Model for the 2000-kg Pickup Truck

APPENDIX B

Typical BARRIER VII Input File

The example input deck for BARRIER VII included in Appendix B corresponds to the critical impact point for test PR-1. All inputs are in English units as specified in the BARRIER VII manual (11).

Missouri Guardrail Posts in Rock - CIP analysis

```
 173   71   28    1  201   73    2    0
  0.0001    0.0001      0.800 300    0       1.0    1
 10   10   10   10   10   10   10
  1            0.0       0.0
  3          75.00       0.0
  5         150.00       0.0
  9         225.00       0.0
 12         281.25       0.0
 13        290.625       0.0
 14       295.3125       0.0
 15         300.00       0.0
 16       304.6875       0.0
 17        309.375       0.0
 18         318.75       0.0
 21         375.00       0.0
 25         450.00       0.0
 29         525.00       0.0
 32         581.25       0.0
 33        590.625       0.0
 34       595.3125       0.0
 35         600.00       0.0
 36       604.6875       0.0
 37        609.375       0.0
 38         618.75       0.0
 44         675.00       0.0
 52         750.00       0.0
 60         825.00       0.0
 66         881.25       0.0
 67        890.625       0.0
 68       895.3125       0.0
 69         900.00       0.0
 70       904.6875       0.0
 71        909.375       0.0
 72         918.75       0.0
 78         975.00       0.0
 84        1031.25       0.0
 85       1040.625       0.0
 86      1045.3125       0.0
 87        1050.00       0.0
 88      1054.6875       0.0
 89       1059.375       0.0
 90        1068.75       0.0
 96        1125.00       0.0
102        1181.25       0.0
103       1190.625       0.0
104      1195.3125       0.0
105        1200.00       0.0
106      1204.6875       0.0
107       1209.375       0.0
108        1218.75       0.0
```

114	1275.00			0.0
122	1350.00			0.0
130	1425.00			0.0
136	1481.25			0.0
137	1490.625			0.0
138	1495.3125			0.0
139	1500.00			0.0
140	1504.6875			0.0
141	1509.375			0.0
142	1518.75			0.0
145	1575.00			0.0
149	1650.00			0.0
153	1725.00			0.0
156	1781.25			0.0
157	1790.625			0.0
158	1795.3125			0.0
159	1800.00			0.0
160	1804.6875			0.0
161	1809.375			0.0
162	1818.75			0.0
165	1875.00			0.0
169	1950.00			0.0
171	2025.00			0.0
173	2100.00			0.0
1	3	1	1	0.0
3	5	1	1	0.0
5	9	3	1	0.0
9	12	2	1	0.0
18	21	2	1	0.0
21	25	3	1	0.0
25	29	3	1	0.0
29	32	2	1	0.0
38	44	5	1	0.0
44	52	7	1	0.0
52	60	7	1	0.0
60	66	5	1	0.0
72	78	5	1	0.0
78	84	5	1	0.0
90	96	5	1	0.0
96	102	5	1	0.0
108	114	5	1	0.0
114	122	7	1	0.0
122	130	7	1	0.0
130	136	5	1	0.0
142	145	2	1	0.0
145	149	3	1	0.0
149	153	3	1	0.0
153	156	2	1	0.0
162	165	2	1	0.0
165	169	3	1	0.0
169	171	1	1	0.0

```
171  173    1    1       0.0
  1  173      0.35
173  172  171  170  169  168  167  166  165  164
163  162  161  160  159  158  157  156  155  154
153  152  151  150  149  148  147  146  145  144
143  142  141  140  139  138  137  136  135  134
133  132  131  130  129  128  127  126  125  124
123  122  121  120  119  118  117  116  115  114
113  112  111  110  109  108  107  106  105  104
103  102  101  100   99   98   97   96   95   94
 93   92   91   90   89   88   87   86   85   84
 83   82   81   80   79   78   77   76   75   74
 73   72   71   70   69   68   67   66   65   64
 63   62   61   60   59   58   57   56   55   54
 53   52   51   50   49   48   47   46   45   44
 43   42   41   40   39   38   37   36   35   34
 33   32   31   30   29   28   27   26   25   24
 23   22   21   20   19   18   17   16   15   14
 13   12   11   10    9    8    7    6    5    4
  3    2    1
100   24
  1     2.29     1.99     37.50   30000.0     6.92     99.5     68.5 0.10 12-Gauge W-Beam
  2     2.29     1.99     18.75   30000.0     6.92     99.5     68.5 0.10 12-Gauge W-Beam
  3     2.29     1.99     9.375   30000.0     6.92     99.5     68.5 0.10 12-Gauge W-Beam
  4     2.29     1.99    4.6875   30000.0     6.92     99.5     68.5 0.10 12-Gauge W-Beam
  5     2.29     1.99    4.6875   30000.0     6.92     99.5     68.5 0.10 12-Gauge W-Beam
  6     2.29     1.99    4.6875   30000.0     6.92     99.5     68.5 0.10 12-Gauge W-Beam
  7     2.29     1.99    4.6875   30000.0     6.92     99.5     68.5 0.10 12-Gauge W-Beam
  8     2.29     1.99     9.375   30000.0     6.92     99.5     68.5 0.10 12-Gauge W-Beam
  9     2.29     1.99     18.75   30000.0     6.92     99.5     68.5 0.10 12-Gauge W-Beam
 10     2.29     1.99     9.375   30000.0     6.92     99.5     68.5 0.10 12-Gauge W-Beam
 11     2.29     1.99    4.6875   30000.0     6.92     99.5     68.5 0.10 12-Gauge W-Beam
 12     2.29     1.99    4.6875   30000.0     6.92     99.5     68.5 0.10 12-Gauge W-Beam
 13     2.29     1.99    4.6875   30000.0     6.92     99.5     68.5 0.10 12-Gauge W-Beam
 14     2.29     1.99    4.6875   30000.0     6.92     99.5     68.5 0.10 12-Gauge W-Beam
 15     2.29     1.99     9.375   30000.0     6.92     99.5     68.5 0.10 12-Gauge W-Beam
 16     2.29     1.99    4.6875   30000.0     6.92     99.5     68.5 0.10 12-Gauge W-Beam
 17     2.29     1.99    4.6875   30000.0     6.92     99.5     68.5 0.10 12-Gauge W-Beam
 18     2.29     1.99    4.6875   30000.0     6.92     99.5     68.5 0.10 12-Gauge W-Beam
 19     2.29     1.99    4.6875   30000.0     6.92     99.5     68.5 0.10 12-Gauge W-Beam
 20     2.29     1.99     9.375   30000.0     6.92     99.5     68.5 0.10 12-Gauge W-Beam
 21     2.29     1.99    4.6875   30000.0     6.92     99.5     68.5 0.10 12-Gauge W-Beam
 22     2.29     1.99    4.6875   30000.0     6.92     99.5     68.5 0.10 12-Gauge W-Beam
 23     2.29     1.99    4.6875   30000.0     6.92     99.5     68.5 0.10 12-Gauge W-Beam
 24     2.29     1.99    4.6875   30000.0     6.92     99.5     68.5 0.10 12-Gauge W-Beam
300    3
  1    21.65     0.00       4.0      4.0     100.0     250.0     250.0 0.10 Simulated Strong Anchor Post
   100.0    100.0     10.0     10.0
  2    21.65     0.00       3.0      3.0     100.0     100.0    150.00 0.10 Second BCT Post
    50.0     50.0      6.0      6.0
  3    21.65      0.0     30.00     4.00     35.25     93.30    175.00 0.10 W6x9 by 6' Long
```

```
    5.0      15.0       6.0      16.0
  1    1    2    4    1  101      0.0      0.0      0.0
  5    5    6   11    1  102      0.0      0.0      0.0
 12   12   13              103      0.0      0.0      0.0
 13   13   14              104      0.0      0.0      0.0
 14   14   15              105      0.0      0.0      0.0
 15   15   16              106      0.0      0.0      0.0
 16   16   17              107      0.0      0.0      0.0
 17   17   18              108      0.0      0.0      0.0
 18   18   19   31    1  109      0.0      0.0      0.0
 32   32   33              110      0.0      0.0      0.0
 33   33   34              111      0.0      0.0      0.0
 34   34   35              112      0.0      0.0      0.0
 35   35   36              113      0.0      0.0      0.0
 36   36   37              114      0.0      0.0      0.0
 37   37   38   66    1  115      0.0      0.0      0.0
 67   67   68              116      0.0      0.0      0.0
 68   68   69              117      0.0      0.0      0.0
 69   69   70              118      0.0      0.0      0.0
 70   70   71              119      0.0      0.0      0.0
 71   71   72   84    1  120      0.0      0.0      0.0
 85   85   86              121      0.0      0.0      0.0
 86   86   87              122      0.0      0.0      0.0
 87   87   88              123      0.0      0.0      0.0
 88   88   89              124      0.0      0.0      0.0
 89   89   90  102    1  120      0.0      0.0      0.0
103  103  104              119      0.0      0.0      0.0
104  104  105              118      0.0      0.0      0.0
105  105  106              117      0.0      0.0      0.0
106  106  107              116      0.0      0.0      0.0
107  107  108  136    1  115      0.0      0.0      0.0
137  137  138              114      0.0      0.0      0.0
138  138  139              113      0.0      0.0      0.0
139  139  140              112      0.0      0.0      0.0
140  140  141              111      0.0      0.0      0.0
141  141  142              110      0.0      0.0      0.0
142  142  143  155    1  109      0.0      0.0      0.0
156  156  157              108      0.0      0.0      0.0
157  157  158              107      0.0      0.0      0.0
158  158  159              106      0.0      0.0      0.0
159  159  160              105      0.0      0.0      0.0
160  160  161              104      0.0      0.0      0.0
161  161  162              103      0.0      0.0      0.0
162  162  163  168    1  102      0.0      0.0      0.0
169  169  170  172    1  101      0.0      0.0      0.0
173    1          301      0.0      0.0      0.0      0.0      0.0
174    3          302      0.0      0.0      0.0      0.0      0.0
175    5          303      0.0      0.0      0.0      0.0      0.0
176    9          303      0.0      0.0      0.0      0.0      0.0
177   15          303      0.0      0.0      0.0      0.0      0.0
178   21          303      0.0      0.0      0.0      0.0      0.0
```

```
179   25              303      0.0      0.0      0.0      0.0      0.0
180   29              303      0.0      0.0      0.0      0.0      0.0
181   35              303      0.0      0.0      0.0      0.0      0.0
182   44              303      0.0      0.0      0.0      0.0      0.0
183   52              303      0.0      0.0      0.0      0.0      0.0
184   60              303      0.0      0.0      0.0      0.0      0.0
185   69              303      0.0      0.0      0.0      0.0      0.0
186   78              303      0.0      0.0      0.0      0.0      0.0
187   87              303      0.0      0.0      0.0      0.0      0.0
188   96              303      0.0      0.0      0.0      0.0      0.0
189  105              303      0.0      0.0      0.0      0.0      0.0
190  114              303      0.0      0.0      0.0      0.0      0.0
191  122              303      0.0      0.0      0.0      0.0      0.0
192  130              303      0.0      0.0      0.0      0.0      0.0
193  139              303      0.0      0.0      0.0      0.0      0.0
194  145              303      0.0      0.0      0.0      0.0      0.0
195  149              303      0.0      0.0      0.0      0.0      0.0
196  153              303      0.0      0.0      0.0      0.0      0.0
197  159              303      0.0      0.0      0.0      0.0      0.0
198  165              303      0.0      0.0      0.0      0.0      0.0
199  169              303      0.0      0.0      0.0      0.0      0.0
200  171              302      0.0      0.0      0.0      0.0      0.0
201  173              301      0.0      0.0      0.0      0.0      0.0
 4424.7   40000.0   20    6    4    0    1
  1      0.055       0.12      6.00      17.0
  2      0.057       0.15      7.00      18.0
  3      0.062       0.18     10.00      12.0
  4      0.110       0.35     12.00       6.0
  5       0.35       0.45      6.00       5.0
  6       1.45       1.50     15.00       1.0
  1    100.75    15.875    1     12.0    1    1    0    0
  2    100.75    27.875    1     12.0    1    1    0    0
  3    100.75    39.875    2     12.0    1    1    0    0
  4     88.75    39.875    2     12.0    1    1    0    0
  5     76.75    39.875    2     12.0    1    1    0    0
  6     64.75    39.875    2     12.0    1    1    0    0
  7     52.75    39.875    2     12.0    1    1    0    0
  8     40.75    39.875    2     12.0    1    1    0    0
  9     28.75    39.875    2     12.0    1    1    0    0
 10     16.75    39.875    2     12.0    1    1    0    0
 11    -13.25    39.875    3     12.0    1    1    0    0
 12    -33.25    39.875    3     12.0    1    1    0    0
 13    -53.25    39.875    3     12.0    1    1    0    0
 14    -73.25    39.875    3     12.0    1    1    0    0
 15    -93.25    39.875    3     12.0    1    1    0    0
 16   -113.25    39.875    4     12.0    1    1    0    0
 17   -113.25   -39.875    4     12.0    0    0    0    0
 18    100.75   -39.875    1     12.0    0    0    0    0
 19     69.25     37.75    5      1.0    1    1    0    0
 20    -62.75     37.75    6      1.0    1    1    0    0
  1     69.25     32.75     0.0     608.
```

```
2     69.25    -32.75     0.0    608.
3    -62.75     32.75     0.0    492.
4    -62.75    -32.75     0.0    492.
1     69.25     37.75
3    853.12       0.0    25.0   62.10     0.0     0.0     1.0
```

APPENDIX C

Force-Deflection Behavior of Bogie Tests

Bogie Test Summary

Test Information

Test Number:	MPR1	
Test Date:	23-Jun-00	
Failure Type:	Soil Failure	

Post Properties

Post Type:	Steel	
Post Size:	W152x23.8	W6x16
Post Length:	134.6 cm	(53.0 in)
Embedment Depth:	61.0 cm	(24.0 in)

Soil Properties

Moisture Content:	0	
Gradation:	47B Sand	
Soil Density, γ_d:	1842	kg/m^3
Compaction Method:	Hand Tamped	

Bogie Properties

Impact Velocity:	2.1 m/s	(4.7 mph)	(6.8 fps)
Impact Location:	54.9 cm	(21.6 in.)	above groundline
Bogie Mass:	966 kg	(2131 lbf.)	

Data Acquired

Accelerometer Data - EDR3
Side View, e-cam
String Potentiometer
Strain Gages

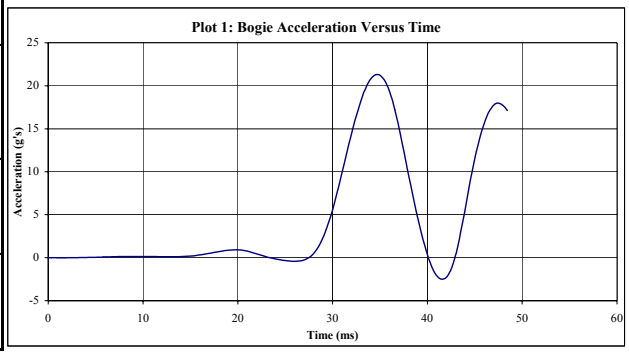

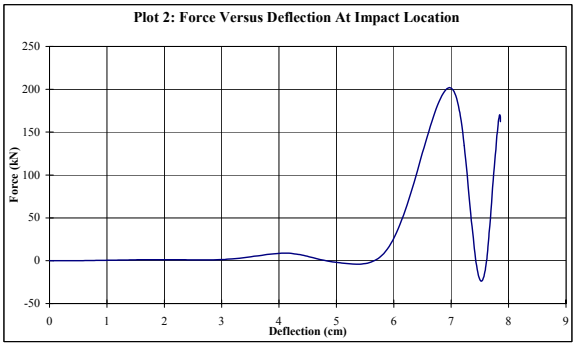

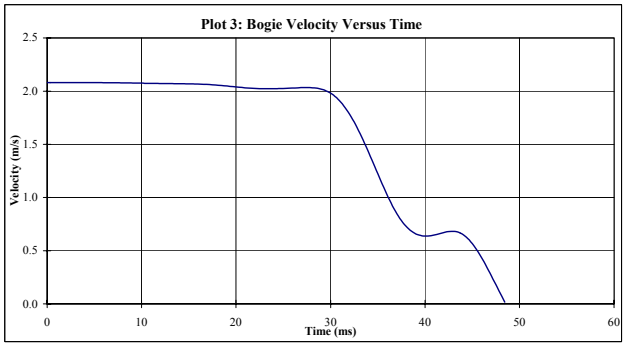

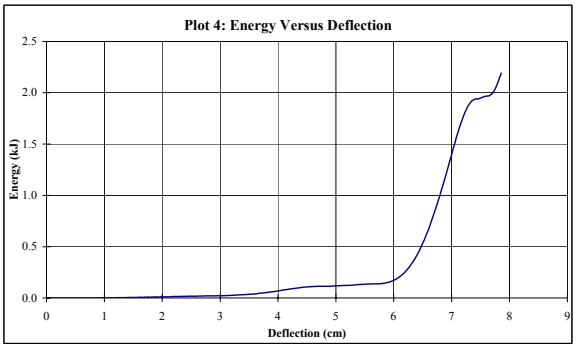

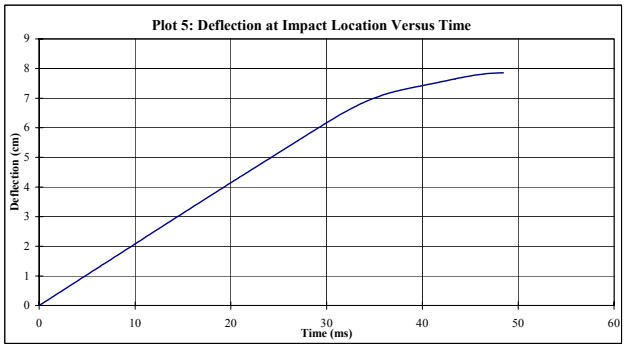

Figure C-1. Accelerometer Data Analysis, Test MPR-1

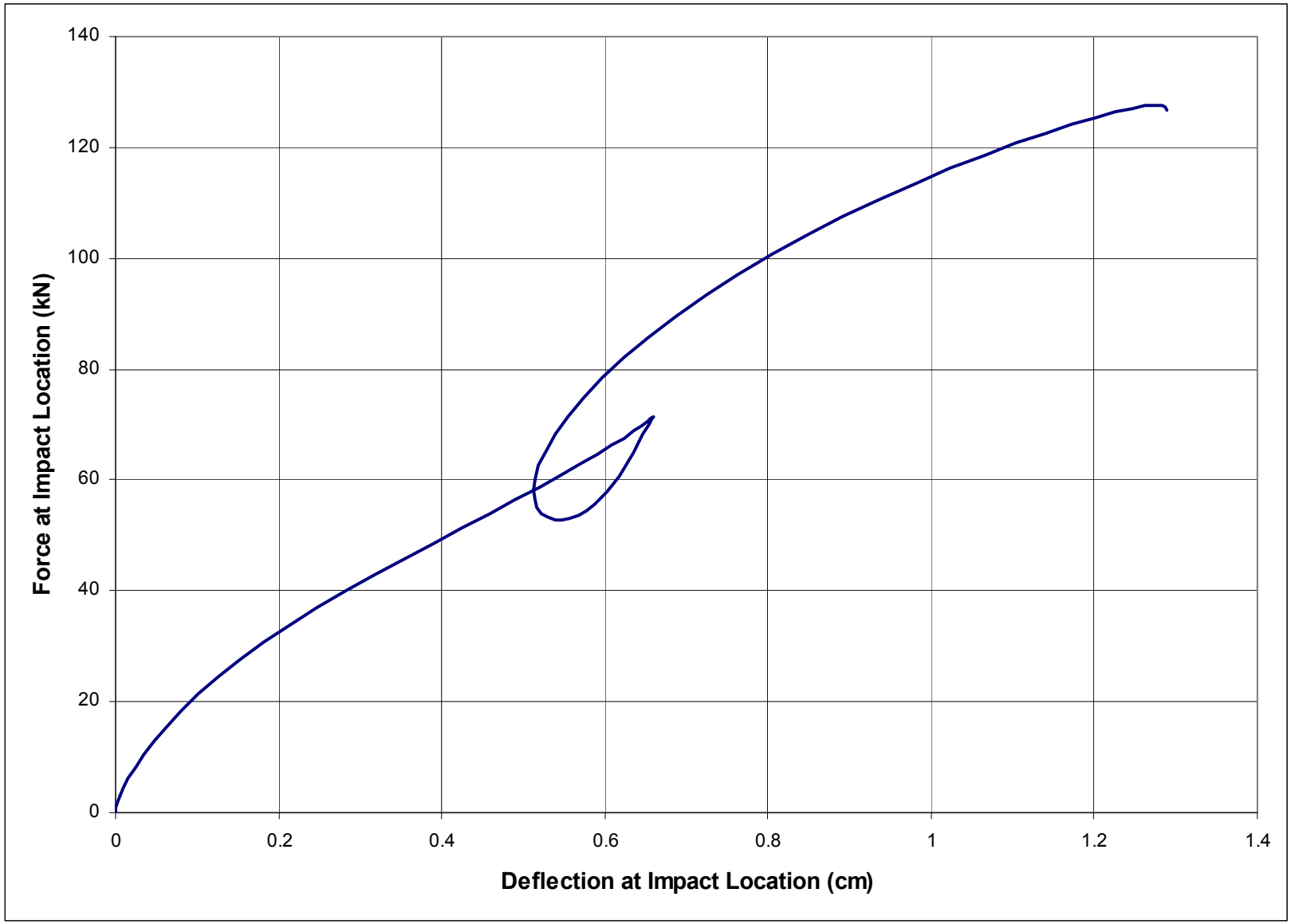

Figure C-2. Force-Deflection Plot Derived from Strain Gauge Data, Test MPR-1

Bogie Test Summary

Test Information

Test Number:	MPR2	
Test Date:	23-Jun-00	
Failure Type:	Soil Failure	

Post Properties

Post Type:	Steel	
Post Size:	W152x23.8	W6x16
Post Length:	134.6 cm	(53.0 in)
Embedment Depth:	61.0 cm	(24.0 in)

Soil Properties

Moisture Content:	0	
Gradation:	47B Sand	
Soil Density, γ_d:	1842	kg/m^3
Compaction Method:	Hand Tamped	

Bogie Properties

Impact Velocity:	4.2 m/s	(9.4 mph) (13.8 fps)
Impact Location:	54.9 cm	(21.6 in.) above groundline
Bogie Mass:	966 kg	(2131 lbf.)

Data Acquired

Accelerometer Data - EDR3
Side View, e-cam
String Potentiometer
Strain Gages

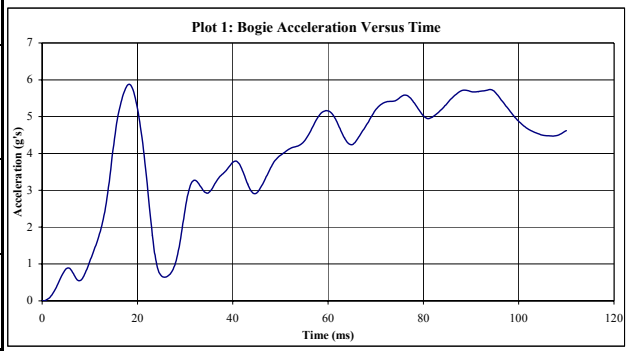

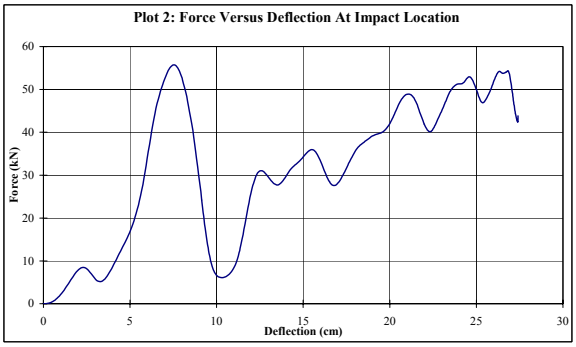

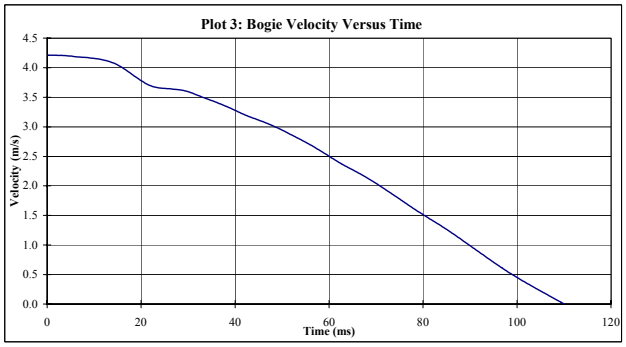

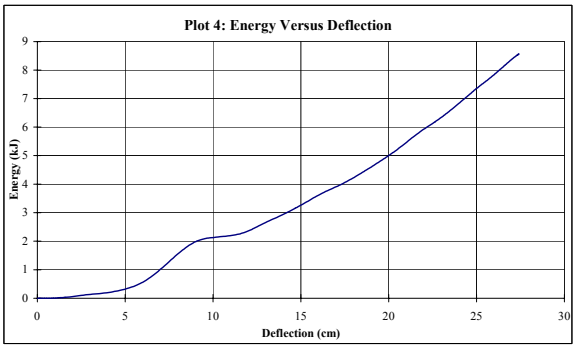

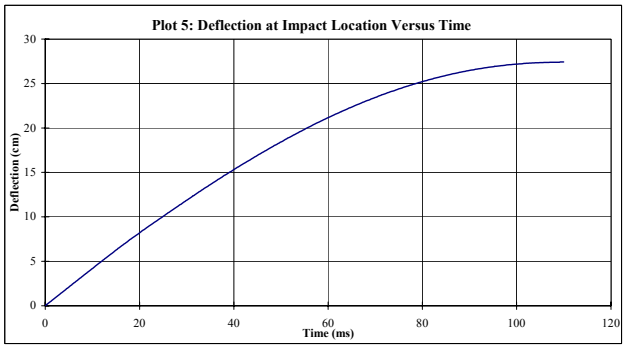

Figure C-3. Accelerometer Data Analysis, Test MPR-2

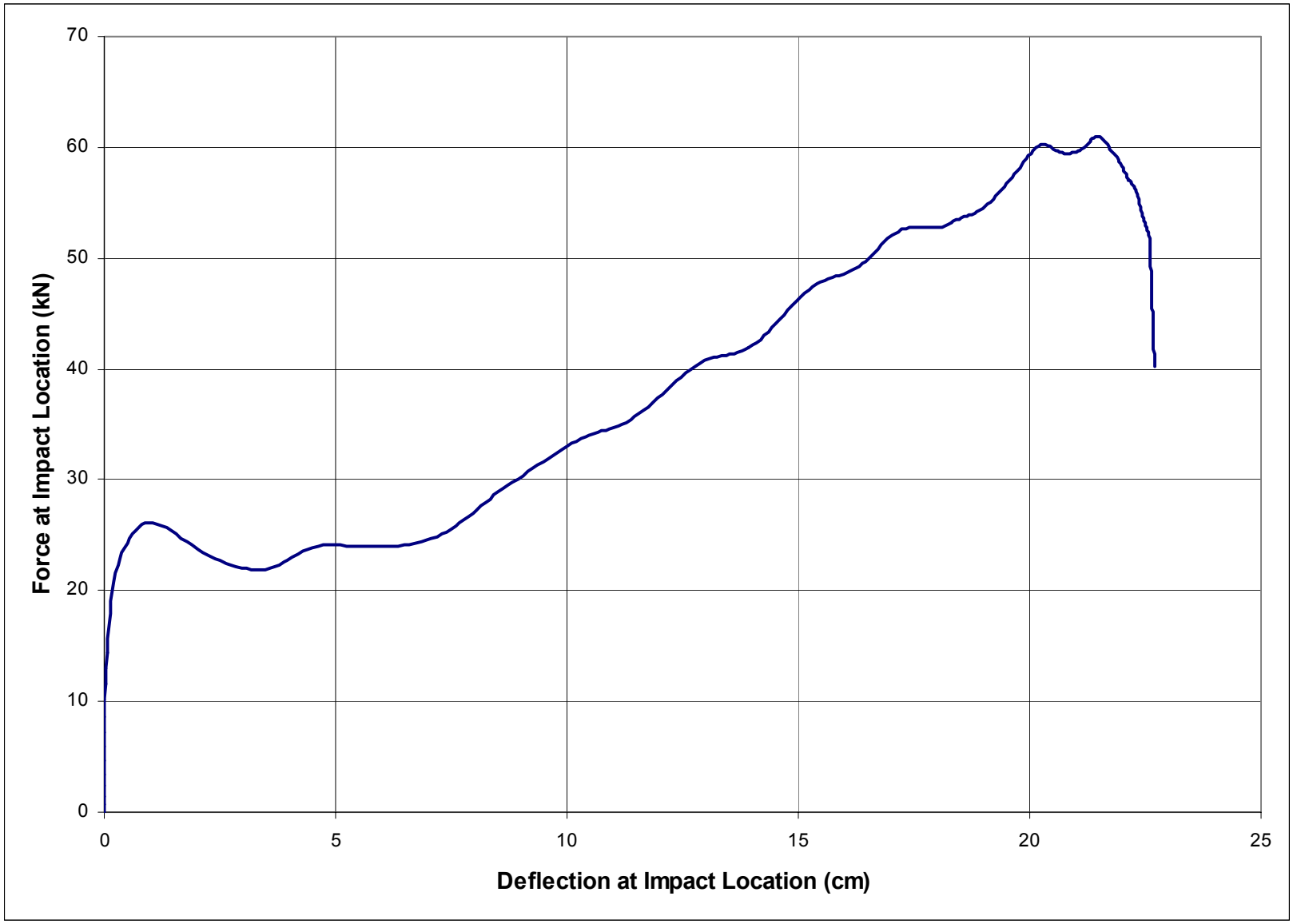

Figure C-4. Force-Deflection Plot Derived from Strain Gauge Data, Test MPR-2

Bogie Test Summary

Test Information

Test Number:	MPR3	
Test Date:	23-Jun-00	
Failure Type:	Soil Failure	

Post Properties

Post Type:	Steel	
Post Size:	W152x23.8	W6x16
Post Length:	134.6 cm	(53.0 in)
Embedment Depth:	61.0 cm	(24.0 in)

Soil Properties

Moisture Content:	0	
Gradation:	47B Sand	
Soil Density, γ_d:	1842	kg/m³
Compaction Method:	Hand Tamped	

Bogie Properties

Impact Velocity:	6.5 m/s	(14.6 mph) (21.4 fps)
Impact Location:	54.9 cm	(21.6 in.) above groundline
Bogie Mass:	966 kg	(2131 lbf.)

Data Acquired

Accelerometer Data - EDR3
Side View, e-cam
String Potentiometer
Strain Gages

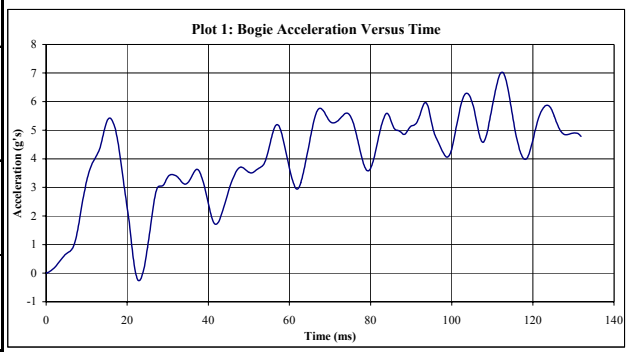

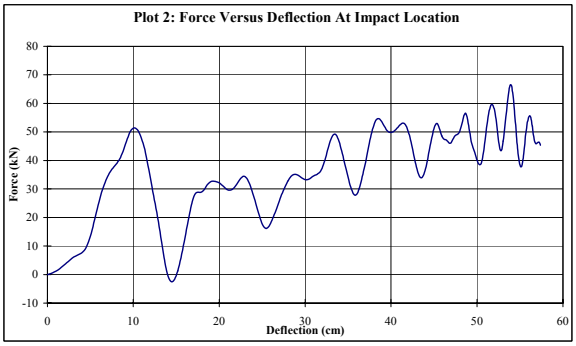

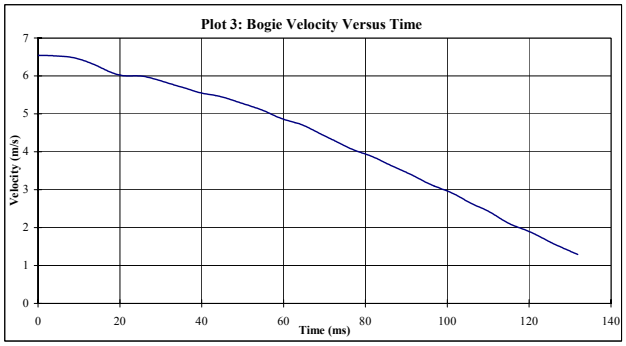

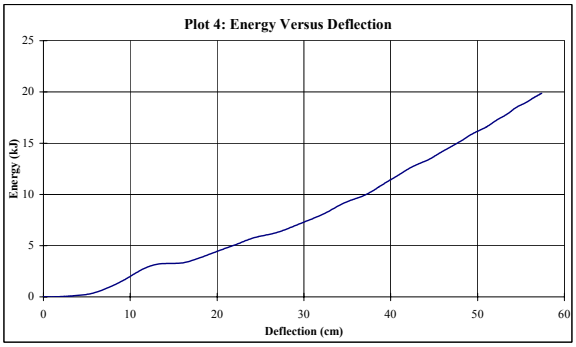

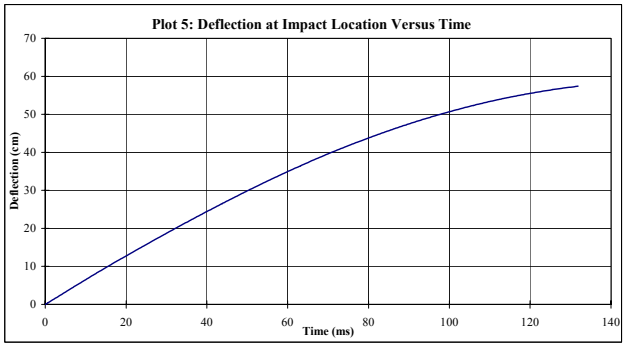

Figure C-5. Accelerometer Data Analysis, Test MPR-3

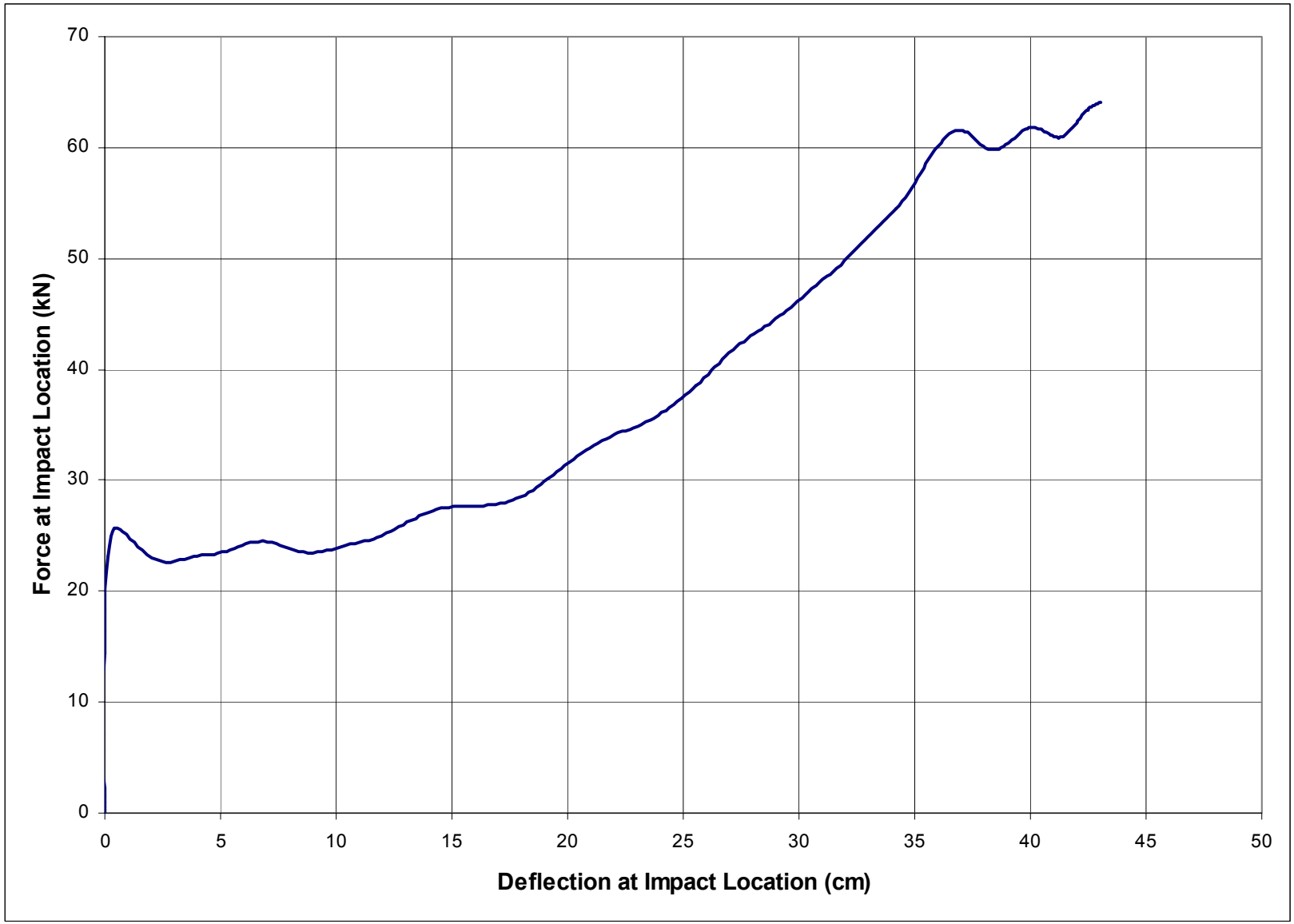

Figure C-6. Force-Deflection Plot Derived from Strain Gauge Data, Test MPR-3

Bogie Test Summary

Test Information

Test Number:	MPR4	
Test Date:	23-Jun-00	
Failure Type:	Soil Failure	

Post Properties

Post Type:	Steel	
Post Size:	W152x23.8	W6x16
Post Length:	134.6 cm	(53.0 in)
Embedment Depth:	61.0 cm	(24.0 in)

Soil Properties

Moisture Content:	0	
Gradation:	47B Sand	
Soil Density, γ_d:	1842	kg/m³
Compaction Method:	Hand Tamped	

Bogie Properties

Impact Velocity:	6.9 m/s	(15.5 mph) (22.8 fps)
Impact Location:	54.9 cm	(21.6 in.) above groundline
Bogie Mass:	966 kg	(2131 lbf.)

Data Acquired

Accelerometer Data - EDR3
Side View, e-cam
String Potentiometer
Strain Gages

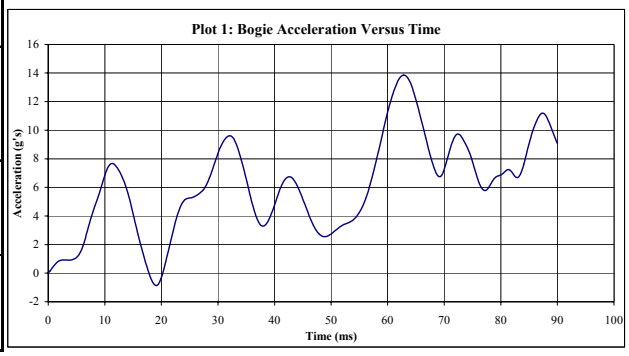

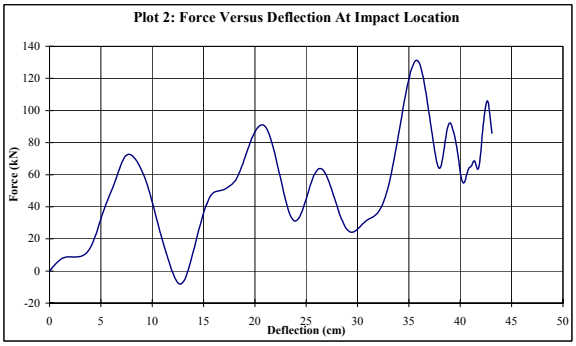

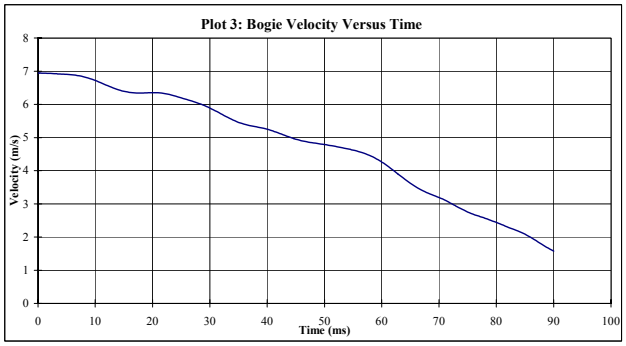

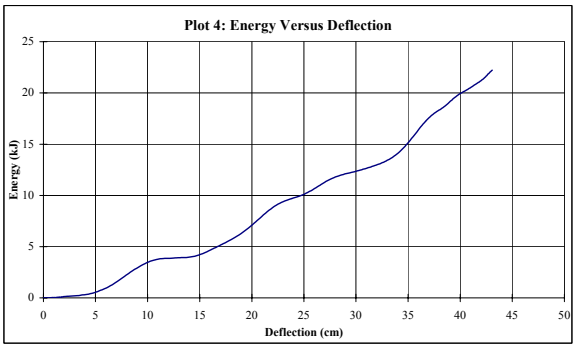

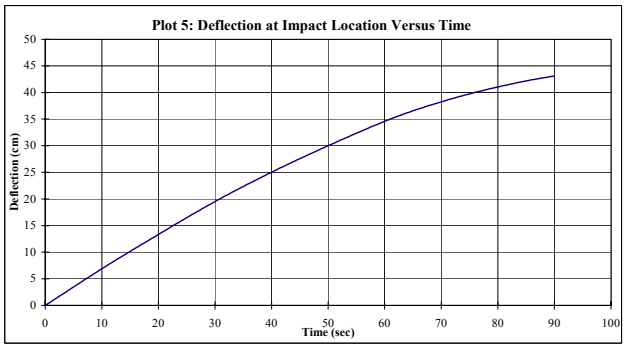

Figure C-7. Accelerometer Data Analysis, Test MPR-4

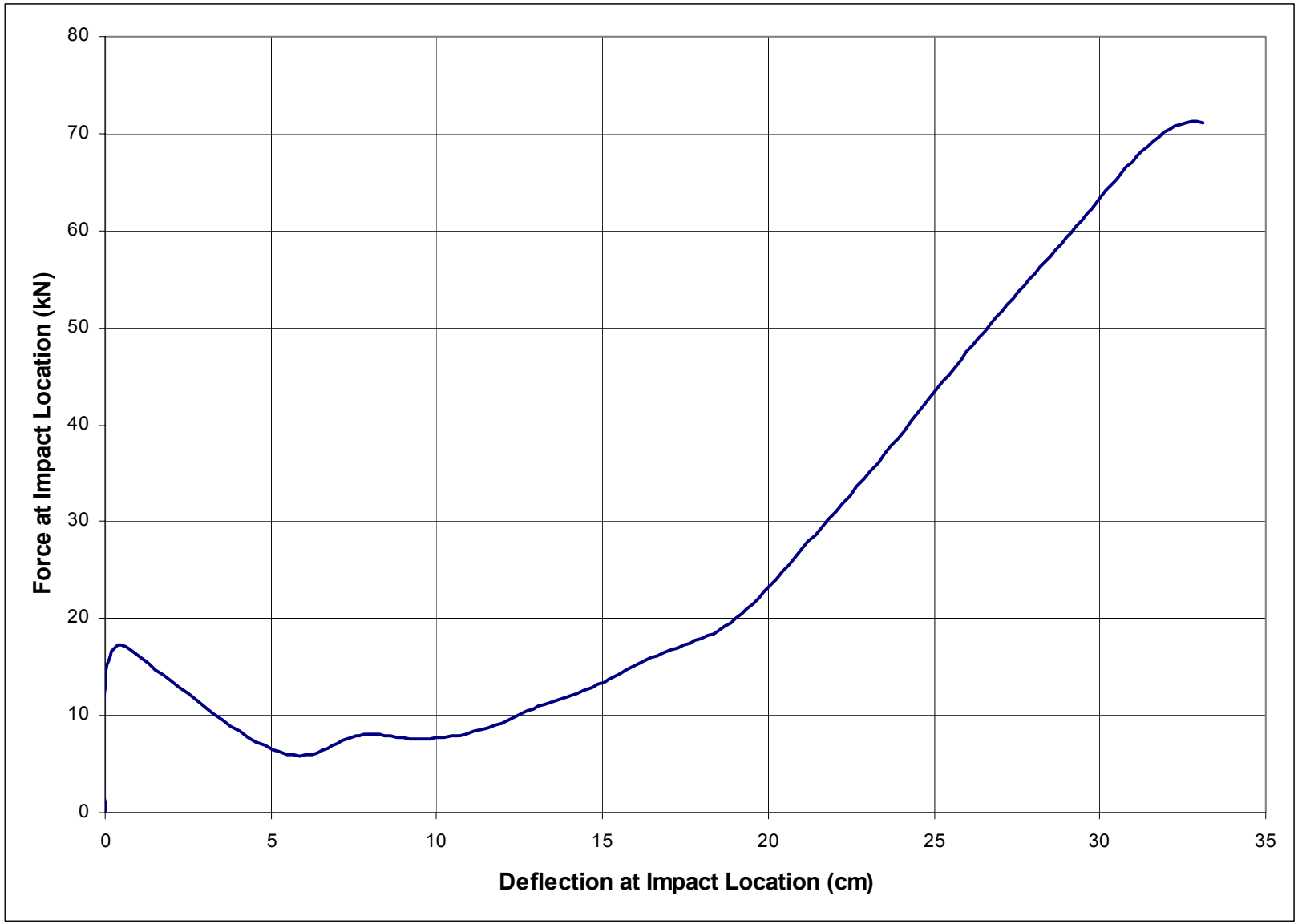

Figure C-8. Force-Deflection Plot Derived from Strain Gauge Data, Test MPR-4

Bogie Test Summary

Test Information

Test Number:	MPR5	
Test Date:	26-Oct-01	
Failure Type:	Soil Failure	

Post Properties

Post Type:	Steel	
Post Size:	W152x23.8	W6x16
Post Length:	134.6 cm	(53.0 in)
Embedment Depth:	61.0 cm	(24.0 in)

Soil Properties

Moisture Content:	0	
Gradation:	ASTM C 33 Coarse Aggregate	
Soil Density, γ_d:	1586	kg/m^3
Compaction Method:	Hand Tamped	

Bogie Properties

Impact Velocity:	6.2 m/s	(13.8 mph) (20.3 fps)
Impact Location:	54.9 cm	(21.6 in.) above groundline
Bogie Mass:	1015 kg	(2237 lbf.)

Data Acquired

Accelerometer Data - EDR3
Side View, e-cam
String Potentiometer
Strain Gages

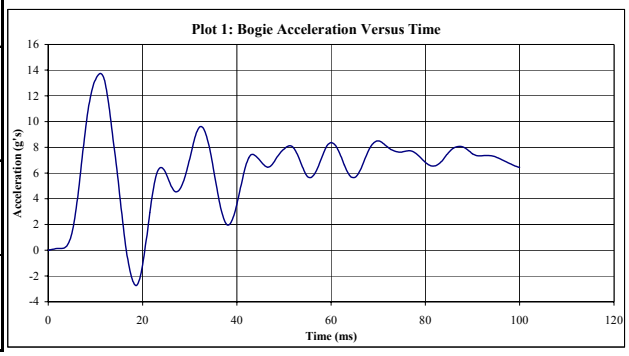

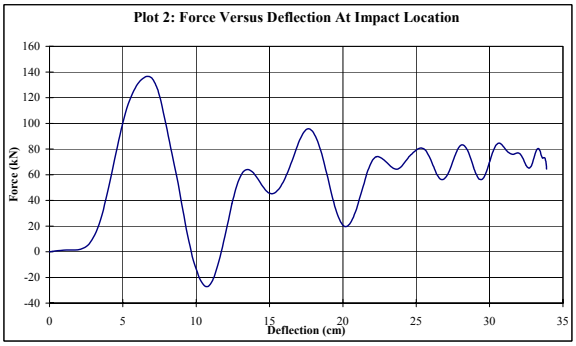

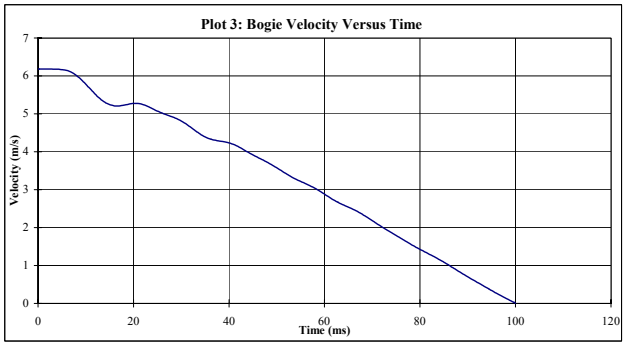

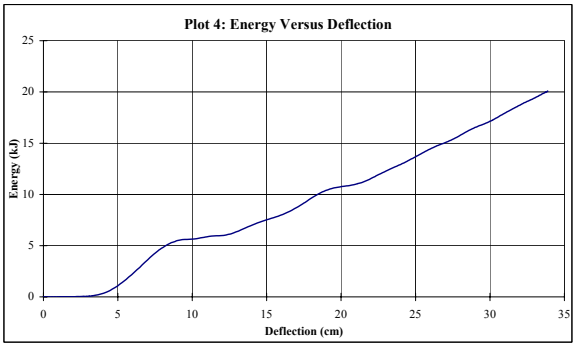

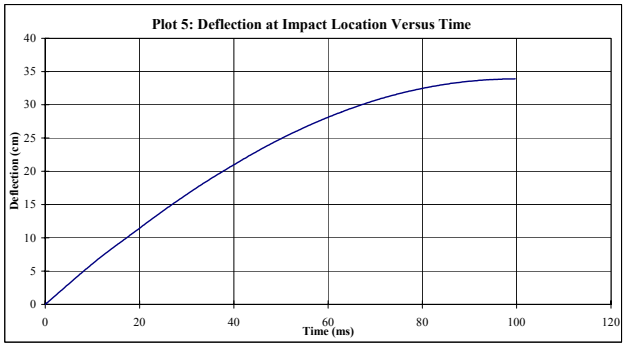

Figure C-9. Accelerometer Data Analysis, Test MPR-5

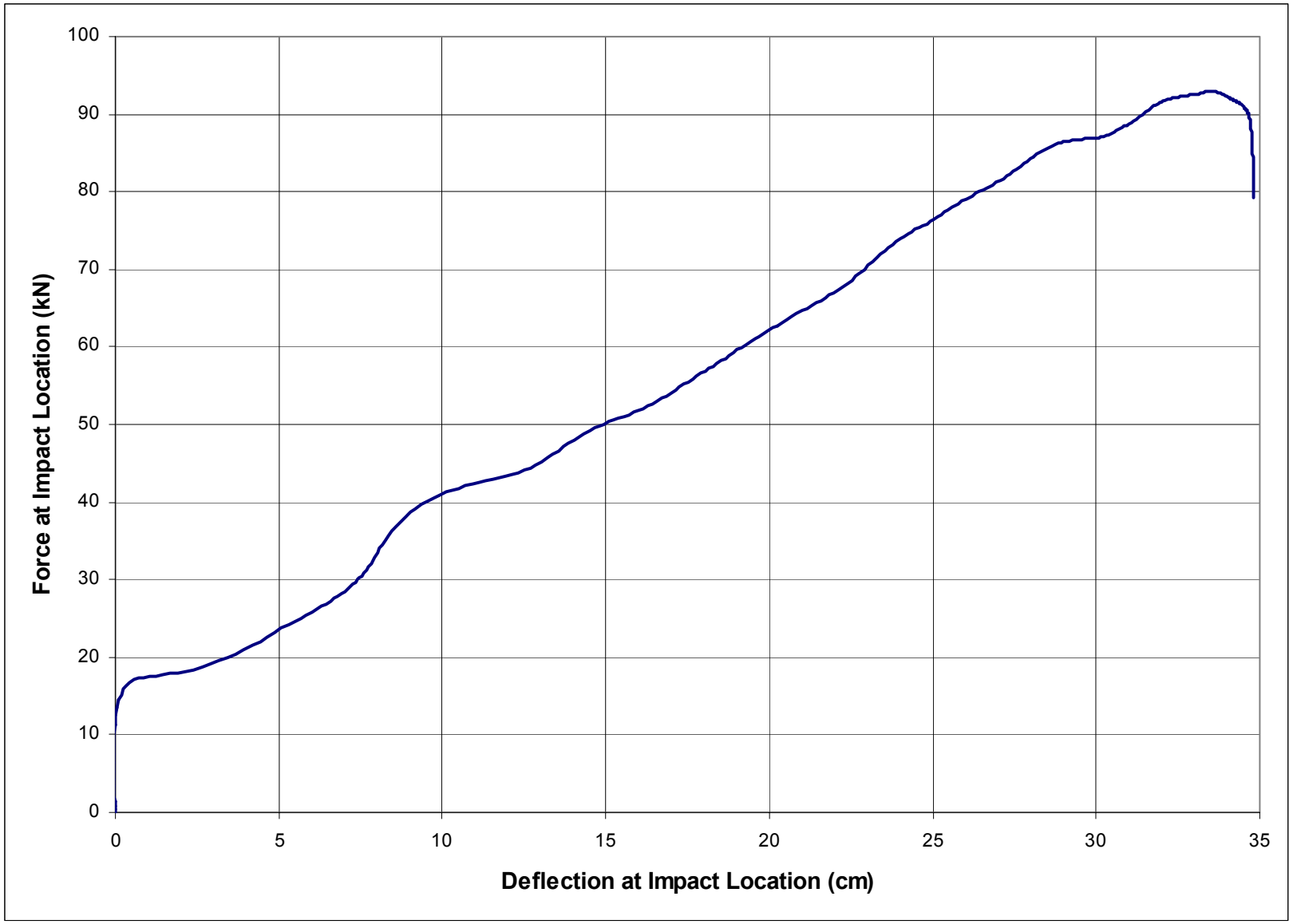

Figure C-10. Force-Deflection Plot Derived from Strain Gauge Data, Test MPR-5

Bogie Test Summary

Test Information

Test Number:	MPR6	
Test Date:	26-Oct-01	
Failure Type:	Soil Failure	

Post Properties

Post Type:	Steel	
Post Size:	W152x23.8	W6x16
Post Length:	119.4 cm	(47.0 in)
Embedment Depth:	45.7 cm	(18.0 in)

Soil Properties

Moisture Content:	0	
Gradation:	ASTM C 33 Coarse Aggregate	
Soil Density, γ_d:	1586 kg/m^3	
Compaction Method:	Hand Tamped	

Bogie Properties

Impact Velocity:	6.8 m/s	(15.2 mph) (22.2 fps)
Impact Location:	54.9 cm	(21.6 in.) above groundline
Bogie Mass:	1015 kg	(2237 lbf.)

Data Acquired

Accelerometer Data - EDR3
Side View, e-cam
String Potentiometer
Strain Gages

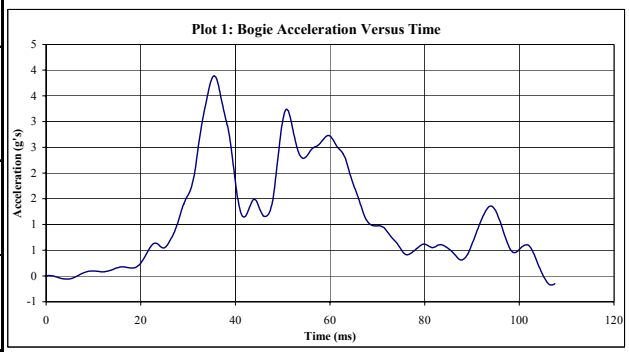

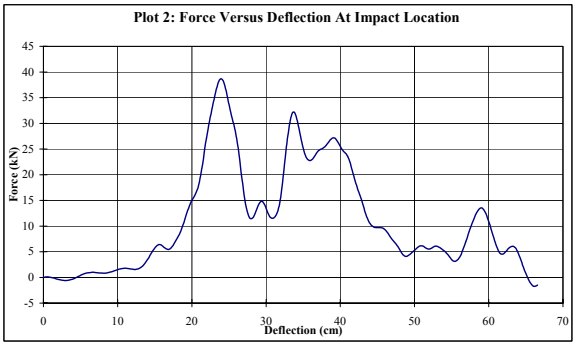

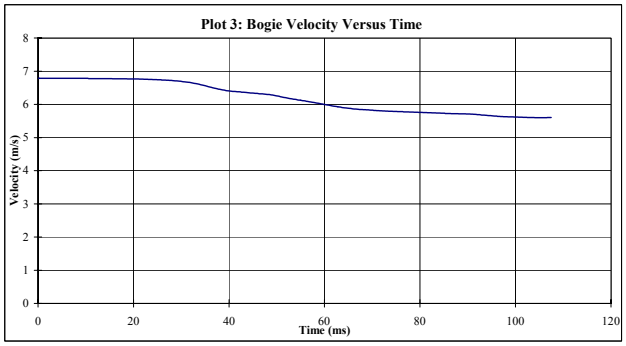

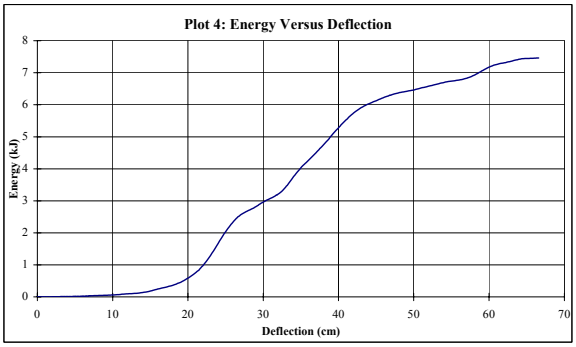

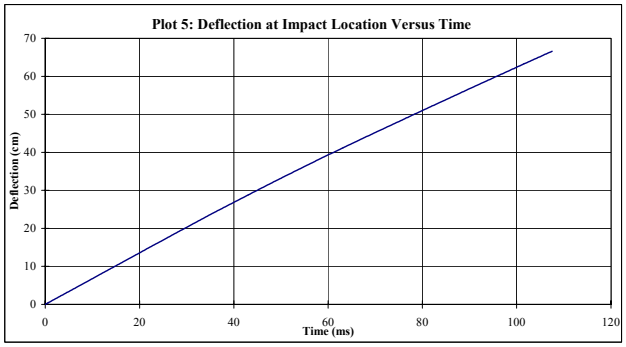

Figure C-11. Accelerometer Data Analysis, Test MPR-6

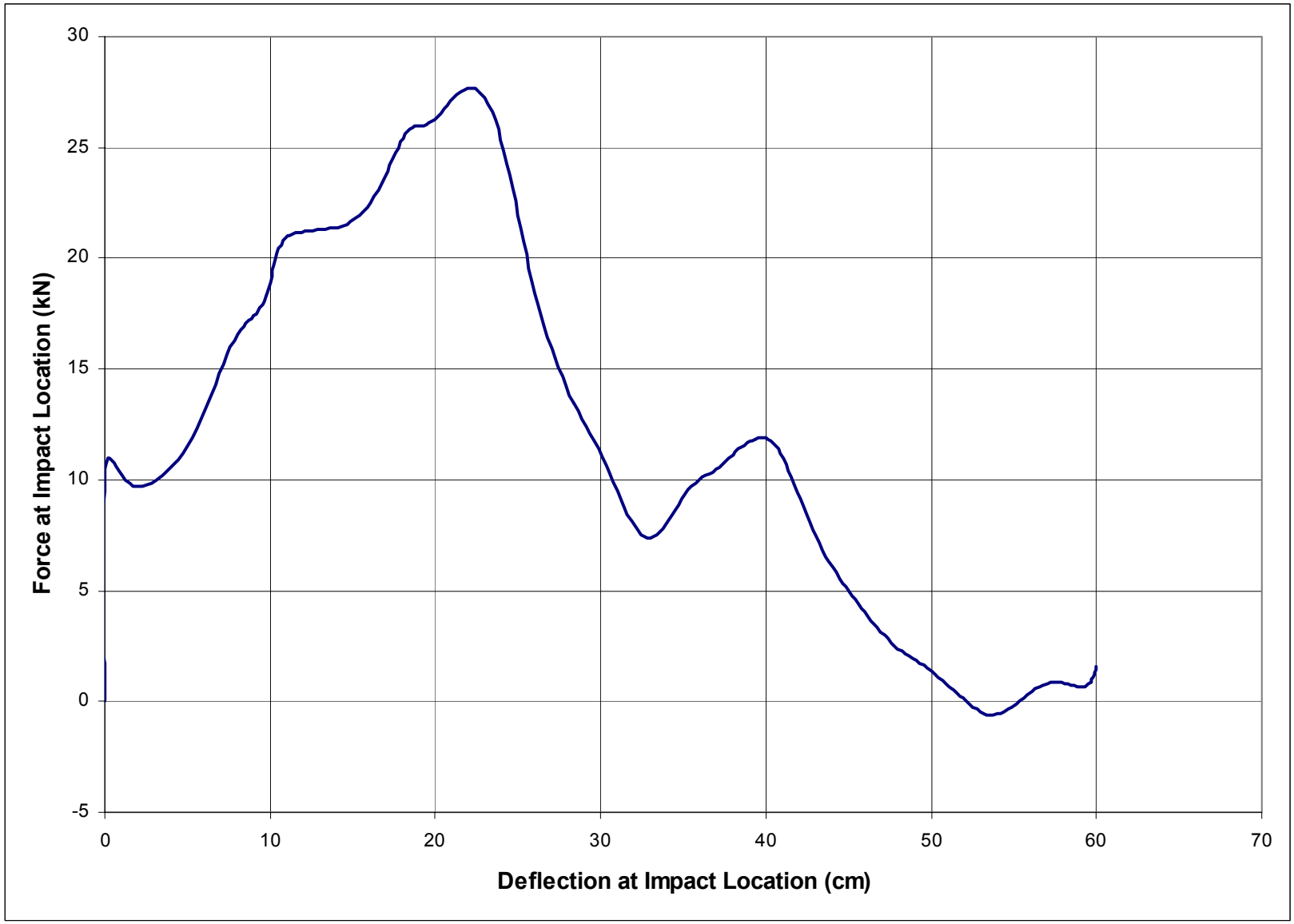

Figure C-12. Force-Deflection Plot Derived from Strain Gauge Data, Test MPR-6

159

Bogie Test Summary

Test Information

Test Number:	MPR7	
Test Date:	30-Nov-01	
Failure Type:	Soil Failure	

Post Properties

Post Type:	Steel	
Post Size:	W152x13.4	W6x9
Post Length:	134.6 cm	(53.0 in)
Embedment Depth:	61.0 cm	(24.0 in)

Soil Properties

Moisture Content:	0	
Gradation:	ASTM C 33 Coarse Aggregate	
Soil Density, γ_d:	1586	kg/m^3
Compaction Method:	Hand Tamped	

Bogie Properties

Impact Velocity:	6.7 m/s	(14.9 mph) (21.9 fps)
Impact Location:	54.9 cm	(21.6 in.) above groundline
Bogie Mass:	1015 kg	(2237 lbf.)

Data Acquired

Accelerometer Data - EDR3
Side View, e-cam

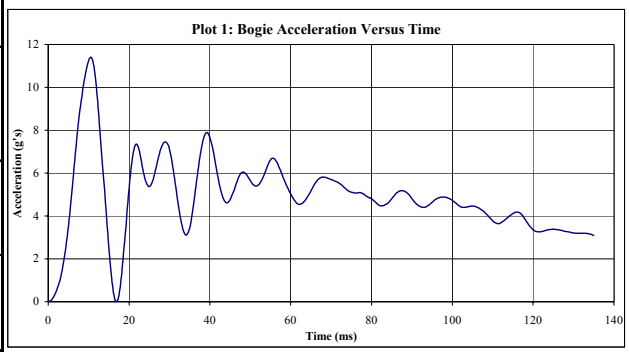

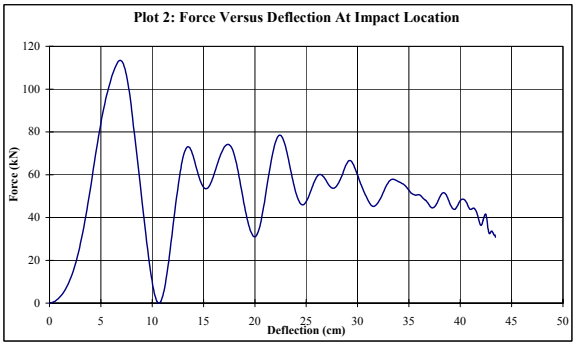

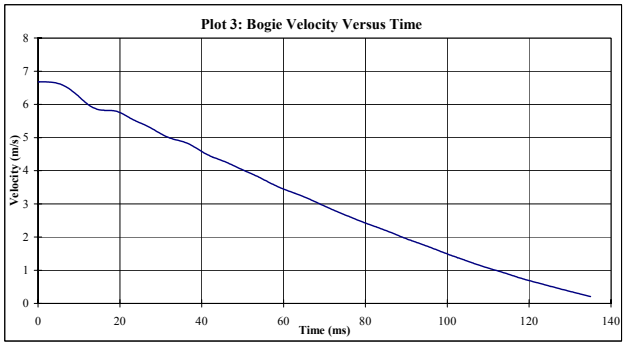

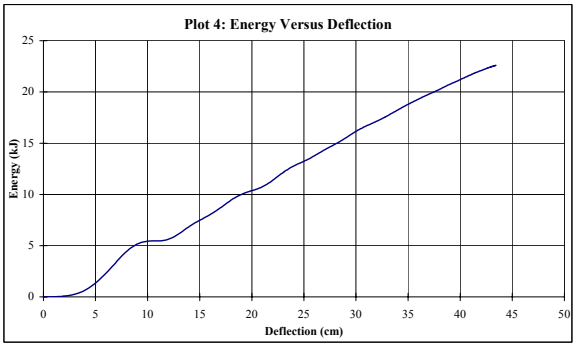

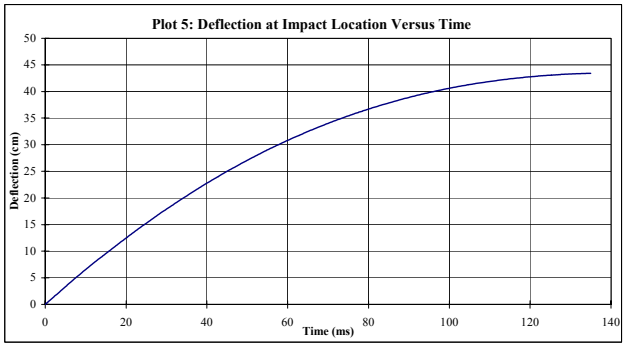

Figure C-13. Accelerometer Data Analysis, Test MPR-7

Bogie Test Summary

Test Information

Test Number:	MPR8	
Test Date:	30-Nov-01	
Failure Type:	Soil Failure	

Post Properties

Post Type:	Steel	
Post Size:	W152x13.4	W6x9
Post Length:	134.6 cm	(53.0 in)
Embedment Depth:	61.0 cm	(24.0 in)

Soil Properties

Moisture Content:	0	
Gradation:	ASTM C 33 Coarse Aggregate	
Soil Density, γ_d:	1586	kg/m^3
Compaction Method:	Hand Tamped	

Bogie Properties

Impact Velocity:	6.0 m/s	(13.5 mph) (19.8 fps)
Impact Location:	54.9 cm	(21.6 in.) above groundline
Bogie Mass:	1015 kg	(2237 lbf.)

Data Acquired

Accelerometer Data - EDR3
Side View, e-cam

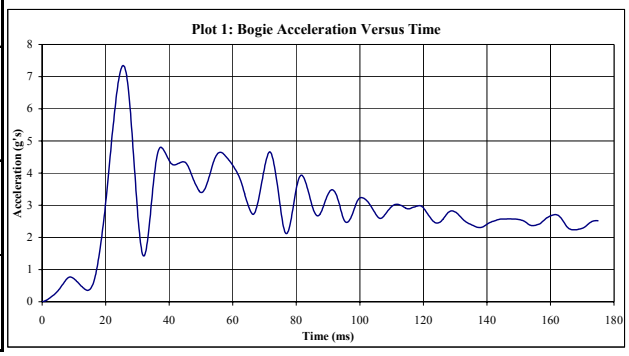

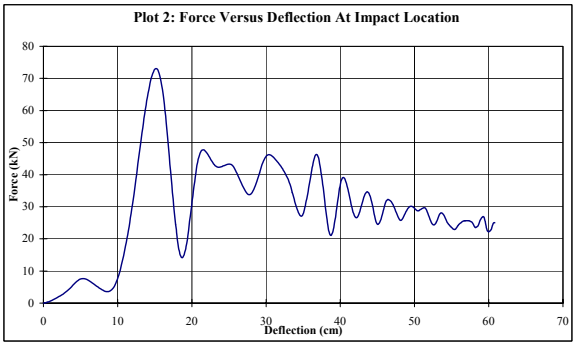

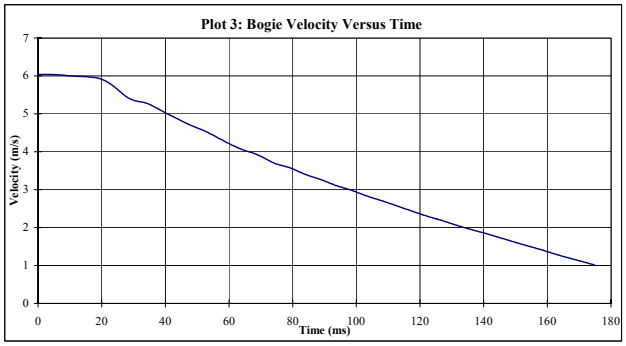

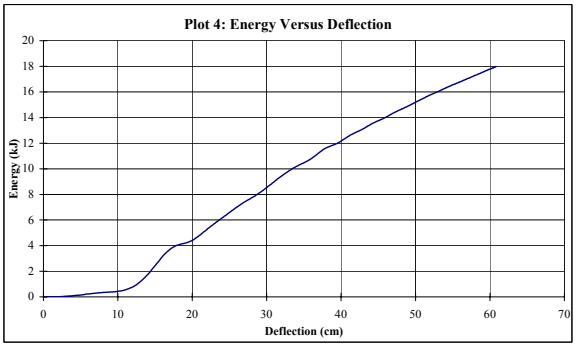

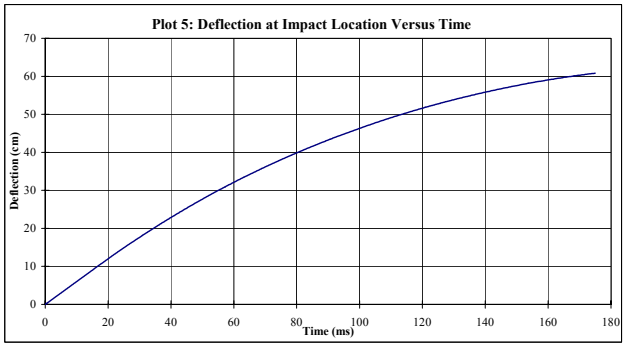

Figure C-14. Accelerometer Data Analysis, Test MPR-8

Bogie Test Summary

Test Information

Test Number:	MPR9	
Test Date:	30-Nov-01	
Failure Type:	Soil Failure	

Post Properties

Post Type:	Steel	
Post Size:	W152x13.4	W6x9
Post Length:	134.6 cm	(53.0 in)
Embedment Depth:	61.0 cm	(24.0 in)

Soil Properties

Moisture Content:	0	
Gradation:	ASTM C 33 Fine Aggregate	
Soil Density, γ_d:	1842	kg/m^3
Compaction Method:	Hand Tamped	

Bogie Properties

Impact Velocity:	6.5 m/s	(14.6 mph) (21.4 fps)
Impact Location:	54.9 cm	(21.6 in.) above groundline
Bogie Mass:	1015 kg	(2237 lbf.)

Data Acquired

Accelerometer Data - EDR3
Side View, e-cam

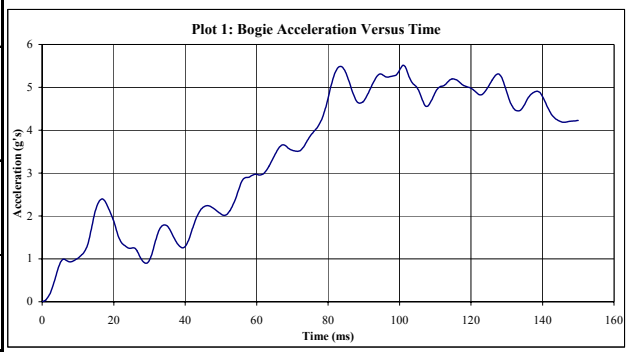

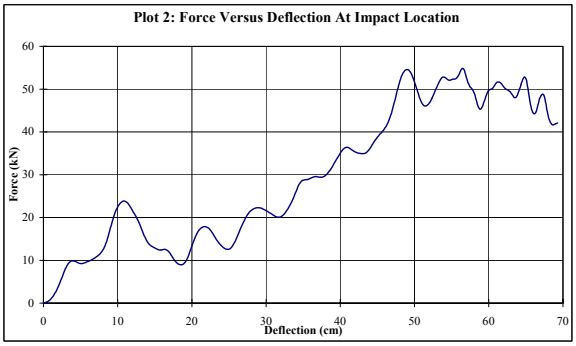

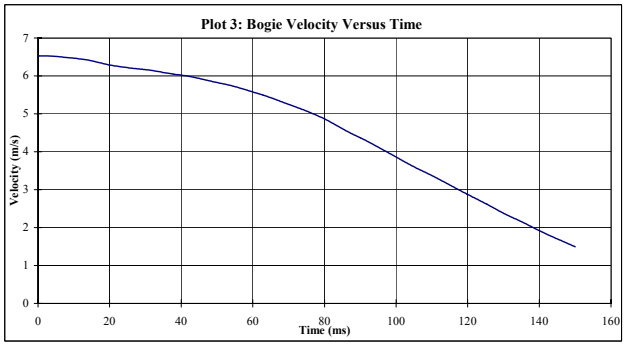

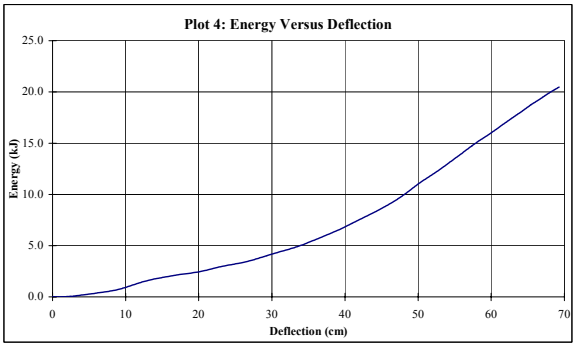

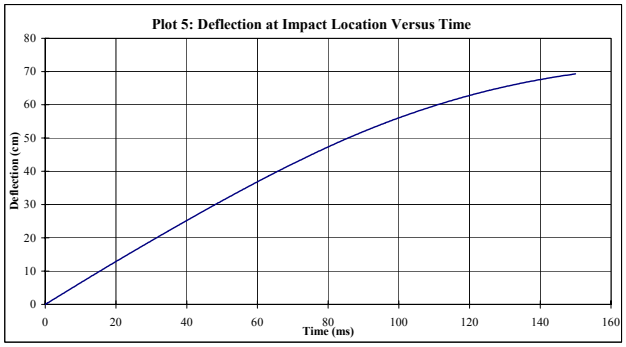

Figure C-15. Accelerometer Data Analysis, Test MPR-9

Bogie Test Summary

Test Information

Test Number:	MPR-10	
Test Date:	25-Sep-02	
Failure Type:	Soil Failure	

Post Properties

Post Type:	Steel	
Post Size:	W152x13.4	W6x9
Post Length:	134.6 cm	(53.0 in)
Embedment Depth:	61.0 cm	(24.0 in)

Soil Properties

Moisture Content:	0	
Gradation:	ASTM C 33 Coarse Aggregate	
Soil Density, γ_d:	1586 kg/m^3	
Compaction Method:	Hand Tamped	

Bogie Properties

Impact Velocity:	8.1 m/s	(18.2 mph) (26.7 fps)
Impact Location:	54.9 cm	(21.6 in.) above groundline
Bogie Mass:	992 kg	(2187 lbf.)

Data Acquired

Accelerometer Data - EDR3
Side View, e-cam

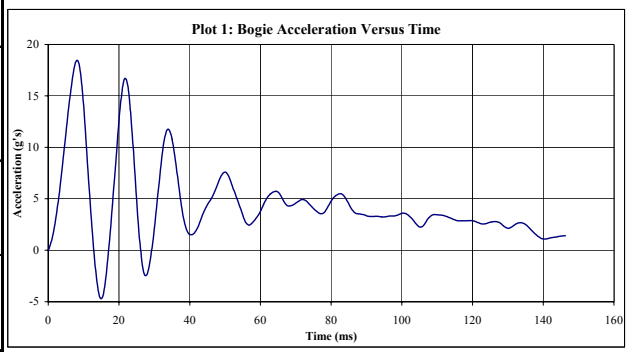

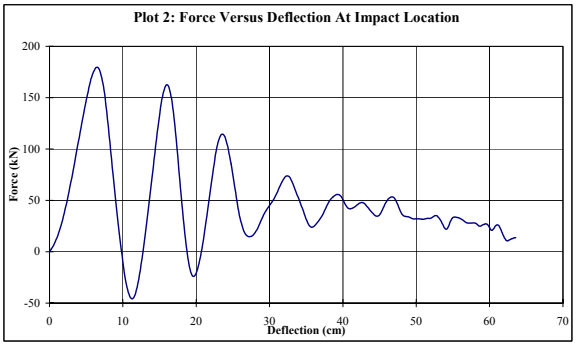

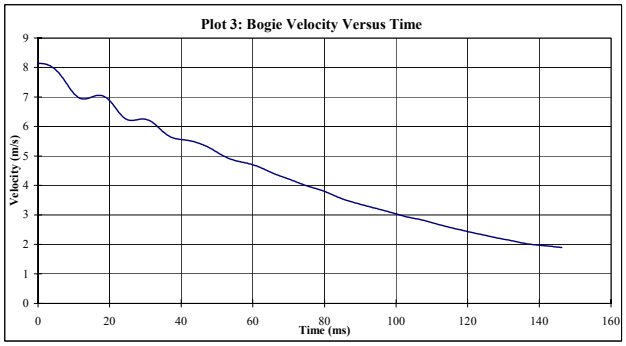

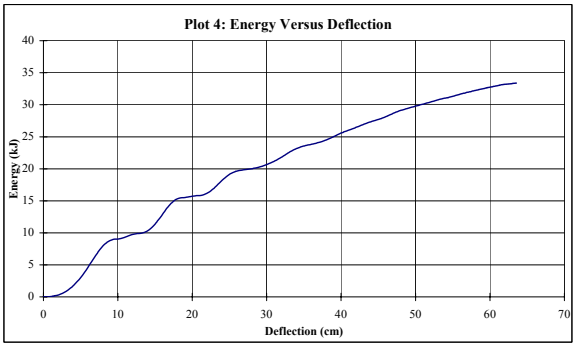

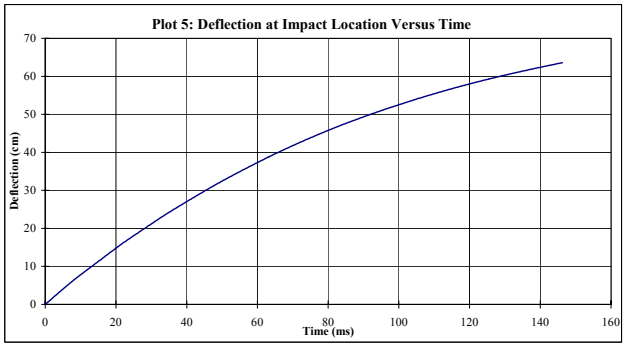

Figure C-16. Accelerometer Data Analysis, Test MPR-10

Bogie Test Summary

Test Information

Test Number:	MPR-11	
Test Date:	25-Sep-02	
Failure Type:	Soil Failure	

Post Properties

Post Type:	Steel	
Post Size:	W152x13.4	W6x9
Post Length:	119.4 cm	(47.0 in)
Embedment Depth:	45.7 cm	(18.0 in)

Soil Properties

Moisture Content:	0	
Gradation:	ASTM C 33 Coarse Aggregate	
Soil Density, γ_d:	1586 kg/m^3	
Compaction Method:	Hand Tamped	

Bogie Properties

Impact Velocity:	7.1 m/s	(15.9 mph) (23.3 fps)
Impact Location:	54.9 cm	(21.6 in.) above groundline
Bogie Mass:	992 kg	(2187 lbf.)

Data Acquired

Accelerometer Data - EDR3
Side View, e-cam

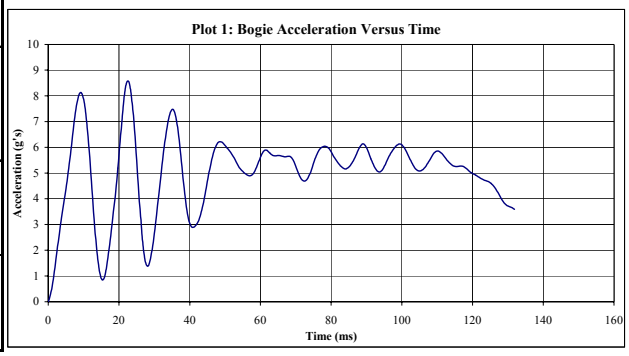

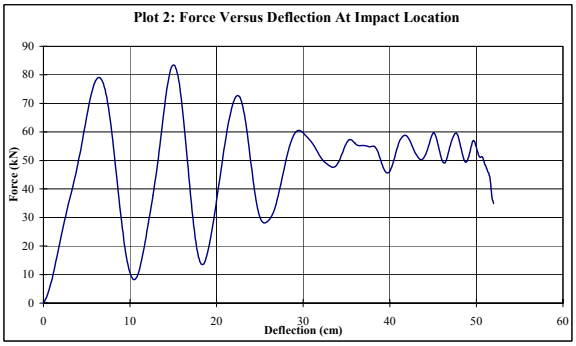

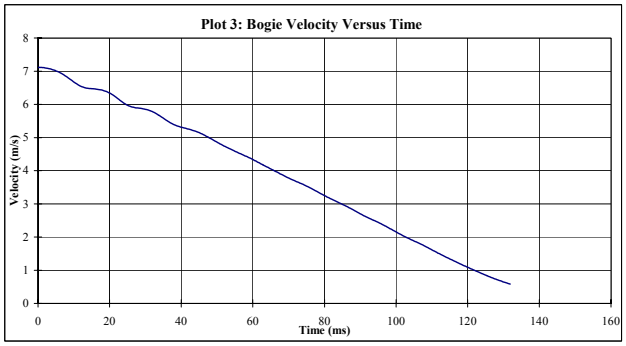

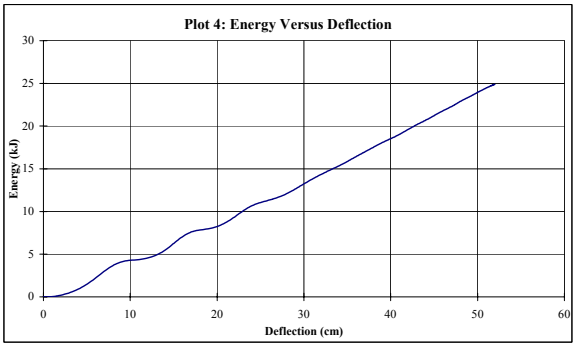

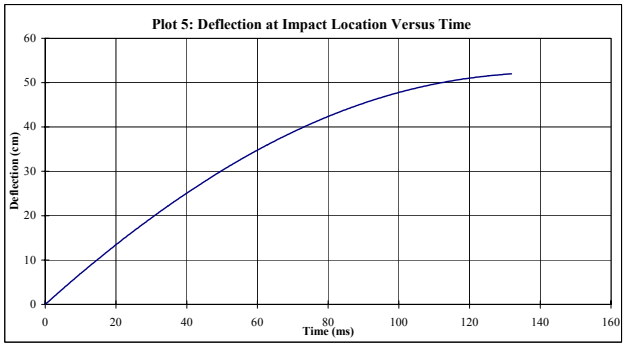

Figure C-17. Accelerometer Data Analysis, Test MPR-11

Bogie Test Summary

Test Information

Test Number:	PRH-1	
Test Date:	24-Nov-99	
Failure Type:	Post Failure	

Post Properties

Post Type:	Steel	
Post Size:	W152x13.4	W6x9
Post Length:	182.9 cm	(6.0 ft)
Embedment Depth:	109.2 cm	(43.0 in)

Soil Properties

Moisture Content:	0	
Gradation:	0	
Soil Density, γ_d:	N/A kg/m³	
Compaction Method:	0	

Bogie Properties

Impact Velocity:	6.7 m/s	(15.0 mph) (22.0 fps)
Impact Location:	54.9 cm	(21.6 in.) above groundline
Bogie Mass:	971 kg	(2142 lbf.)

Data Acquired

Accelerometer Data
Side View, S-VHS

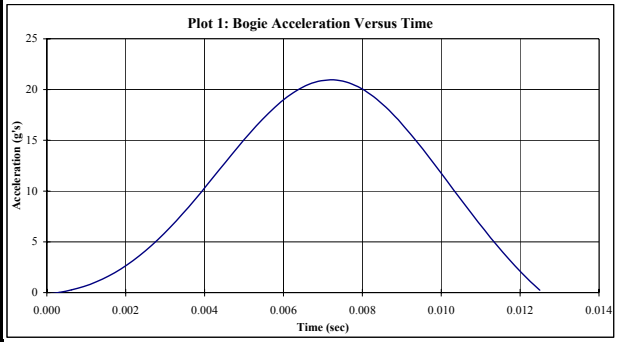

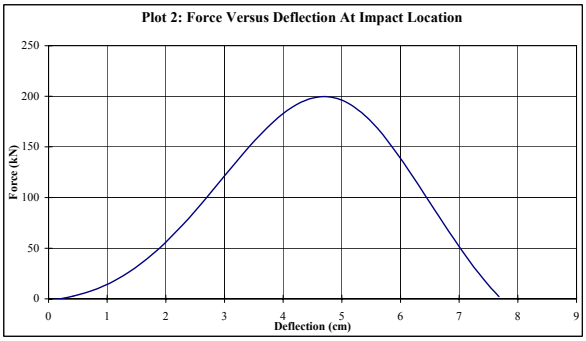

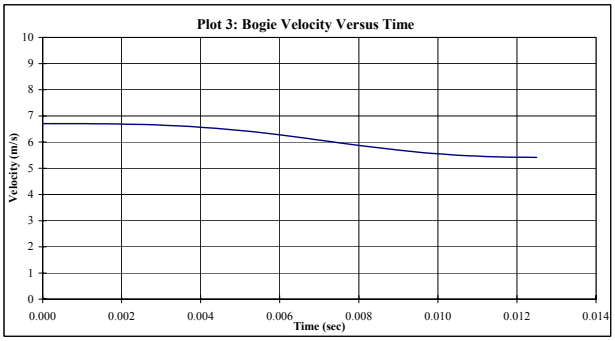

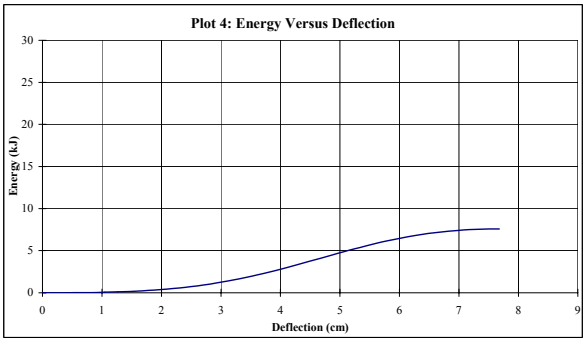

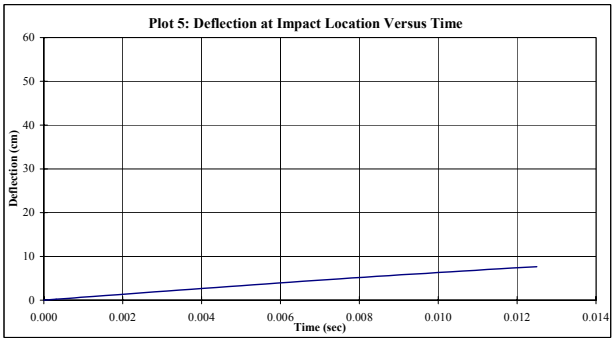

Figure C-18. Accelerometer Data Analysis, Test PRH-1

APPENDIX D

Accelerometer Data Analysis, Test PR-1

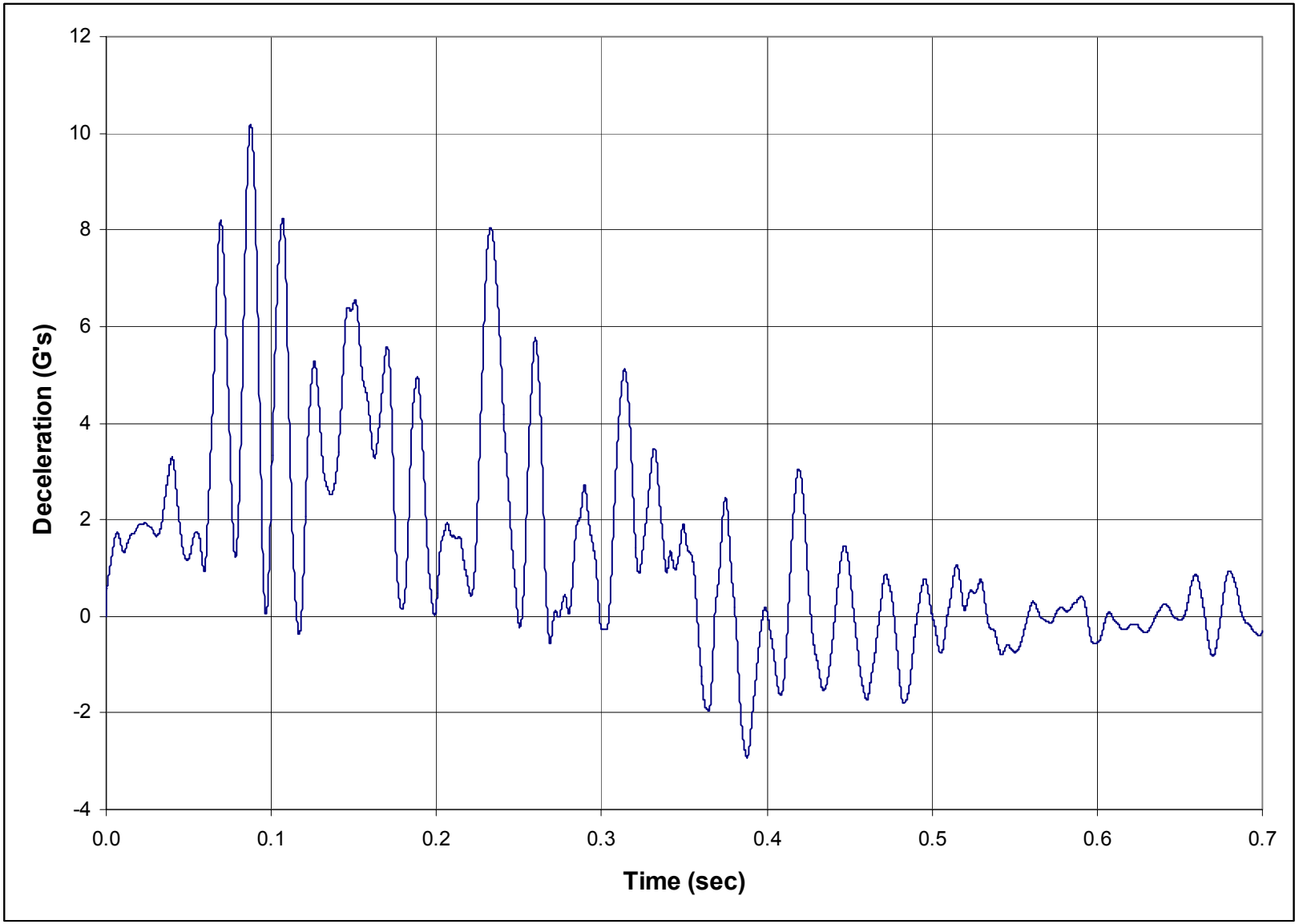

Figure D-1. Graph of Longitudinal Deceleration, Test PR-1

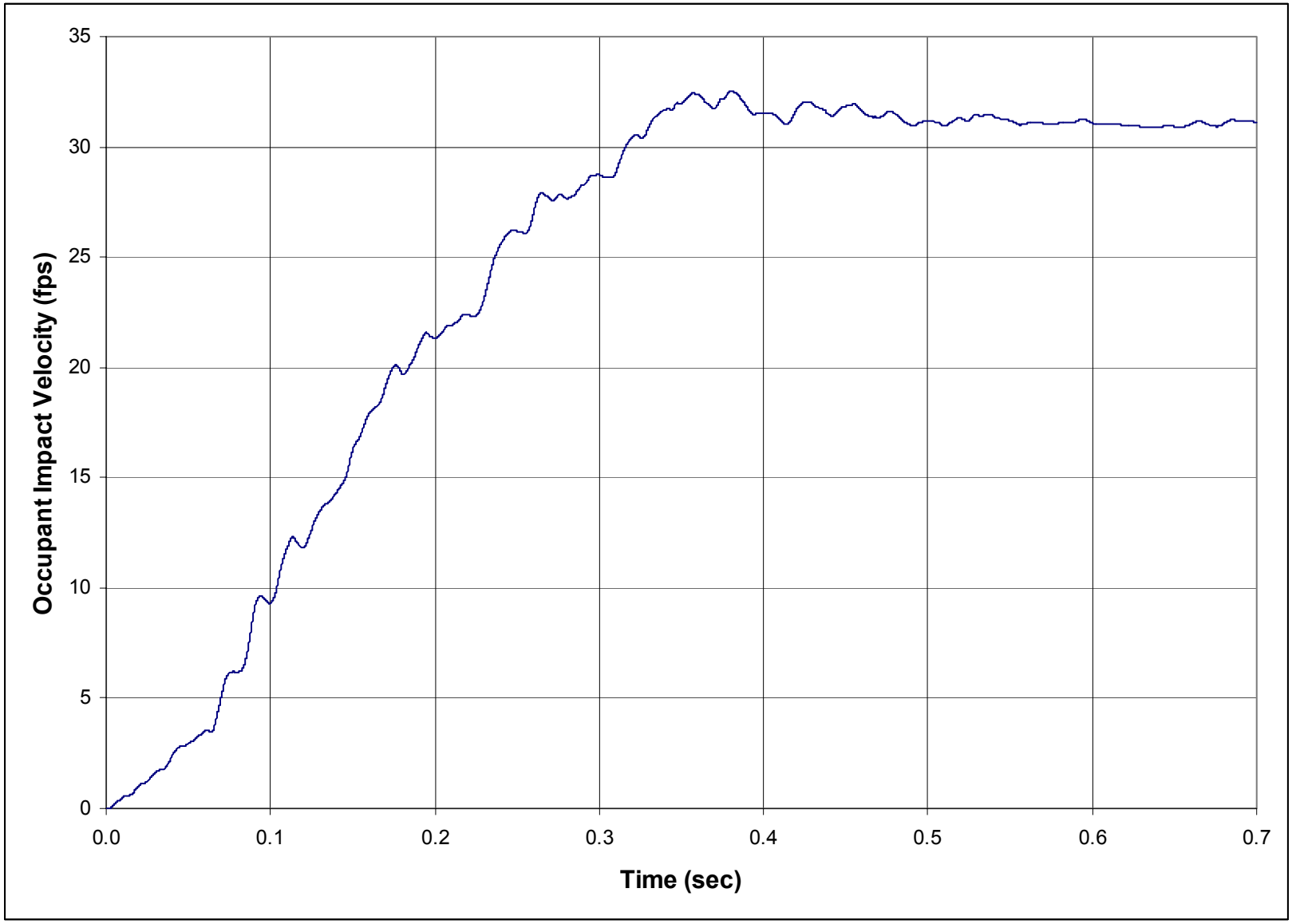

Figure D-2. Graph of Longitudinal Occupant Impact Velocity, Test PR-1

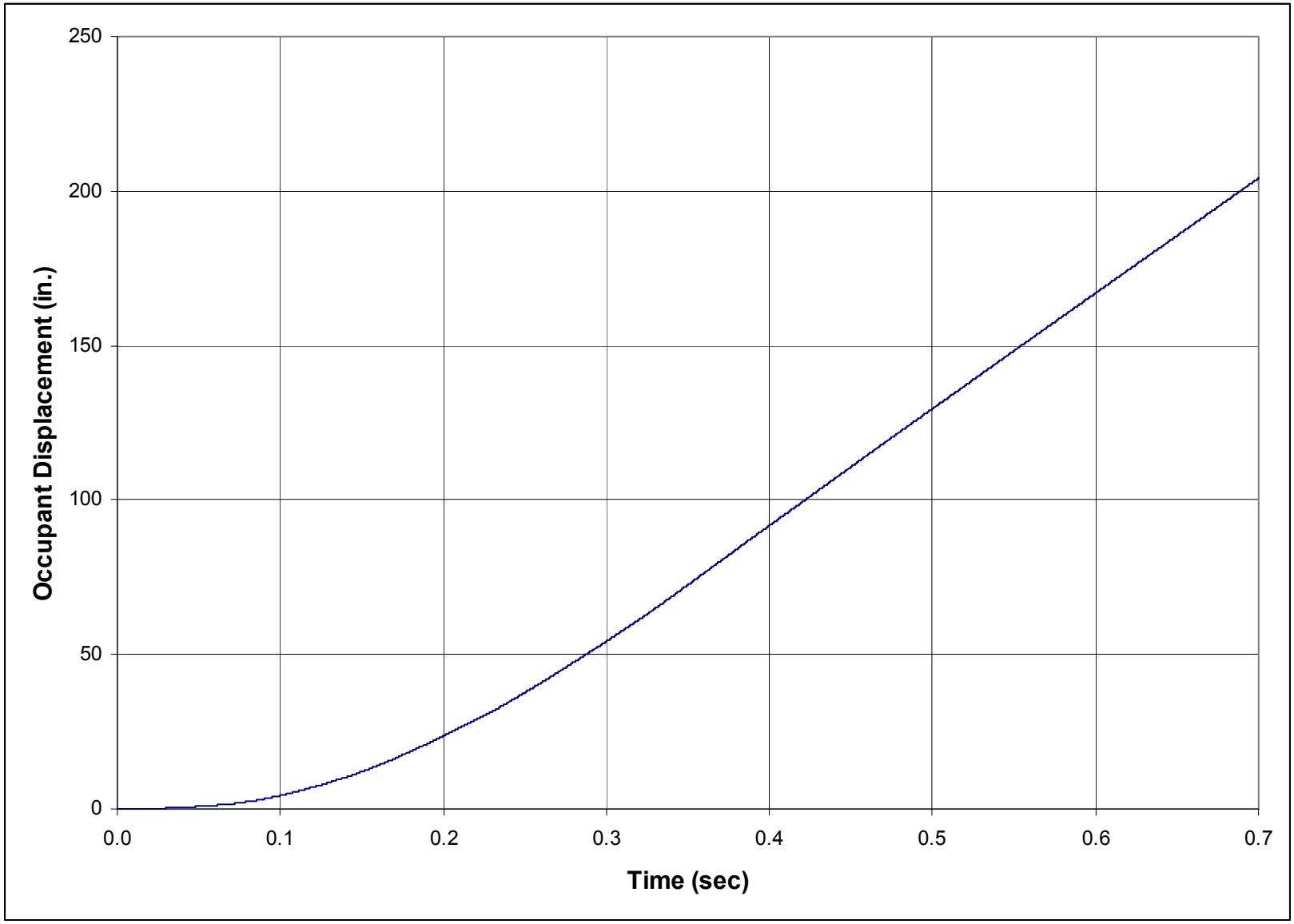

Figure D-3. Graph of Longitudinal Occupant Displacement, Test PR-1

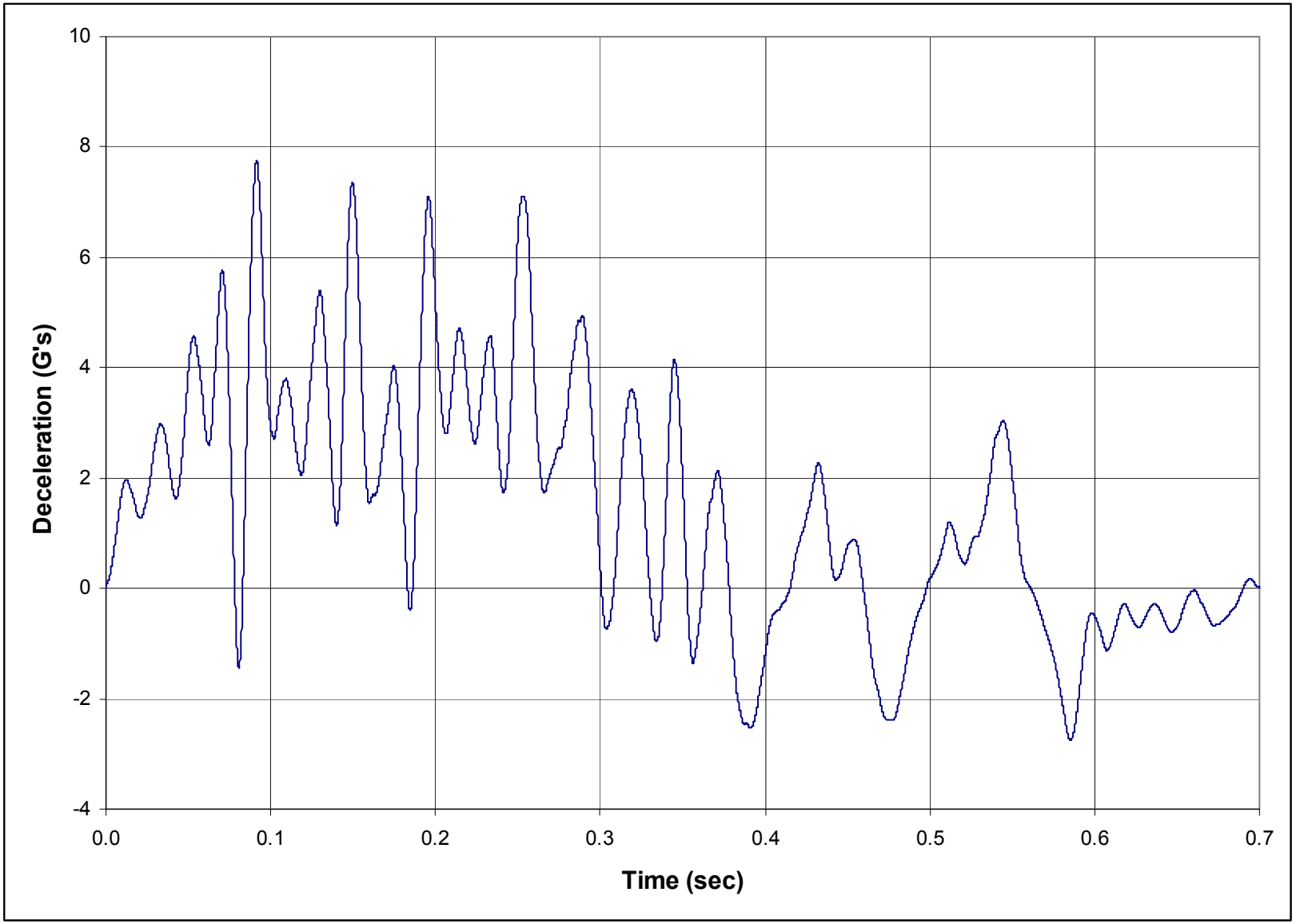

Figure D-4. Graph of Lateral Deceleration, Test PR-1

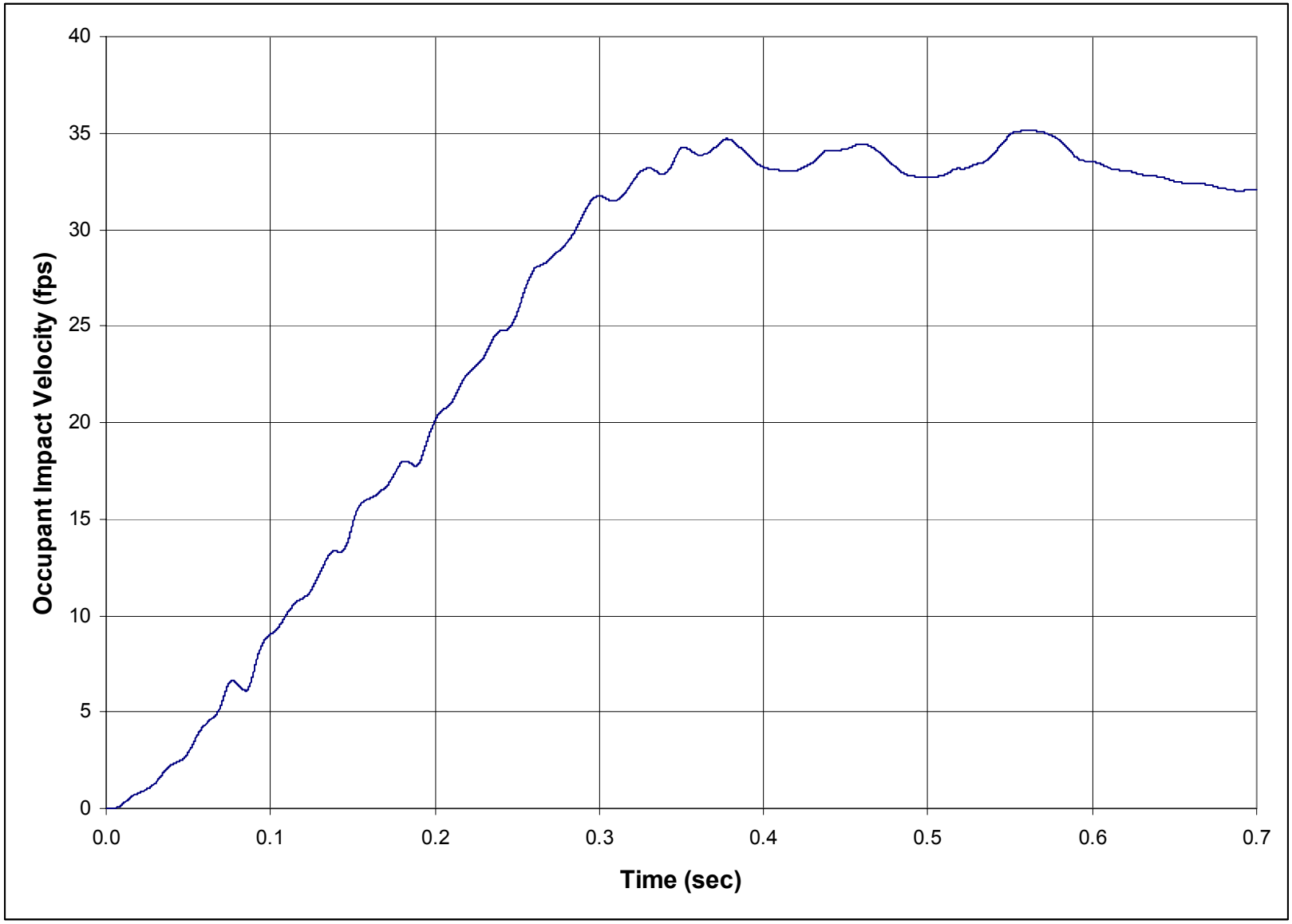

Figure D-5. Graph of Lateral Occupant Impact Velocity, Test PR-1

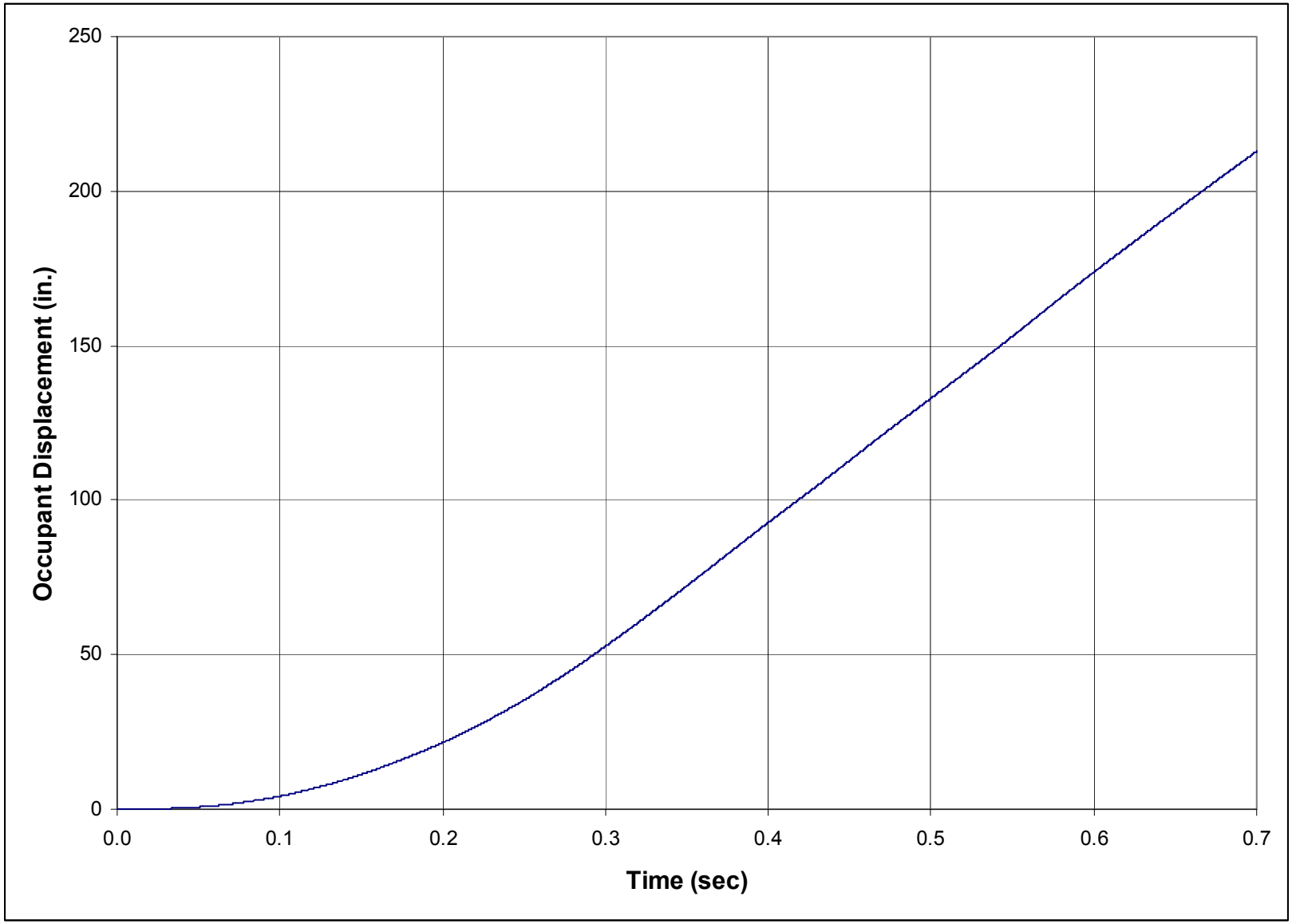

Figure D-6. Graph of Lateral Occupant Displacement, Test PR-1

APPENDIX E

Roll and Yaw Data Analysis, Test PR-1

Figure E-1. Graph of Roll and Yaw Angular Displacements, Test PR-1

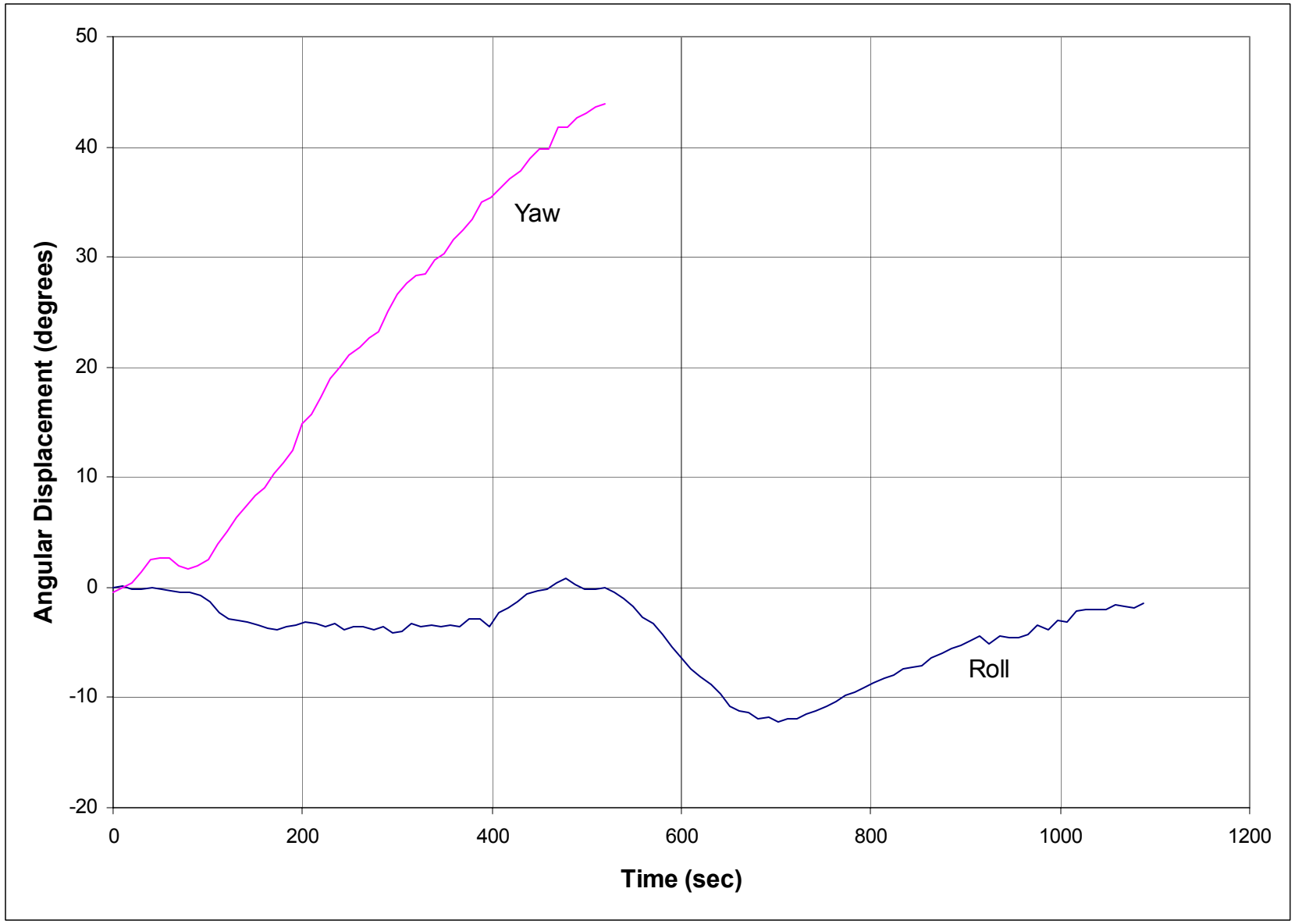

Figure E-1. Graph of Roll and Yaw Angular Displacements, Test PR-1